Graduate School ETD Form 9
(Revised 01/14)

PURDUE UNIVERSITY
GRADUATE SCHOOL
Thesis/Dissertation Acceptance

This is to certify that the thesis/dissertation prepared

By Jinghua Zhong

Entitled MODELING AND ADAPTIVE ROBUST MOTION CONTROL OF PIEZOELECTRIC ACTUATORS

For the degree of Doctor of Philosophy

Is approved by the final examining committee:

Bin Yao

Arvind Raman

Peter H. Meckl

Jianghai Hu

To the best of my knowledge and as understood by the student in the *Thesis/Dissertation Agreement. Publication Delay, and Certification/Disclaimer (Graduate School Form 32)*, this thesis/dissertation adheres to the provisions of Purdue University's "Policy on Integrity in Research" and the use of copyrighted material.

Bin Yao

Approved by Major Professor(s): _____

_____

Approved by: David C. Anderson 02/13/2014

Head of the Department Graduate Program Date

MODELING AND ADAPTIVE ROBUST MOTION CONTROL OF PIEZOELECTRIC ACTUATORS

A Dissertation

Submitted to the Faculty

of

Purdue University

by

Jinghua Zhong

In Partial Fulfillment of the

Requirements for the Degree

of

Doctor of Philosophy

May 2014

Purdue University

West Lafayette, Indiana

ProQuest LLC.
789 East Eisenhower Parkway
P.O. Box 1346
Ann Arbor, MI 48106 - 1346

To my parents and my wife.

ACKNOWLEDGMENTS

I'd like to first and foremost thank my major professor, Dr. Bin Yao, and my committee members, Drs. Arvind Raman, Peter Meckl, and Jianghai Hu, for their enormous patience during my long struggle in the pursuit of this degree. It will be more than 10 years from the day I arrived at Purdue when this dissertation is finally submitted.

Dr. Yao taught me almost everything I know about controls and helped me along my research. I now work in the industry on problems that are completely unrelated to my Ph.D. research, but the design philosophies I learned at Purdue prove more useful than ever. Drs. Raman, Meckl and Hu gave me valuable feedback during my preliminary exam and my final defense, and Dr. Meckl corrected numerous typos and grammatical errors in my dissertation.

I'd also like to thank some of my former groupmates, Dr. Shreekant Gayaka, for his friendship and many discussions, Dr. Phanindra Garimella, for helping me make sense of adaptive robust control for the first time when I started my research, and Dr. Song Liu, for his help and the best food I've had at Purdue.

Volunteering for the Purdue Graduate Student Government and its annual job fair was a big part of my life at Purdue, and along the way I met some great people, such as Leonardo Bachega, Marriner Merrill, and Salvador Acuña. Their support made it possible for me to secure a fellowship for my 6th and "final" year.

The constant reflection on life by David Foster Wallace and his perspective on the day-to-day mundaneness have been an inspiration and source of courage for me. May you rest in peace. 3D Realms released Duke Nukem Forever after 15 long years and shamed me into finishing. I never imagined I would fail to graduate before DNF.

My parents sent me to the US in 2001, and since then I have never spent enough time with them, even through their many illnesses. They gave me everything.

And last but not least, I thank my wife Jessie for her love and bearing with me during the past two years as I was finishing my dissertation. This would not have been possible without your many sacrifices.

TABLE OF CONTENTS

Page

LIST OF FIGURES

LIST OF TABLES

ABSTRACT

Zhong, Jinghua Ph.D., Purdue University, May 2014. Modeling and Adaptive Robust Motion Control of Piezoelectric Actuators. Major Professor: Bin Yao, School of Mechanical Engineering.

High performance motion trajectory tracking can be achieved on a piezoelectric stack actuator stage by the combination of a new hysteresis model, judicious modeling of the dominant dynamics, and adaptive robust control design.

A new hysteresis model for piezoelectric actuators is proposed. Inspired by the similarity between pre-sliding friction and piezoelectric hysteresis, the Dahl friction model is extended with non-local memory to model piezoelectric hysteresis. Asymmetry in hysteresis loops is accommodated with a shaping function, which eliminates the need for having different parameters for different branches of the hysteresis loops. All parameters of the hysteresis model can be identified from the outer-loop alone, and the identified model reduces hysteresis nonlinearity from 14 percent of the actuator range to less than 1 percent.

A low-order dynamic model is developed by recognizing the domain switching dynamics of the actuator as the dominant dynamics when the resonant frequency of the stage is far beyond the application bandwidth. The piezoelectric dynamics is well approximated by a feed-through gain and a first-order nonlinear dynamics driven by the input with hysteretic disturbances.

Based on the parameterized model, an adaptive robust controller is designed to achieve (a) guaranteed transient error under the assumption of bounded uncertainties and disturbances; and (b) asymptotic tracking in the presence of parametric uncertainties only. Good tracking performance is achieved for large amplitude trajectories up to 100 Hz even when the hysteresis is entirely attenuated as an unknown disturbance. With additional model compensation from the hysteresis model, the

final tracking errors are more than two orders of magnitude smaller than previously reported in literature on an identical actuator.

For single-loop periodic trajectories, performance can be improved without using an explicit hysteresis model. By approximating the unknown but periodic uncertainty with harmonic basis functions and adapting their amplitudes online, non-parametric uncertainty from unknown hysteresis is significantly reduced. Experimental results demonstrate tracking error down to the sensor noise level for sinusoidal trajectories up to 100 Hz with moderate amplitudes and less than one percent for large amplitudes.

1. INTRODUCTION

1.1 Motivation

Positioning stages based on piezoelectric actuators (PEA) are widely used in high-precision positioning and tracking applications. The actuators are able to produce sub-nanometer displacements by means of the inverse piezoelectric effect. Their resolution is only limited by the resolution and noise level of driving electronics. They are also capable of generating very large pushing forces, which deliver very high bandwidth in typical positioning mechanisms where low-inertia stage and high-stiffness flexures are used [1].

Piezo-actuators are crucial components in equipments for nanotechnology. Instead of using a single open-loop piezo-tube scanner to generate motion in all three dimensions, modern scanning probe microscopes (SPM) employ feedback-controlled piezoelectric scanning stages to achieve higher accuracy and longer range of motion in the X-Y plane. The throughput of probe-based nanofabrication techniques, especially those based on nanolithography or indentation using the scanning tip in Atomic Force Microscopes (AFM), relies heavily on the control performance of the piezoelectric actuators [2].

Besides SPMs, piezoelectric actuators are also used in optical fiber aligners, dual-stage hard-drive reading heads, cutting tool compensation, and other applications where extremely high positioning accuracy and/or large force is needed. Research on the motion control of piezoelectric actuator stages has not only remained active for the past three decades but also seen a steady increase.

When driven by a slow voltage at small strain levels, the behavior of piezoelectric actuators is governed by the classical equation of linear piezoelectricity [3, 4], which describes a quasi-static linear relationship between applied electric field and generated

stress. The linear piezoelectric constant along the main axis is a key parameter in the specification of piezoelectric actuators and provides a good approximation for the input-to-output gain in open-loop operations if the frequency and range are low.

However, as the demand for range and driving frequency increases for today's applications, we are faced with major nonlinearity inherent in piezoelectric materials, in particular hysteresis, which results from ferroelectric phase transitions of dipole domains in piezo actuators. It leads to severe positioning errors if not properly modeled and compensated. Voltage-driven piezo actuators, especially "soft" ones designed to achieve a longer range, can have hysteresis as much as 15% of the total travel.

Piezoelectric actuators display significantly reduced hysteresis when driven by charge instead of voltage [5], because polarization (charge/area) is directly related to charge [6]. However, despite many recent advances in the design of charge amplifiers [7], the implementation complexity and cost of such techniques limited their application. No commercial charge amplifiers that can drive the stages at the same range and frequencies as a voltage driver are yet available from leading piezoelectric actuator manufacturers. Hysteresis compensation and high-bandwidth tracking control under voltage-driven conditions remains both challenging and important.

1.2 Literature Review

1.2.1 Piezoelectricity

Piezoelectricity, discovered by the Curie brothers in 1880, is the fundamental property that enables piezoelectric materials to be used as sensors and actuators. The prefix "piezo-" is derived from the Greek word "piezein" — "to press." [1] The term itself summarizes the effect: electric charge generation under applied pressure or stress. When used for sensing, this direct effect produces voltages that can be measured when stress is applied.

[1] Webster's New World Collegiate Dictionary, 4th Ed.

Piezoelectric actuators produce displacements by means of the converse piezoelectric effect, which generates strains and displacements under an applied electric field. It needs to be distinguished from simple electrostriction, which is common to all dielectric materials, including piezoelectric materials. Under electrostriction, dielectric materials are polarized almost linearly along the external electric field. No remnant strain remains when the external field is removed [8, 9].

The strain generated from converse piezoelectric effect is mostly irreversible. It comes from the spontaneous polarization of the dipole domains in piezoelectric materials. Below the Curie temperature, these domains have two stable configurations. When the external field is large enough to overcome the energy barrier between the two states, dipole domains that are not aligned with the external field will switch to the opposite state. Strain generated from this effect is much larger than that of the electrostriction, therefore most piezoelectric actuators are manufactured to exploit this property. Unfortunately, it is also the source of hysteresis in such actuators.

The combined effect of electrostriction and converse piezoelectricity constitutes the highly nonlinear response we observe in piezoelectric actuators. When these actuators are used at very low strain levels, the input-output relationship is dominated by the reversible polarization and is almost linear. In this case, the classical constitutive equation of linear piezoelectricity is a widely accepted standard [3]. When driven at much higher strain levels, the hysteresis effect dominates and requires much more complicated models.

1.2.2 Hysteresis Compensation

Hysteresis is also a Greek name. Its origin, "hysterein," means to lag behind [10]. Systems with hysteresis do not return to the same output level when the input reverts to a previously applied value at steady state. While the input-output map of a hysteresis loop looks similar to the phase-shift observed in the response of a linear dynamical system, the phenomenon is unrelated to phase delays; it persists when the

input frequency approaches zero. For piezoelectric materials, the output depends on the polarization of the dipole domains that are reoriented by the external field. The "lag" is a direct result of the bi-stability of domains.

Hysteresis models of piezoelectric actuators can generally be categorized into two classes [11, 12]: "Physical" models based on domain level physics, often derived from thermodynamics laws or statistical mechanics, and purely phenomenological models. The term "physical" is a bit of a misnomer here, as no physical equations can describe the domain dynamics of piezoelectric materials well enough. Many phenomenological modifications and assumptions are necessary even for a single domain [4].

Physical Models

Physical models are derived from the balance of free energy at the lattice or domain level. They provide good approximations for the dynamics of single crystal piezoceramics since the entire bulk is a single domain [4,9]. For polycrystalline piezoceramics, an ensemble of domain level dynamics is needed, with a separate set of parameters for each subset of domains [13]. They cannot be computed in real time even for a small number of domains. Since almost all piezo-actuators are made of polycrystals to have a longer usable range, physical models are unsuitable for control design.

A subclass of these models, sometimes called "meso-scopic" parameterized models, are derived from the same principles of statistical mechanics at the domain level, but the models are parameterized by the distribution of coercive fields measured at the macroscopic level [14]. Though the models are too complicated and nonlinear for real-time control, they provide valuable insight to the origin of hysteresis loop shapes in an actuator.

Seelecke defines an effective electric field for a domain as the difference between the externally-applied electric field and the internal field from its neighboring domains. Domains switch alignment when the effective electric field overcomes the coercive

field inherent to each domain. If we consider a single domain alone, which has equal and opposite coercive fields, the domain with the weakest coercive fields will switch first in both directions, which means the ascending and descending curve should be symmetric. The internal field from the neighboring domains, however, provides a nonlinear bias field as the polarization changes, causing asymmetry in the hysteresis loops. While such an interpretation may not be physically true, it is a useful one that agrees with experimental observations within the limited range of the actuator. It also motivates a friction-inspired model that will be detailed in the next chapter.

Phenomenological Models

Phenomenological models are purely based on the observed hysteresis. They are not limited to the description of piezoelectric hysteresis. In fact, many of the popular models are applied first to magnetic materials or friction induced hysteresis. Such models include the Duhem model, Maxwell's model, the Preisach model, their variants, and many others [15,16]. Some of them use simple curve fitting techniques with either polynomial or special functions [17,18]. Though not physically based, they are easy to implement and provide very good approximations for simple input profiles. However, they are not necessarily easy to identify and do not usually provide enough accuracy when used for static inverse compensation.

Preisach Models An important class of models are the Preisach model and its variants, which approximates the hysteresis with a set of relay operators that switch at different input levels. Frenec Preisach first applied this model to hysteresis in magnetic materials in 1935 [19]. The distribution of switching thresholds, called the Preisach distribution function or the Everett function, can be approximated by known functions or an interpolation of experimental data.

Mayergoyz's encyclopedic book on hysteresis [20] has been the definitive source for the Preisach model since its first edition in 1991. For a more concise and recent presentation, Szabo et al. have an easy-to-follow summary of the scalar model and its

identification procedures [21]. Smith's book on models of smart materials also contains a good introduction on the basic Preisach model, though it's used in a different interpretation in later chapters for his energy models [22]. Further development and solutions for special types of distribution functions can be found in [23–25].

The Preisach model is very successful in capturing the basic properties of piezoelectric hysteresis due to the natural analogy between the relays and the physical domains of piezoelectric materials. Therefore it is commonly used for static feedforward compensation when dealing with low frequency trajectories [26]. Memory effects and minor loop closure, observed in piezoceramics, are automatically satisfied by the Preisach model.

However, it is not without disadvantages: (i) a large set of quasi-static experiments are required to build a look-up table, (ii) the typical static model is only accurate for a low and narrow frequency range, and (iii) the inversion becomes difficult when piezoelectric dynamics due to broad spectrum of domain-switching time constants are included [9]. It is therefore not a good choice for high bandwidth real-time motion control.

Models with Non-local Memory

Preisach models, or any models that are summations of basic hysteretic elements, have inherent non-local memory. Non-local memory can also be incorporated into hysteresis models by explicitly keeping track of all reversal points in hysteresis loops.

Bashash and Jalili model the hysteresis as an input nonlinearity [27, 28]. Observing the similarity between minor-loops and their parent-loops, minor-loops are constructed with scaled and shifted portions of the major loop. The ascending branch and descending branch of the major loop are approximated with special functions of the input voltage. For specific implementation, both exponential functions and polynomials up to the 3rd order have been used. The model is then inverted and used as a static feedforward. While they are easy to use, curve-fitting models give little

insight into the structure of the hysteresis and require complicated loop experiments to identify the scaling and shifting factors needed for minor-loops.

Takács used a similar technique to model ferromagnetic hysteresis. His model, called the $T(x)$ model, centers around the function $T(x) = A_0 x + B_0 \tanh(C_0 x)$, which describes the ferromagnetic saturation effect [18]. Even though Takács's model is entirely phenomenological, the $T(x)$ function essentially describes the anhysteretic curve in ferromagnetic materials, which is conceptually similar to the cumulative distribution function of internal field in Smith and Seelecke's model for ferroelectric materials. However, their similarity ends there. All minor-loops in Takács's model are described using scaled and shifted versions of the $T(x)$ function, which is completely phenomenological.

Models with Local Memory Only

With no memory of the loading history, these models cannot fully describe the hysteresis in piezoelectric actuators. Many of them originate from friction research. Some are rate-independent and potentially applicable to simple piezo hysteresis loops, such as the Duhem model, the Bouc-Wen model, the Dahl model for pre-sliding friction, and the Bliman-Sorine model. The others are rate-dependent and general enough to model stick-slip friction that are not observed in piezo hysteresis, such as the LuGre friction model. A more thorough review of friction models can be found in an excellent survey article by Olsson et al [29].

1.2.3 Dynamic Modeling and Control Design

Creep Dynamics and Resonance Dynamics

The domain-switching dynamics are characterized by a broad spectrum of time constants. In a step response, the dynamic process is manifested as a slow drift following a quick initial jump. This drift is almost always modeled separately as the

creep dynamics. It is either considered negligible [12] or compensated in a feedforward loop [30], even though its dynamics is largely within the bandwidth of typical applications and should be considered the dominant dynamics, whereas the stage resonance dynamics is often much higher and canceled by notch filters. Such modeling oversight is quite understandable, because the frequency response for piezo actuator stages is usually obtained at very small output amplitude to avoid distortion from hysteresis, therefore not showing the dynamics of domain-switching.

Resonance dynamics typically includes the first vibrational mode of the actuator stage and is commonly modeled as a second order linear system [31]. For piezo actuator stages with a larger mass and more than one degrees of freedom, the lowest few vibrational modes are often close in frequency and need to be included in the model for better performance [32].

Controller Design

To compensate the hysteresis effect and achieve higher positioning accuracy, almost all existing schemes attempt to model and invert the hysteresis. The inverted input is used as a feedforward signal, and the inversion error and other plant dynamics are compensated using feedback control.

Ge and Jouaneh used the Preisach model and PID feedback [26], and more recently Basash and Jalili used a special curve-fitting model and sliding mode control [31], just to name a few. Since their hysteresis model is identified from either quasi-static inputs or inputs with a narrow frequency band and applied statically, it is difficult to improve the tracking error for high frequency motion.

Dynamic inversion based on online adaptation has also been attempted by many researchers. The problem is made simpler when the trajectories are periodic or repetitive, because the dipole domains that will switch in the next cycle will be similar, so the loop shape remains almost identical. In [33], a set of relays similar to those of the Preisach model are used, and the set of parameters for the relays are adapted online,

but their method is limited by the requirement of periodicity and monotonicity in the trajectory and is only valid for operations of very low frequency.

Also based on properties of the Preisach model, Leang and Devasia designed an iterative learning controller (ILC) and avoided the offline identification of Preisach relay parameters [34, 35]. Their approach yields excellent final tracking accuracy, but works only for very slow trajectories that satisfy input-output monotonicity on individual Preisach loop branches and takes many cycles to converge.

Cruz and Hayward likened the hysteresis to a phase delay and uses a tuned phaser to reduce hysteresis [36]. It does not require identification of the hysteresis but works only for single-frequency trajectories. It also needs to be tuned whenever a different operating frequency is applied, which greatly limits its usefulness. The model is also inherently flawed because hysteresis is not really a phase delay. In addition, other nonlinear piezoelectric effects such as the slow drifting [35] and the broad spectrum of domain switching time constants [9] are not accounted for in all these methods.

1.2.4 Recent Advances

It will be 4 years after my research was finished when this dissertation is finally submitted in 2014. During this time, the field of hysteresis modeling and piezoelectric actuator control has continued to evolve. The following survey brings the literature review up to date with recent advances.

System Design and Driving Methods

Piezoelectric actuators can be driven by voltage, current or charge drivers. Voltage drivers are most common despite having the most hysteresis, whereas piezoelectric actuators driven by charge are largely free of hysteresis.

Charge can be measured in a voltage-driven system by inserting a capacitor in series with the actuator, even though the range will be reduced unless the driving voltage is increased correspondingly, because the actuator and the capacitor will have the

same charge and similar voltage across them. Minase et al. compared voltage, charge and capacitor insertion methods for driving piezoelectric actuators in a comprehensive review [37]. Instead of measuring charge, Ishikiriyama and Morita measured the change in permittivity, which has the same benefit of being linear to strain with little hysteresis [38].

Salah et al. used charge feedback for position control [39]. Huang et al. used a switched capacitor charge pump [40]. Zhang et al. used a charge driver and its output voltage as an additional feedback to reduce hysteresis [41], and Fleming, in a separate paper, designed such circuits [42]. The leakage current in charge drives were characterized by Sheng et al. for better compensation [43]. Current control is less straightforward than charge control, but current drivers or current feedback is much easier to implement, and it still has the benefit of bypassing the hysteresis [44].

Fleming and Leang integrated a force sensor on a piezoelectric actuator to provide force feedback [45]. In the resulting system, hysteresis is reduced, and the frequency of the zero in each pole-zero pair is always lower than that of the pole, making it much easier to achieve good damping.

Despite the progress in alternative driving hardware, simple voltage-driven systems remain the only commercially available systems with high performance.

Variants of Preisach Models

Preisach-like models remain popular, and rightfully so. Given their general nature, they will always fit when sufficiently many hysterons/operators are used, and minor-loop wipe-outs are automatically satisfied. Their high computational cost is becoming less of an issue on new hardware. Iyer and Tan demonstrated the inverse compensation of a Preisach model on an FPGA (Field Programmable Gate Arrays) device where the inverse operators are calculated and summed in parallel [46].

Preisach models are not limited to symmetric hysteresis, even though they are most often applied to symmetric hysteresis loops. Asymmetry can be incorporated

by using asymmetric hysterons and/or weighting functions. Jang, Chen and Lee used a Preisach-model feedforward with a PID feedback loop on a piezoelectric actuator with asymmetric hysteresis [47]. Jiang et al. (not to be confused with Jang) modeled the asymmetric hysteresis with a modified Prandtl-Ishlinskii model [48]. In Chapter 2, we show how asymmetry can be introduced through a shaping function without using Preisach models or modifying the basic hysteresis model itself.

Peng and Chen combined the classical Preisach hysteresis inverse with H_2-optimal control [49]. Liu (Lei) et al. used an SVD-based method to identify Preisach parameters when the dicretization level is low and the corresponding least-squares problem becomes ill-conditioned [50]. The identified Preisach model is then used with a PI controller for scanning control [51]. Minase et al. identified the Preisach hysteresis model and creep parameters using an unscented Kalman filter [52]. Al Janaideh et al. proposed an analytical generalized Prandtl-Ishlinskii model inversion for hysteresis compensation [53]. They and Li applied the results to a stop-operator-based Prandtl-Ishlinskii model in the compensation of hysteresis for a piezoelectric actuator [54]. Though theoretically novel, their results provide limited benefit in experimental performance, as hysteresis inversion is only part of the motion tracking problem.

Edardar, Tan and Khalil were not the first to use a Prandtl-Ishlinskii hysteresis inverse with sliding-mode control, but they were the first to analytically choose the coefficient of the sliding-mode components based on inversion error bounds [55, 56]. They went on to use singular perturbation to analyze the behavior of a fast linear system preceded by a hysteresis operator, which has been a common model structure for piezoelectric actuators [57]. Esbrook and Tan also performed harmonic analysis to evaluate the Fourier series of the outputs of hysterons subject to sinusoidal and sawtooth signals [58].

The Maxwell model is a superposition of first-order linear systems, as opposed to the Preisach model, which is a superposition of static operators such as switch and play. Liu (Yanfeng) et al. used fractional-order Maxwell models to directly

incorporate creep dynamics into the model [59]. They also preshape the trajectory using the linear plant dynamics to reduce feedforward error [60].

Non-Preisach Models

Bashash and Jalili produced some of the best results in controlling a single piezoelectric actuator before their focus shifted to 3-dimensional systems. They proposed a simple constitutive model of hysteresis with minor loops and designed adaptive sliding-mode feedback controllers to suppress the error of the feedforward model [61]. Similar results using adaptive sliding-mode control (but with different hysteresis models) were also published by Huang, Tan and Lee [62]. After demonstrating its effectiveness on a one-dimensional actuator [63], Bashash and Jalili applied their robust adaptive approach to coupled parallel flexure actuator stages [64]. Jalili's monograph on piezoelectric-based vibration control contains a comprehensive review of their results and related work [65].

Cao and Chen used the discrete form of Duhem model and ARMA-based identification of its parameters [66]. The Bouc-Wen model was used by Rakotondrabe as hysteresis feedforward [67]. Liu, Chang and Li designed model-reference adaptive controllers around a hysteretic system described by the Bouc-Wen model and showed its effectiveness on a piezo-positioning stage [68]. Li and Xu used adaptive sliding mode control with perturbation estimation assuming a Bouc-Wen-like hysteresis model [69].

Li and Xu also used Dahl-model based hysteresis compensation in the positioning control of piezoelectric actuators on an XY manipulator [70]. This may be the only recent reference in which the Dahl model is used. Their work was focused on single loops and made no extensions to the Dahl model to capture more complicated loops. Our results using a modified Dahl model that predicts minor loops are discussed in Chapter 2.

For single-frequency tracking, Gu and Zhu approximated the hysteresis combined with the dynamic phase lag by ellipses [71, 72], which is similar in concept to the earlier phaser approach by Cruz-Hernandez and Hayward [36].

Compensation without Hysteresis Models

For complex but periodic trajectories, especially those encountered in surface scanning, iterative and repetitive controllers can effectively achieve high accuracy without using explicit hysteresis models. The early work by Leang, Zou and Devasia showed good results using iterative learning control (ILC) [73, 74]. The same approach was also used by Liu et al. at around the same time [75].

Inversion-based feedforward control and iterative control (IIC) approaches continued to be actively developed by Zou's group. Wu and Zou quantified the bound of the feedforward error and used it in the design of an H_∞ robust feedback controller [76]. Yan, Zou and Lin showed excellent tracking performance of their IIC controller in scanning a pentagram pattern [77]. The same approach was later applied to 3-dimensional positioning by Yan, Wang and Zou [78]. Wang's dissertation in 2013 provides the most recent and complete exposition of their results [79].

Besides being explicitly modeled or iteratively canceled, hysteresis has also been treated simply as an unknown disturbance. Yi, Chang and Shen used a disturbance observer to compensate for hysteresis [80]. Liaw and Shirinzadeh modeled the hysteresis nonlinearities of a piezo flexure stage as multiplicative uncertainties that are functions of the position and adapted the parameters along with a sliding-mode robust controller [81].

Gu et al. designed a robust adaptive control framework around a backlash-like hysteresis model preceding a linear plant [82]. Their approach occupies a middle ground between complete hysteresis model inversion methods and (non-repetitive) model-less methods, and their experimental performance is comparable to most of the recent results.

When driven at low strain, the hysteresis effect is less prominent and the (sometimes very low-frequency) resonant dynamics of an actuator stage can be dominant in motion tracking. For this scenario, Aphale et al. presented the modeling of an XY stage and the design of an H_∞-based controller that achieves fast and accurate tracking of low-amplitude triangular signals [83].

Final Remark

The research results in this dissertation remain relevant and competitive. New hardware design did not eliminate the need for hysteresis compensation, the hysteresis control paradigms remain largely unchanged, and experimental performance saw very little improvement despite the theoretical advances.

1.3 Objective

Existing modeling and control schemes for piezoelectric actuators require complex offline identification for hysteresis compensation. They overlook the domain switching dynamics as the dominant dynamics in the case where the resonance dynamics is fast and much beyond the closed-loop bandwidth.

In this dissertation, we will show the dominant dynamics of a piezoelectric actuator, develop a control-oriented model that captures the major characteristics of the dominant dynamics and yet simple enough for adaptive dynamic compensation, and design adaptive robust controllers to achieve high performance motion tracking for piezoelectric actuators. A hysteresis compensation model will also be developed with an emphasis on easy implementation and identification.

1.4 Organization

The rest of the dissertation is organized as follows.

Chapter 2 details the development of a model for hysteresis compensation with an emphasis on easy implementation and identification. Experimental results show excellent static linearity with hysteresis compensation.

Chapter 3 presents the development of a control-oriented model for a piezo-stage with negligible resonance dynamics and the corresponding design of an adaptive robust controller. Experimental results are provided to demonstrate the performance of the controller both with and without hysteresis feedforward.

Chapter 4 shows that tracking performance can be further improved under the same framework when the desired trajectories are periodic. For such trajectories, the unknown but periodic portion of the dynamics can be approximated by a superposition of harmonic basis functions. Experimental results show a decreasing trend in tracking error as more harmonic terms are used.

Finally, Chapter 5 concludes the dissertation with a summary of contributions and lists some of the problems from the current research for future research.

The results are presented in this order to be more logical, but they were not obtained in the same order over the course of the research. The dynamic model and the adaptive robust controller in Chapter 3 were obtained before the various methods of hysteresis compensation were developed. The harmonic approximation in Chapter 4 was done next, and the hysteresis "friction" model in Chapter 2 happened last after repeated failures to find a model that's simple and useful.

2. MODELING AND COMPENSATION OF HYSTERESIS

2.1 Model Structure

Piezoelectric actuators or stages are commonly modeled as a system with linear dynamics preceded by a hysteresis nonlinearity, and a hysteresis inverse is constructed to cancel the hysteresis [12, 30] (Figure 2.1a). While such a formulation has been shown to work for many point-to-point or single-loop trajectories, it inherently assumes that the hysteresis depends only on the input and domain polarization happens instantaneously. Neither of these assumptions are physically true.

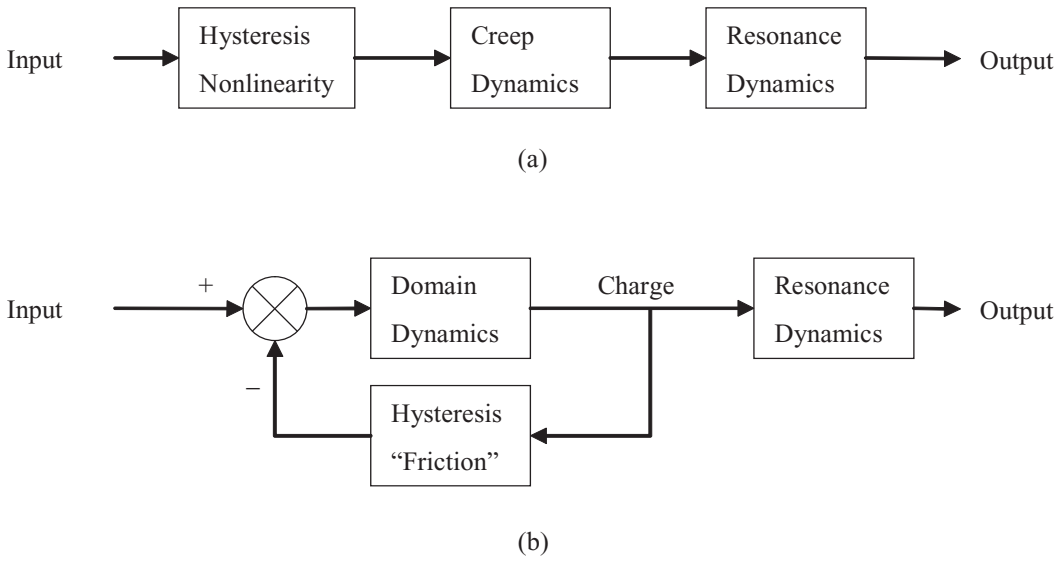

Figure 2.1. Model structure. (a) Common model structure; (b) Proposed model structure.

In this dissertation, the hysteresis is modeled as a feedback friction-like nonlinearity that depends on the output of the actuator (Figure 2.1b). Such a formulation is motivated by the following factors:

1. The "memory" of the actuator depends on the domains that have switched in the past. Only domains that have switched under the applied voltage affect the branching of hysteresis in the future. As we will show in the next chapter, the switching of domains is far from instantaneous. The number of domains that have switched directly relates to the charge output of the actuator.

2. In semi-physical models such as Seelecke's energy-based model, the energy barrier of domains is a function of the polarization that corresponds to the distribution of domain barriers, which predicts the barrier that needs to be overcome for the domain that hasn't yet switched [13]. This is essentially a rate-independent relationship from polarization/charge output to a corresponding barrier that causes hysteresis.

3. The hysteresis in a piezoelectric actuator, when viewed from output to input after removing a linear slope, is remarkably similar to hysteresis caused by pre-sliding friction (Figure 2.2). Pre-sliding friction only depends on displacement and has been extensively studied in the past. A simple friction model may be a natural place to start in modeling the piezoelectric hysteresis as a feedback nonlinearity.

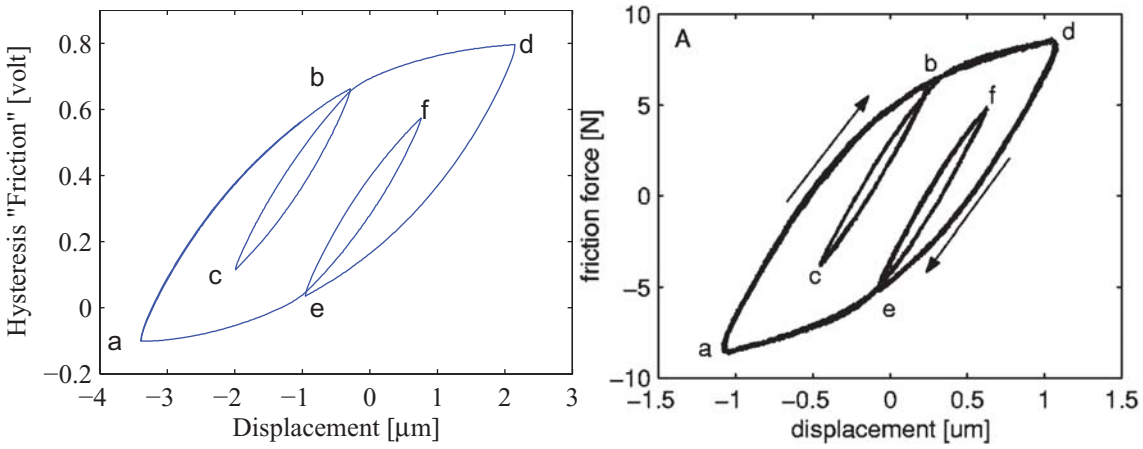

Figure 2.2. Left: Piezoelectric hysteresis; Right: Typical pre-sliding friction. (Reprinted with permission from [84]. Copyright 2004, American Institute of Physics.)

2.2 Hysteresis in a Piezoelectric Stack Actuator

2.2.1 The Big Picture

The hysteresis loop we observe in stack actuators is only part of a much larger hysteresis loop, sometimes referred to as the "butterfly" loop due to its shape (Figure 2.3). During manufacturing, piezoelectric actuators are subject to a large external electric field while being cooled down from above the Curie temperature, such that all domains are aligned with the external field. The piezo amplifier normally does not allow a large negative voltage to be applied to the actuator. When depoled to the other direction, the actuator may produce negative displacement with an increasing input, making it useless for actuation.

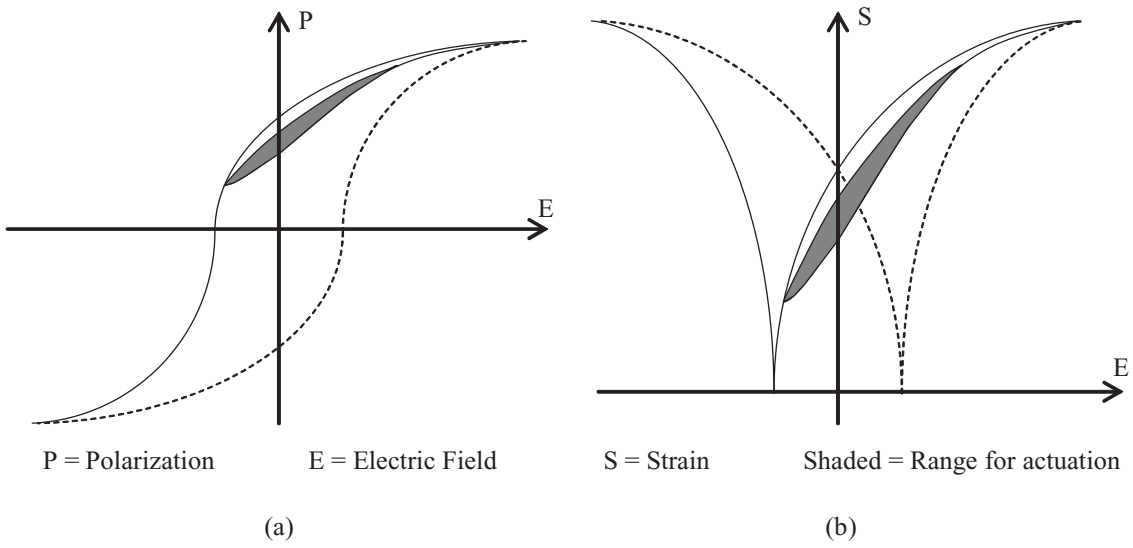

Figure 2.3. Actuator range within a full "butterfly" hysteresis. (a) Polarization; (b) Strain.

2.2.2 Experimental Setup

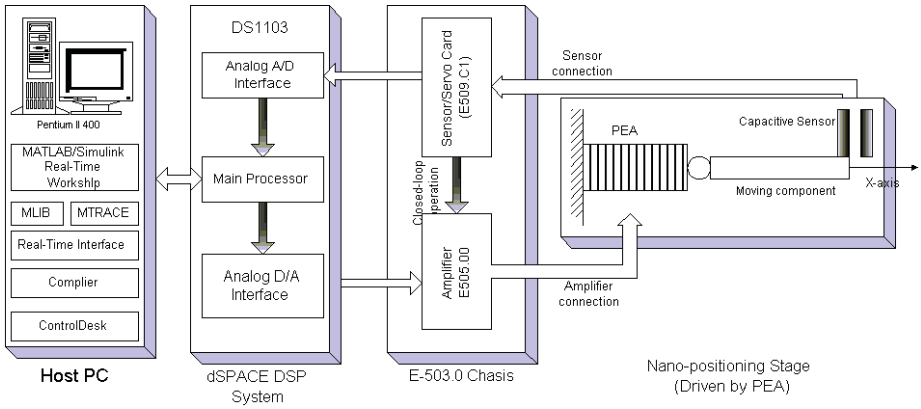

Figure 2.4. Experimental setup.

The experimental setup consists of four parts (Figure 2.4): the positioning stage with integrated capacitive displacement sensor, a low-voltage driving amplifier, a dSPACE DS1103 controller board, and a generic PC for dSPACE ControlDesk. The base of the stage is screw-mounted on a massive vibration isolation table to minimize induced vibrations in the supporting structure. The capacitive sensor signal has a noise level of ± 0.003 volt, which corresponds to ± 3.6 nm of displacement. The driving amplifier (Physik Instrumente E501.00) has an output range of -20 to 120 volts and a bandwidth above 2kHz, a decade higher than our desired frequency range, so its electrical dynamics are considered negligible. It amplifies the control voltage signal from the dSPACE board by a factor of 10. All input signals in the following results are the pre-amplified control voltage from dSPACE.

2.2.3 Full-loop Initialization

Piezoelectric actuators have non-local memory. The output from a starting position depends on all the minor loops that had been formed before the actuator settled into this position. To obtain consistent results in experiments, we need to initialize the actuator by driving it with the full range of available voltage, so that it starts from a known outer-loop after all minor loops have been wiped out.

Since the pre-amplified input is limited to [-2V, $+10$V], we first ramp up to $+10$V and then come back to -2V before starting the experiments. This is demonstrated in Figure 2.5, where the stage output measurement saturates at 12μm when the input exceeds roughly 7.5V, because the analog input on dSPACE has been saturated, even though the actuator can move beyond 12μm. After the initialization loop, the 2nd loop is generated by ramping up to $+7$V. The actuator reaches -3μm at -2V and 11μm at $+7$V. We consider this 14μm loop the largest usable loop and define it as the major loop that no subsequent experiments should exceed.

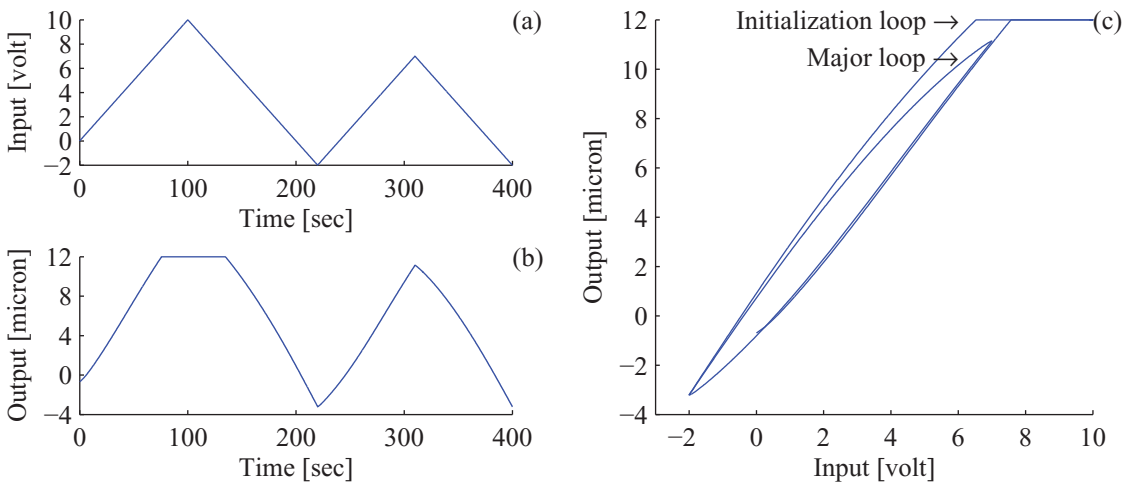

Figure 2.5. The initialization loop and the major loop.

The experiments intended to show the true hysteresis need to run with pseudo-static input signals to exclude dynamic phase lag. The input rate is set to 0.1V/s, at which the actuator consistently forms closed hysteresis loops with negligible creep, and it is slow enough not to excite the resonance dynamics of the actuator and stage.

Throughout the dissertation, the following terminologies will be used:

Major-loop The largest loop formed by the actuator within its usable range.

Minor-loop Any loop smaller than the major-loop

Outer-loop The larger of two connected loops

Inner-loop The smaller of two connected loops

2.2.4 Asymmetry in Loop Shape

Though the small hysteresis loop in Figure 2.2 is highly symmetric around its center, the hysteresis loops at a bigger scale warp to the right and become asymmetric as the actuator goes toward the upper end of its range (see the major loop in Figure 2.5.c). The distortion is similar to strain-hardening and can be interpreted in several

ways. For instance, Smith and Seelecke modeled this phenomenon as a distribution of internal field exerted by the switched domains to their opposing neighbors [14] [13]. As the strain[1] increases, the internal field increases nonlinearly as the majority of domains switch into one direction, causing the effective domain barrier and therefore the shape of the loops to become asymmetric. A similar phenomenon is observed in magnetic materials and modeled by the mean field theory [86]. The flexure springs in the stage may also exhibit a small amount of hardening but is likely not the main source, as the same distortion is seen in standalone actuators that are not mounted on flexure stages [13].

2.3 Hysteresis Modeling

Based on observations in the previous section, we now separate the hysteretic input-output relationship of the actuator into several apparent components (Figure 2.6). The effective barrier for the next switching domain, as the displacement changes, is a combination of both the switching barrier inherent to the domain and the counteracting internal field from its neighbors, if we adopt the modeling perspective of Smith and Seelecke. Though we cannot measure and isolate the two, the domain barrier is 2-fold symmetric and hysteretic, whereas the internal field is nonlinear but not hysteretic.

After removing a linear component from each, the remaining domain barrier will be highly similar in shape to pre-sliding friction described by the Dahl friction model, as we have shown in Figure 2.2. The nonlinear curve from the internal field depends only on the excess of domains in the positive direction, therefore it can be captured by a function of displacement, which can be fitted using a high-order polynomial.

[1]The distribution function in Seelecke's energy model is actually between electric field and polarization, not strain. Even though the relationship between polarization and strain/displacement is nonlinear and generally considered quadratic [22], the relationship is one-to-one in the actuator range. The nonlinear relationship can be safely lumped to the shaping functions defined later in the chapter. In addition, Georgiou and Mrad have shown that in the range typically used for actuation, the relationship between polarization and strain is highly linear (Figure 1 in [85]).

The two linear components are combined into the overall linear gain of the system. In the next sections, we will model and identify each of these components.

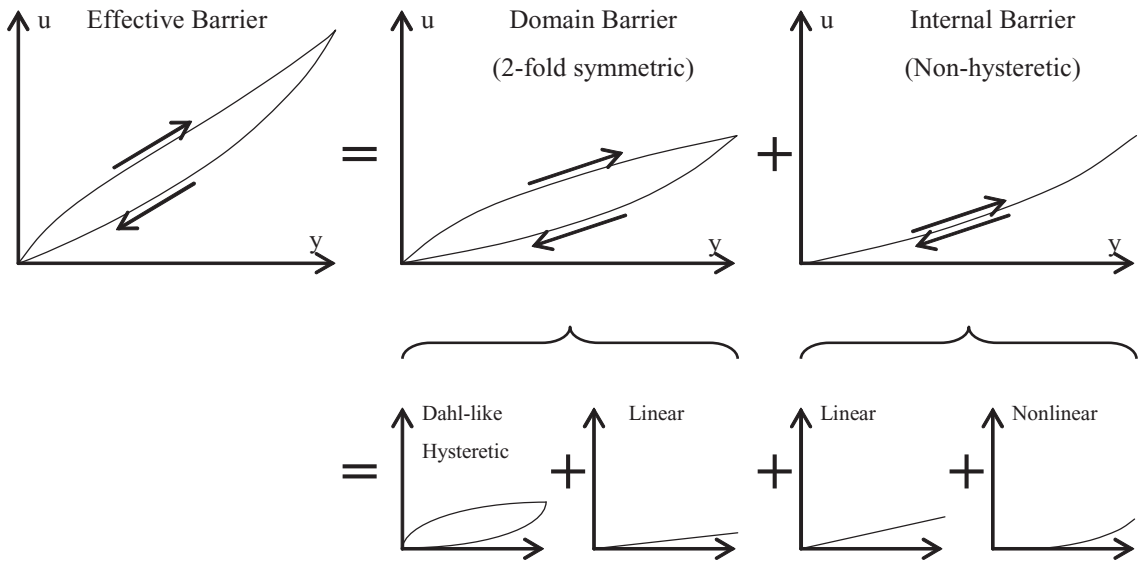

Figure 2.6. Components of a piezoelectric hysteresis.

2.3.1 The Dahl Friction Model

In 1968, Philip R. Dahl of the Aerospace Corporation developed a model for pre-sliding friction in ball bearings [87]. Inspired by the stress-strain relationship in solid mechanics, Dahl proposed a differential equation in displacement,

$$\frac{dF}{dx} = \sigma \left(1 - \frac{F}{F_c}\text{sgn}(v)\right)^{\alpha}, \tag{2.1}$$

where F is the friction force, x the displacement, σ the stiffness coefficient, F_c the Coulomb friction force, v the velocity, and α the exponential order that determines the shape of the curve. If we set the initial condition such that $|F_0| < F_c$, F will converge to F_c at steady-state as displacement goes towards infinity. Dahl's model can also be expressed in the time domain by observing that

$$\frac{dF}{dt} = \frac{dF}{dx}\frac{dx}{dt} = \frac{dF}{dx}v = \sigma \left(1 - \frac{F}{F_c}\text{sgn}(v)\right)^{\alpha} v. \tag{2.2}$$

We prefer the displacement form (2.1), because the friction force is only a function of displacement and the sign of velocity, not the value of velocity. When $\alpha = 1$, equation (2.1) is a simple 1st-order linear filter in displacement.

Bliman and Sorine defined the total distance covered by the relative motion in space, $s = \int_0^t |v(\tau)|\, d\tau$, as their new "time" variable and extended Dahl's model to a higher-order linear model in the space variable s [88, 89]. Their model has the form

$$\begin{aligned} \frac{dx_s}{ds} &= Ax_s + Bv_s \\ F &= Cx_s, \end{aligned} \tag{2.3}$$

where the velocity in space $v_s = \frac{dx}{ds} = \text{sgn}(v)$. Adopting Bliman and Sorine's space variable and defining the friction state as z, we can rewrite the 1st-order Dahl's model in a concise and normalized form

$$\begin{aligned} \frac{1}{\sigma}\frac{dz}{ds} + z &= \text{sgn}(v) \\ F &= F_c z, \end{aligned} \tag{2.4}$$

which clearly shows the behavior of the model — a low-pass filter in displacement with an exponential decay rate σ.

2.3.2 Enforcing Loop Symmetry

The Dahl model only forms closed and symmetric loops between two equal and opposite values of z, not arbitrary reversals. To enforce a symmetric loop between any two reversal points, we can extend the Dahl model by adding z_r, the friction state z at the last reversal, to the right-hand side of 2.4, which is equivalent to resetting z to start from zero at the reversal and assigning the previous value of z to z_r such that the output remains continuous. With the additional term, the model becomes

$$\frac{1}{\sigma}\frac{dz}{ds} + z = z_r + \text{sgn}(v), \tag{2.5}$$

whose output starts from z_r and converges to $z_r + 1$ if the displacement has reversed toward the positive direction or $z_r - 1$ toward the other.

2.3.3 Adding Non-local Memory

Equation (2.5) depends only on the last reversal point and has no memory of the past reversals. If the displacement continues after a loop has been closed, the model will not follow the parent loop (Figure 2.7).

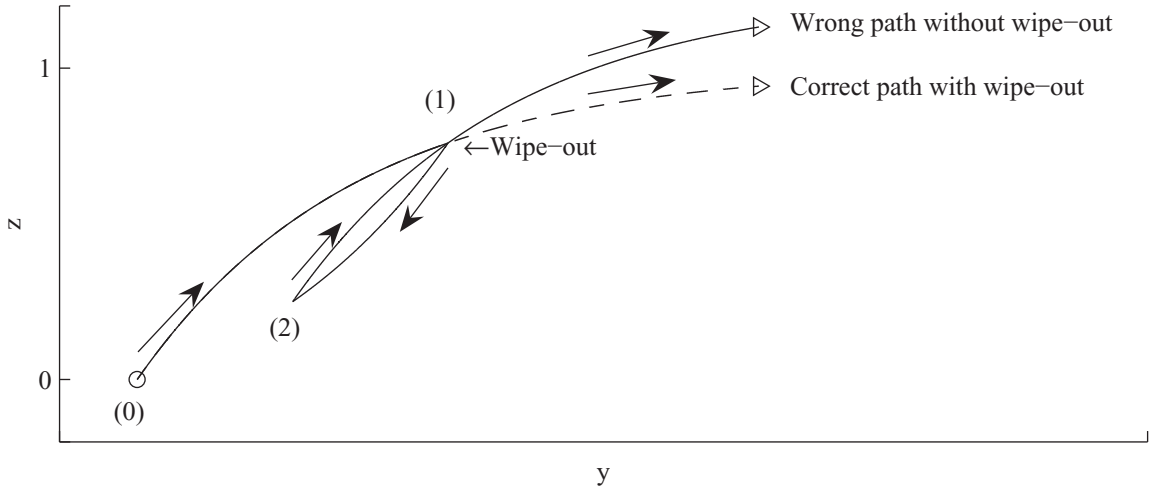

Figure 2.7. Model behavior with and without non-local memory.

To correctly wipe out a minor loop, we further extend the local memory of z_r in equation (2.5) by recording all past reversal points from the major-loop and replacing the initial value to that of the immediate parent loop whenever a loop is closed. A similar technique to implement the memory has been used in the integrated Leuven model for pre-sliding friction [90]. The final model becomes

$$\frac{1}{\sigma}\frac{dz}{ds} + z \;=\; z_i + \mathrm{sgn}(v), \tag{2.6}$$

where z_i is the initial condition for the i-th reversal. The reversal index i grows with each reversal that forms a new minor loop (Figure 2.8). At each reversal, both y and z are added to a memory stack. After the i-th reversal, if y crosses y_{i-1}, which is the reversal point on its parent loop, i is decremented by 2, erasing both reversal points that form the minor loop, and z_i now corresponds to the initial state of the parent

loop, as if the minor loop never happened. The memory arrays are initialized to have $z_{(-2)} = 1$ at $y_{(-2)} = +\infty$ and $z_{(-1)} = 0$ at $y_{(-1)} = -\infty$, such that the model output will be bounded by a fictitious infinite major loop that cannot be wiped out.

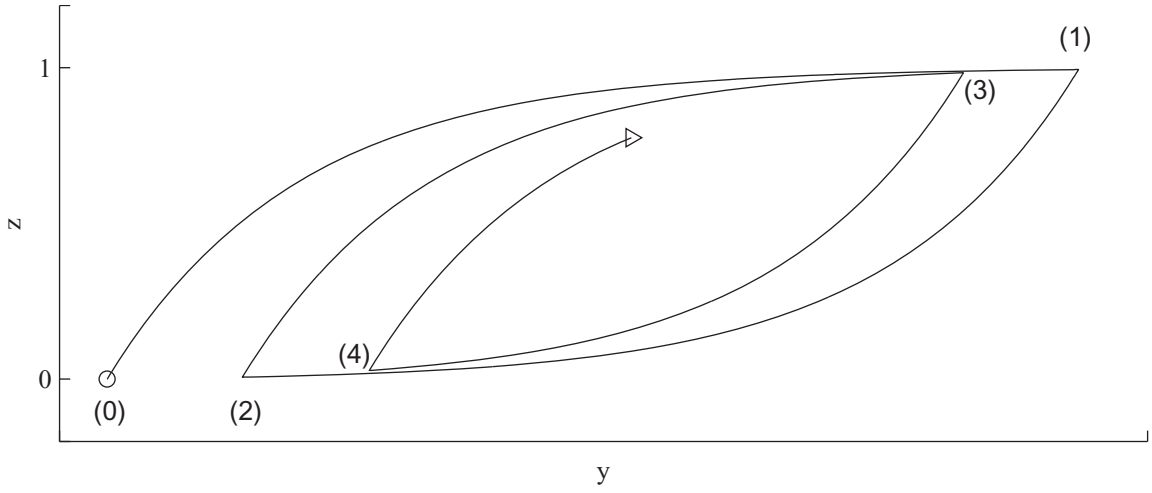

Figure 2.8. Reversal index.

2.3.4 Adding Asymmetry

In section 2.2.4, we have mentioned that asymmetry in hysteresis loops may be attributed to an internal field that increases nonlinearly with the strain output. While analytical distribution functions based on the phase fraction of the domains have previously been used to model this nonlinearity [13], we do not know the phase fraction of the actuation range, because a full depoling loop cannot be applied to the actuator.

Ni et al. observed significant hardening distortion in the restoring force of wire cable isolators and modeled it as a separate nonlinear force that adds to the output of a Bouc-Wen model as a shaping function, which is approximated by a 3rd-order polynomial [91]. For even more drastic distortions such as widening of loops at large displacement, Al-Majid and Dufour further extend Ni's approach to define enveloping functions to shape their symmetric model output [92]. Using extra shaping functions

for asymmetry keeps the core of the hysteresis model simple and easy to identify. Since the asymmetry in piezoelectric actuator loops is quite mild, a polynomial shaping function is sufficient.

2.3.5 The Final Hysteresis Friction Model

Combining the symmetric hysteresis model with memory and the shaping function, the total hysteresis friction in our system is given by

$$\begin{aligned} u_h &= u_{h_1} + u_{h_2} \\ u_{h_1} &= h_1 z \\ u_{h_2} &= \sum_{i=2}^{N} h_i y^i \end{aligned} \tag{2.7}$$

where $h_1$is the magnitude of the symmetric hysteresis friction and h_i are the coefficients of the polynomial shaping function. And the total input of the system is

$$u = \frac{1}{k} y + u_h \tag{2.8}$$

where k is a linear gain from u to y.

2.4 Parameter Identification

By the nature of our model, the outer-loop contains all the information needed for identification. To simplify presentation, the coordinates are shifted such that (u, y) start from $(0, 0)$. The hysteresis state z starts from zero and reaches z_r at the upper reversal point.

The ascening part of the loop is denoted $u_a(y)$ and the descending part $u_d(y)$, both spanning the same range of y. the non-hysteretic part of the input $\frac{y}{k} + \sum_{i=2}^{N} h_i y^i$ is shared by both curves, whereas the hysteretic component u_h is different. A polynominal order $N = 4$ has been picked because the next term improves the fit by less than 0.1%.

Differentiating u by y, we have

$$\frac{du}{dy} = \frac{du_{h_1}}{dy} + \frac{1}{k} + 2h_2 y + 3h_3 y^2 + 4h_4 y^3 \tag{2.9}$$

where the term $\frac{du_{h_1}}{dy}$ depends on the direction of the curve.

$$\begin{aligned} \frac{du_{h_1}}{dy} &= h_1 \frac{dz}{dy} \\ &= h_1 \frac{dz}{ds} \cdot sgn(v) \\ &= \begin{cases} \sigma h_1 - \sigma u_{h_1} & \text{along } u_a(y), \\ \sigma h_1 + \sigma u_{h_1} - \sigma h_1 z_r. & \text{along } u_d(y). \end{cases} \end{aligned} \tag{2.10}$$

In the ascending direction, the derivative becomes

$$\begin{aligned} \frac{du_a}{dy} &= \sigma h_1 - \sigma u_{h_1} + \frac{1}{k} + 2h_2 y + 3h_3 y^2 + 4h_4 y^3 \\ &= (\sigma h_1 + \frac{1}{k}) + \sigma(-u_a) + (\frac{\sigma}{k} + 2h_2)y \\ &\quad +(\sigma h_2 + 3h_3)y^2 + (\sigma h_3 + 4h_4)y^3 + (\sigma h_4)y^4 \end{aligned} \tag{2.11}$$

and in the descending direction,

$$\begin{aligned} \frac{du_d}{dy} &= \sigma h_1 + \sigma u_{h_1} - \sigma h_1 z_r + \frac{1}{k} + 2h_2 y + 3h_3 y^2 + 4h_4 y^3 \\ &= (\sigma h_1 + \frac{1}{k} - \sigma h_1 z_r) + \sigma(u_d) + (-\frac{\sigma}{k} + 2h_2)y \\ &\quad +(-\sigma h_2 + 3h_3)y^2 + (-\sigma h_3 + 4h_4)y^3 + (-\sigma h_4)y^4. \end{aligned} \tag{2.12}$$

The unknown parameters can now be identified from the sum and difference of these two derivatives. The parameters σ, h_2, h_3, h_4 can be identified through least squares from the sum

$$\frac{d(u_d + u_a)}{dy} = \sigma(u_d - u_a) + h_2(4y) + h_3(6y^2) + h_4(8y^3) + (2\sigma h_1 + \frac{2}{k} - \sigma h_1 z_r), \tag{2.13}$$

and the remaining parameters h_1 and k can be obtained, again by least squares, after substituting the known parameters identified from (2.13) into the difference

$$\frac{d(u_d - u_a)}{dy} = \sigma(u_d + u_a - 2h_2 y^2 - 2h_3 y^3 - 2h_4 y^4) - \frac{\sigma}{k}(2y) - \sigma h_1 z_r. \tag{2.14}$$

The numerical values for all the parameters are

$$\begin{aligned} k &= 1.961 \\ \sigma &= 0.356 \\ h_1 &= 1.292 \\ h_2 &= 3.12 \times 10^{-3} \\ h_3 &= 1.36 \times 10^{-4} \\ h_4 &= 9.04 \times 10^{-6} \end{aligned}$$

2.5 Model Validation

All parameters in our model are identified using the outer-loop alone. If the proposed model is valid, the model should correctly produce all loop shapes and wipe out minor-loops when the initial conditions are matched. Unless otherwise noted, all experiments in this section are initialized to start from -2V after a full-loop initialization. The hysteretic friction u_h predicted by the model is subtracted from the true input to show the compensated input-output relationship.

2.5.1 First-order Reversals

First-order reversal loops are the most similar to their parent loops and often used for hysteresis modeling and identification. Both lower reversals and upper reversals are compensated well by the proposed hysteresis model (Figures 2.9 and 2.10). Without compensation, the hysteresis in the actuator causes a difference of up to 1.9 micron at the same input, which is 14% of the actuation range. When the predicted "friction" is subtracted from the input, the input-output relationship becomes highly linear with a residue of 0.13 micron, which is less than 1% of the actuation range.

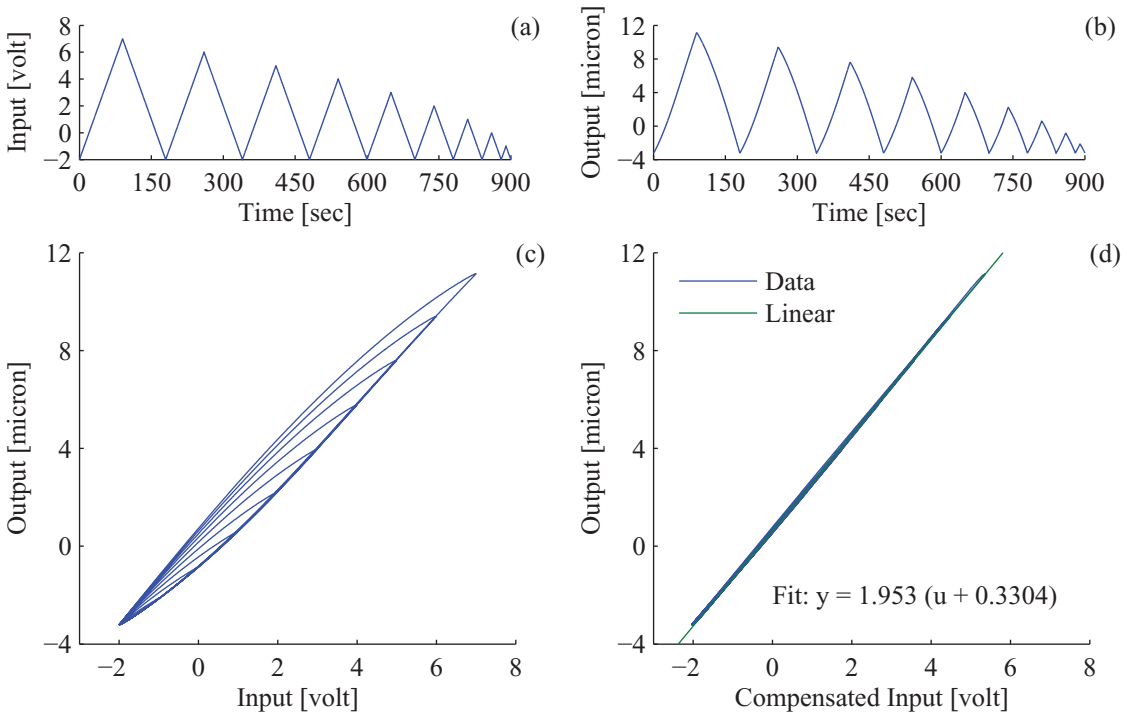

Figure 2.9. 1st-order reversals from the ascending branch of the major-loop. (a) Input; (b) Output; (c) Hysteresis before compensation; (d) Hysteresis after compensation.

2.5.2 High-order Reversals with Decreasing Amplitude

In this experiment, the input alternates with decreasing amplitude to form higher-order reversal curves. The most inner reversal in Figure 2.11 corresponds to an 8th-order minor-loop. Again, the input-output relationship becomes linear with the same gain with a residue of 0.12 micron when we subtract the predicted hysteresis from the input.

2.5.3 Wiped-out Minor Loops

Figure 2.12 shows a more challenging trajectory that contains 3 minor loops on each side of major loop. When the actuator returns from a minor-loop, once it gets

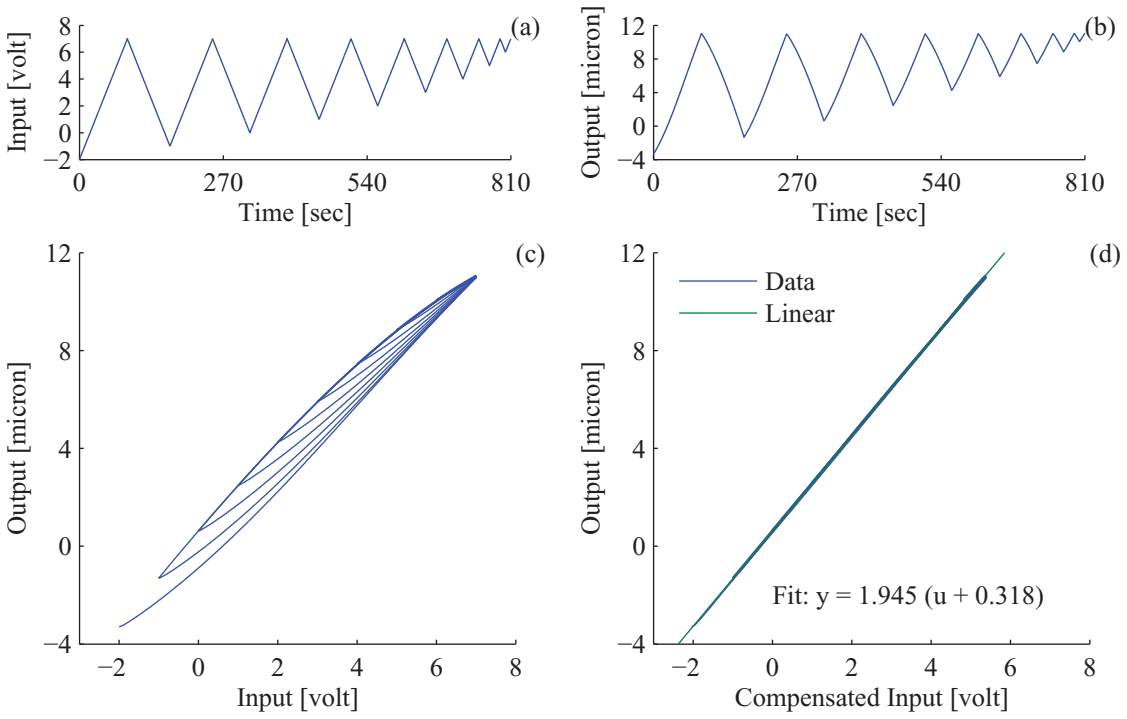

Figure 2.10. 1st-order reversals from the descending branch of the major-loop. (a) Input; (b) Output; (c) Hysteresis before compensation; (d) Hysteresis after compensation.

past the previous reversal point on the parent loop, the output continues on the parent loop as if the minor loop never happened. As we can see in Figure 2.12.d, the model correctly predicts all the minor loops.

2.5.4 Unmatched Initial Conditions

In practice, a full-loop initialization cannot always be done before the desired trajectory. If no information on the previous loading history is available, the hysteresis model will not correctly predict the hysteresis until all minor loops within the trajectory are wiped-out. However, once the output trajectory has reached both extrema, all minor-loops previously contained between them will be wiped out, after which only a constant offset remains.

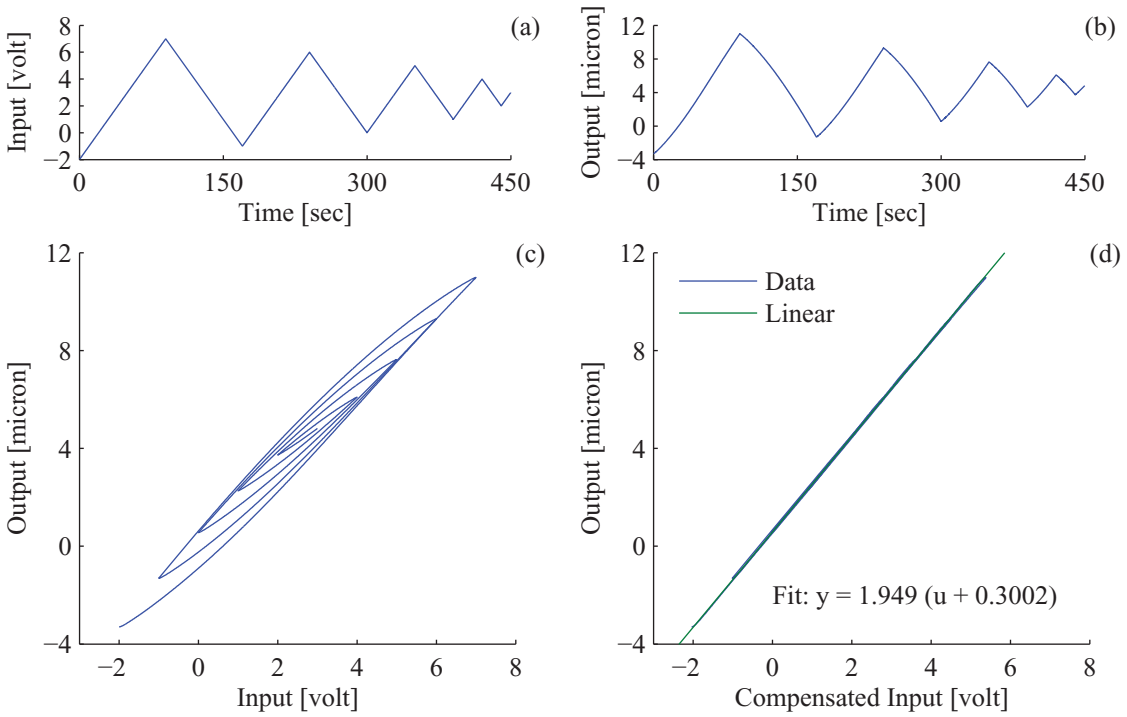

Figure 2.11. Minor-loops with decreasing amplitude. (a) Input; (b) Output; (c) Hysteresis before compensation; (d) Hysteresis after compensation.

The experiment in section 2.5.2 is repeated from zero input without the initialization loop (compare Figure 2.13). The model starts with no knowledge of previous minor-loops and fails to cancel the hysteresis until the maximum displacement is reached. Since the normalized friction state is always bounded, the prediction error never exceeds the width of the original hysteresis loop. Being an uncertainty with a known bound, it can be attenuated in subsequent controller design. It also has no effect on steady-state error because it becomes a constant after a finite time when the the largest loop has been formed. Note that the constant offset in this experiment is much different from that of the correctly initialized one.

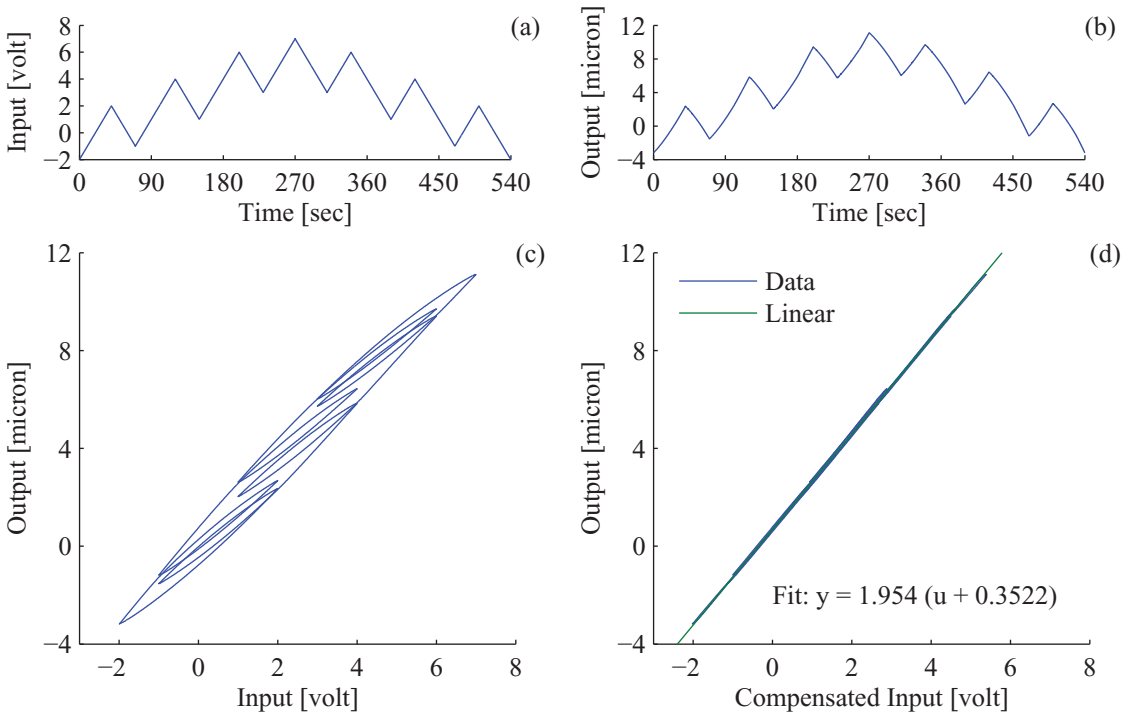

Figure 2.12. Minor-loops branching from both sides of the major loop. (a) Input; (b) Output; (c) Hysteresis before compensation; (d) Hysteresis after compensation.

2.6 Feedforward Compensation of Hysteresis

The model and linear gain identified so far can be used to control the actuator in open-loop. We start with a pseudo-static triangular trajectory, which has a ramp rate of 0.2 micron per second and a span of 10 microns. This is close to the input rate at which we drove the actuator to collect data for hysteresis identification. At such low speed, the identified model is expected to have an almost perfect fit.

The tracking error is less than 0.11 micron everywhere, which is 1.1% of the actuation span. After the first ascending curve, the subsequent segments are all within a 0.05-micron band, suggesting that the actuator is settling into a very repeatable loop whose hysteresis is well described by the model. A linear fit of the curve y vs. y_d in Figure 2.14.b has a slope of exactly 1 and an offset of only 23 nm.

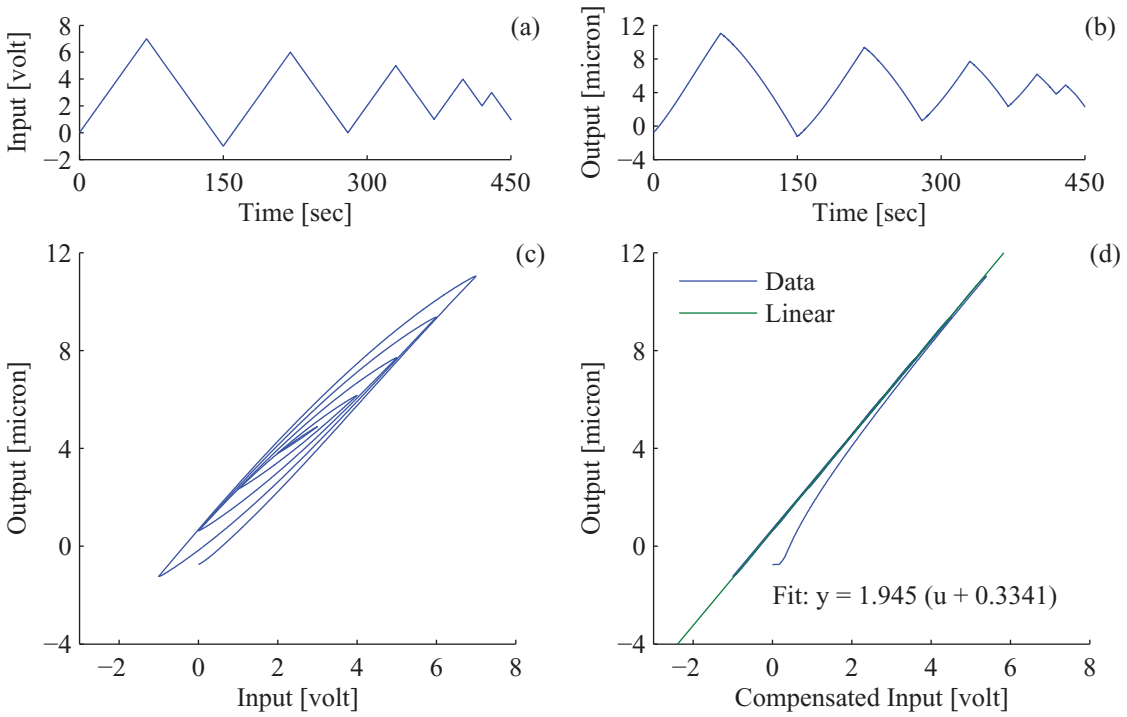

Figure 2.13. Compensation with unmatched initial conditions. (a) Input; (b) Output; (c) Hysteresis before compensation; (d) Hysteresis after compensation.

As the ramp rate increases, tracking error starts to grow. At 2 microns per second (Figure 2.14.d), the largest tracking error is 0.235 micron during part of the first ascending curve, after which the input-output relationship again remains very linear and consistent in both directions — $y = 0.965y_d + 0.166$ with a maximum residual of 0.043.

When the ramp rate reaches 40 microns per second (Figure 2.14.f), equivalent to a 2-Hz triangular wave with 10 microns peak-to-peak, the error has become too large for the feedforward controller to be useful by its own, but the compensated loop after the first ascending curve is still fairly linear with $y = 0.92y_d + 0.37$ with a maximum residual of 0.059. The hysteresis, when defined as the difference between the ascending output and descending output, is still within 0.11 micron.

Most of the error comes from the fixed feedforward gain, which is no longer a good fit for faster trajectories. The hysteresis between ascending curves and descending curves is quite constant except where the actuator reverses direction. Constant offsets are easily compensated by any closed-loop controller with integral control, and an unknown but constant input gain can be compensated by adaptive control. These will be addressed in the next chapter.

Running the initialization loop is essential for open-loop feedforward control. Figure 2.15 shows that the error and offset become as big as the original hysteresis even for the slowest speed if we skip the initialization and start from an unknown loop state. However, the initialization may not be necessary if a closed-loop controller is used to attenuate the error from the mismatched hysteresis model.

2.7 Implementation and Interpretation of the Dahl Hysteresis Model

The hysteresis model has been implemented in C from a direct discretization of equation 2.6 using forward difference. Such a straightforward implementation has the benefit of extremely low computational cost, but numerical accuracy will suffer if the displacement becomes too large in each step of integration, which happens when either the sampling frequency is too low or the trajectory speed is too high. The trajectories in our experiments are not fast enough to cause numerical problems.

If numerical accuracy must be guaranteed regardless of step size in displacement, we can use the analytic solution of equation (2.6) instead of integrating the hysteresis model along the desired trajectory. For example, if the actuator reverses direction at position y_i with hysteresis friction z_i and now goes in the positive direction with $y > y_i$, the new inner loop is calculated as $z = z_i + (1 - \exp(-\tau * (y - y_i)))$.

In other words, the extended Dahl model is nothing more than fitting an exponential decay function to the outer hysteresis loop, if it hasn't been obvious. The higher-order variants, such as the Bliman-Sorine model, are more general by allowing a superposition of exponential and sinusoidal functions. It is entirely possible to

achieve the same accuracy using polynomials or combinations of other special functions.

The advantage of the Dahl model thus lies not in its accuracy but in its brevity of expression and simplicity of implementation. We can identify its parameters using least squares, because the differential model is linear in both states and parameters. The solution function, which is a common exponential function, enforces the shape of hysteresis we desire without much special handling that may be necessary for other functions. Even though other functions may fit equally well, they cannot be calculated simply by integrating linearly along the reference trajectory.

These remarks are more personal preferences than engineering requirements. However, the mathematical form of the model should be simple when the hysteresis encountered in the actuator is simple. A general model that will fit everything but cannot be computed in a short sampling period is not a good model in application.

2.8 Conclusion

The Dahl friction model, with the addition of reversal history and a shaping function, correctly predicts the hysteresis observed in a common Piezoelectric stack actuator. All parameters of the new model can be identified from the outer-loop alone. The hysteresis is reduced from 14% to less than 1% of the actuation range. When initial conditions are unmatched, the modeling error remains bounded within the largest uncompensated hysteresis. Once the actuator goes through the largest loop in the trajectory that wipes out all unknown minor loops, the modeling error becomes a constant that can be compensated by feedback control, which will the the subject of Chapter 3.

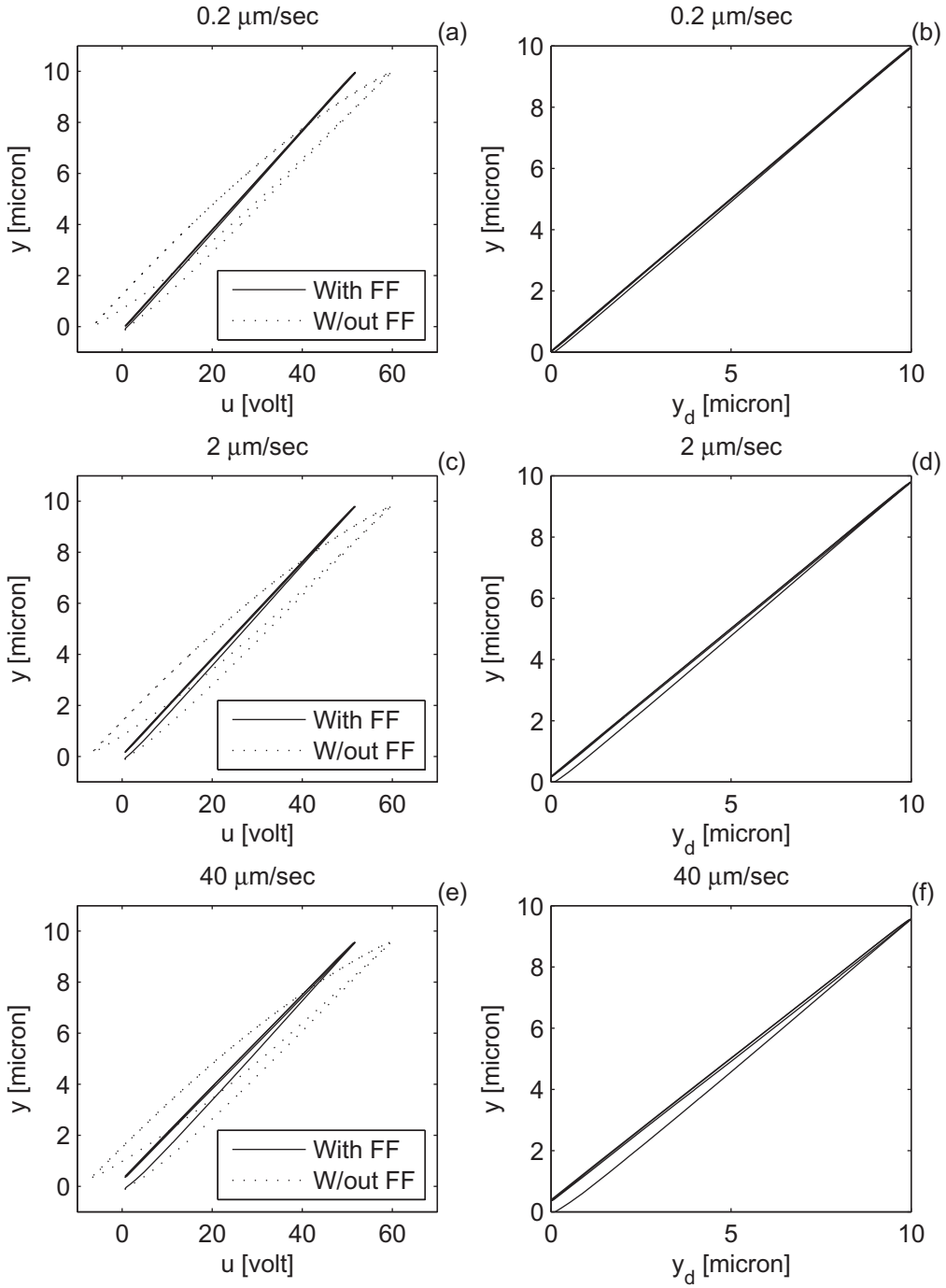

Figure 2.14. Actuator response with feedforward compensation is very good at low speed but degrades at higher speed. (a-b) Output vs. input and reference at 0.2 μm/sec; (c-d) Output vs. input and reference at 2 μm/sec; (e-f) Output vs. input and reference at 40 μm/sec.

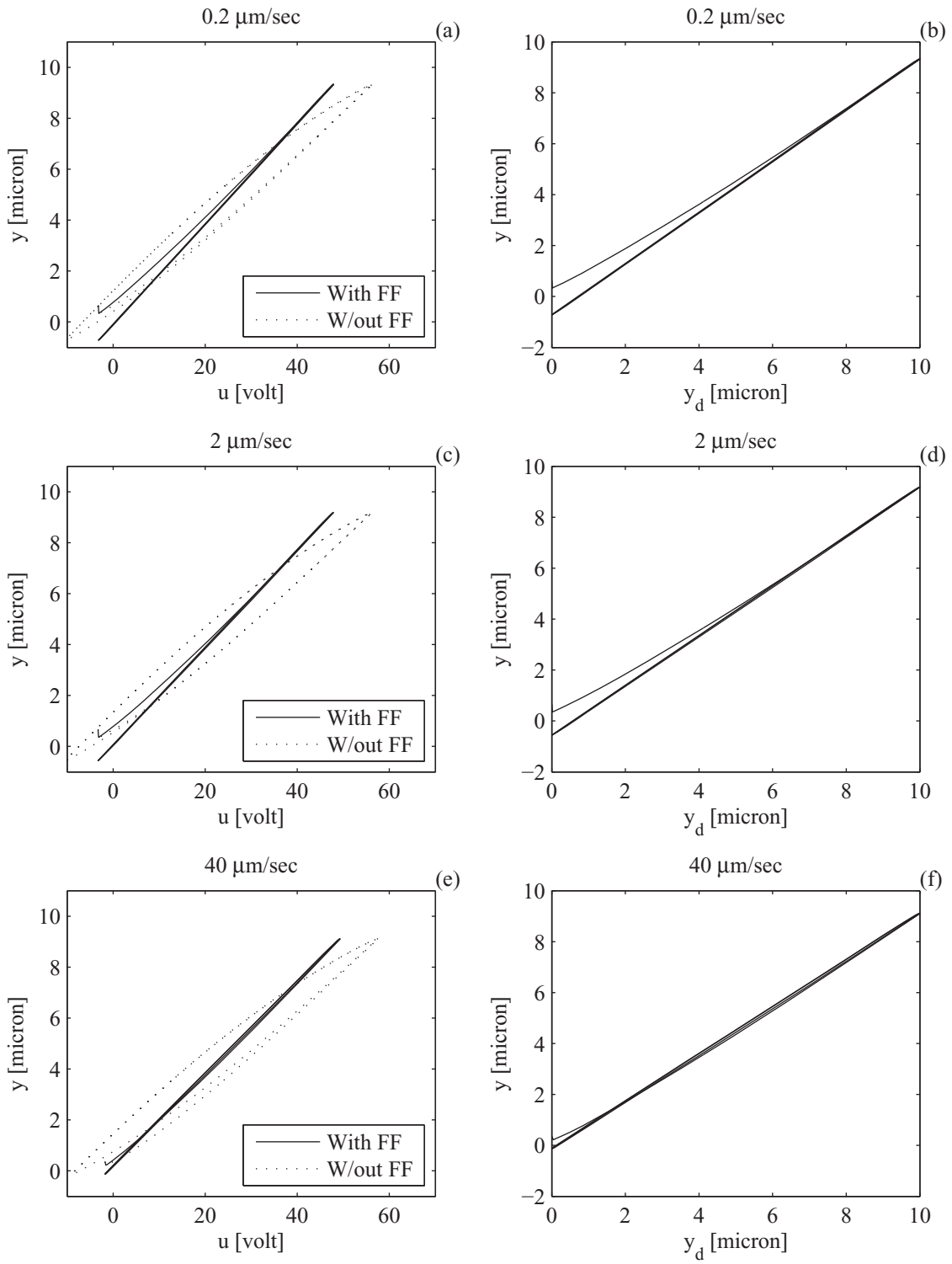

Figure 2.15. Actuator response with feedforward compensation but no initialization will have significant error but will still be linear after the first upper reversal point. (a-b) Output vs. input and reference at 0.2 μm/sec; (c-d) Output vs. input and reference at 2 μm/sec; (e-f) Output vs. input and reference at 40 μm/sec.

3. DYNAMIC MODELING AND FEEDBACK CONTROL OF A PIEZOELECTRIC ACTUATOR WITH NEGLIGIBLE RESONANCE DYNAMICS

In Chapter 2, we have developed a hysteresis model that can be used for feedforward control. In this Chapter, we will identify the dominant dynamics of the actuator and design a feedback controller that adapts the gain, rejects an input disturbance, but assumes no structural knowledge of the hysteresis. They will then be combined for the best performance.

In the frequency range where only the piezoelectric dynamics dominate, high tracking accuracy is possible through an integration of adaptive robust control strategy with a control-oriented modeling of nonlinear piezoelectric effects. Specifically, the fast and slow dynamics of the total stage displacement due to various piezoelectric effects including the rate-dependent hysteresis nonlinearity, the drifting, and the broad spectrum of domain switching time constants are first identified.

With the control structure in mind, a simple first-order nonlinear model with unknown parameters and bounded disturbances is used to capture the essence of the fast and slow dynamics. An adaptive robust controller (ARC) is designed to effectively compensate for the effect of unknown model parameters and bounded disturbances, which provides an on-line adaptation-based dynamic model compensation that minimizes tracking errors. Experimental results demonstrate the effectiveness of the approach even without adding hysteresis feedforward [93,94]. When the hysteresis friction model is added as a disturbance feedforward, the uncertainty from hysteresis is further reduced to achieve excellent tracking performance.

3.1 Introduction

In this chapter, we will take a holistic approach to the modeling and control of a piezoelectric positioning stage. Specifically, we will significantly reduce the complexity of the model needed to capture all the nonlinear piezoelectric effects for precision motion control designs through the use of advanced adaptive robust control strategy [95–97] and on-line parameter adaptation. We recognize that, though the time constants of domain switching dynamics have a broad spectrum and cause various nonlinear effects (e.g., the slow drifting phenomenon in [35] can be considered as the effect of the domain switching dynamics having large time constants), in the frequency of interest, the piezoelectric dynamics can be separated into the fast and slow dynamics.

In terms of controller design, the effect of slow dynamics can be captured by an unknown slow-changing bounded disturbance and the fast dynamics can be approximated well by a first-order nonlinear dynamics with unknown static gain and time constant driven by a hysteresis function of the input. By further approximating the hysteretic function via simple linear functions with unknown gain and bounded approximation error, we obtain a first order nonlinear model linearly parameterized by four unknown parameters only, which is sufficient to capture the major characteristics of various piezoelectric hysteresis nonlinearities for controller designs.

Adaptive robust control (ARC) [95–97] is then applied to compensate for the effect of unknown parameters and the bounded slow-varying disturbances effectively through the use of a discontinuous projection based on-line parameter estimation method. The uncompensated unknown nonlinearities and the effect of transient parameter estimation errors are further attenuated by fast robust feedback embedded in the ARC design [98]. As a result, the time consuming identification of the exact hysteresis piezoelectric nonlinearities is avoided while excellent tracking performance is achieved.

3.2 Dynamics of a Piezoelectric Stage System

3.2.1 The Positioning Stage System

The system to be controlled is a commercially available nano-positioning stage driven by a piezoelectric actuator with an integrated capacitive position sensor, produced by Polytec PI (Model number P753.11C). The unit has a total measurable travel of 12 μm when it is driven by an applied control voltage of -2 to 10 volts (amplified by 10 through the amplifier). We will limit our experiments to a range within $\pm 2.4\mu$m, as the stage requires very high power to operate at its full range at high frequencies, which causes potential saturation in the driving amplifier. Since the goal of this paper is higher accuracy at high frequencies, we prefer a higher available operating frequency to a longer range of travel. In this range, the actuator already exhibits a very noticeable amount of hysteresis.

Piezoelectric actuators have non-local memory because different portions of dipole domains switch under different loading history [9, 20]. To ensure that all our experiments start from a comparable internal polarization state, we apply the same loading history before each of the experiments for modeling. The control input slowly ramps up (0.1V/s) from 0 to 10V, then down to -2V and holds at -2V for 10 seconds (Figure 3.1), before any of the following experiments are started. By doing so, almost all of the domains that can switch in the available input range of -2 to 10V would have been switched back to a negative state at the terminal input of -2V. The initial positions after such initialization are within tens of nanometers of each other and considered practically the same.

The hysteresis caused by dipole domain switching is often considered rate independent at low velocities, as in most of the Preisach-based models which assume the domains switch instantaneously and the same domain will switch at the same input level. *The assumption that the same domain will switch at the same input level may be reasonable*, as demonstrated by the steady-state responses of the stage under two different inputs with the same final value, a pseudo-static (0.1V/s) ramp input from

0 to 2V, and a step input from 0 to 2V, shown in Figure 3.2. In the step response, the stage does not immediately jump to the same output level that the ramp input reaches at 2V, but slowly and eventually converges to almost the same output level after 20 seconds. The convergence of outputs shows that steady-state outputs of the stage for various monotonic inputs with the same steady-state input magnitude but different ramping-up rate is indeed rate-independent. The portion of dipole domains that will eventually switch will be the same if the prior loading history and the next steady-state monotonic input level are the same.

However, *the switching of the domains cannot be assumed to occur instantaneously and independent of input loading rate*. As a consequence, rate-dependent hysteresis loops will occur in reality, as shown in Figure 3.3 where the hysteresis loops corresponding to the responses of the actuator to a 4 volt peak-to-peak triangular input at three different input loading rates are plotted. The loops start from almost the same initial positions but are very different from each other in terms of the subsequent hysteresis loops. The hysteresis loop for the triangular input with the slowest input rate of 0.1V/s forms a closed loop during the entire duration of the experiment, while the other two change with time though eventually converge to some steady-state loops. As seen from Figure 3.3, the hysteresis loop for the input rate of 10V/s does not reach the same output level as the loops with slower input rates do when the input reaches 2V.

As will be seen from the frequency responses of the stage obtained using small amplitudes of sinusoidal input signals in subsection 3.2.2, for frequencies up to 300Hz studied in this paper, the phase lags caused by the resonance and amplifier dynamics of the stage are negligible. Considering that the fastest input rate used in Figure 3.3 only translates to 1.25Hz if such input is periodically applied, we can conclude that the observed rate-dependence phenomena are entirely due to hysteresis of the piezo-actuator. At higher input rates, one can expect to observe even greater differences in terms of steady-state hysteresis loops. A model that captures the rate-dependence of the hysteretic output is thus necessary for better compensation.

The experimental tests above reveal that the hysteresis of the actuator is *rate-dependent* and does not form a well-defined single loop when the input rate increases, which might be the reason why simple Preisach-based implementations are so hard to identify and work only for a low and narrow frequency range, because rate-independence, loop closure and IO monotonicity are some of the fundamental requirements of the classical Preisach models. The rate-dependence of the loops also implies that dipole domain switching, the cause of the piezo hysteresis, can not be considered instantaneous even for low input rates, which is one of the emphases of this dissertation.

3.2.2 Identification of the Plant Model

The total response of the stage consists of two major components: a fast resonance response that dominates the dynamics in the short travel and high frequency range, and a hysteretic response due to dipole domain switching in piezoelectric materials, which resembles a nonlinear relaxation process [11, 99].

Resonance Dynamics of the Stage

The frequency response for the resonance dynamics of the stage has previously been identified using a sinusoidal sweep excitation signal from $0 - 12.8$kHz [11]. The amplitude of the output is restricted to 40nm to avoid distortion from hysteresis as much as possible. The experimental bode plots remain almost identical under different input offsets (-1,0,2,3V), implying the linear nature of this dynamics (Figure 3.4). The stage has two very close resonance peaks at 5100 and 5800 kHz. Below 300Hz, there is negligible phase delay and the gain stays almost constant. Therefore, for operating frequencies in this range, the resonance and amplifier dynamics are negligible and the displacement output of the stage is entirely due to the displacement of the piezoelectric actuator. To be conservative, we limit our closed-loop bandwidth to 200Hz and our desired trajectories to 100Hz.

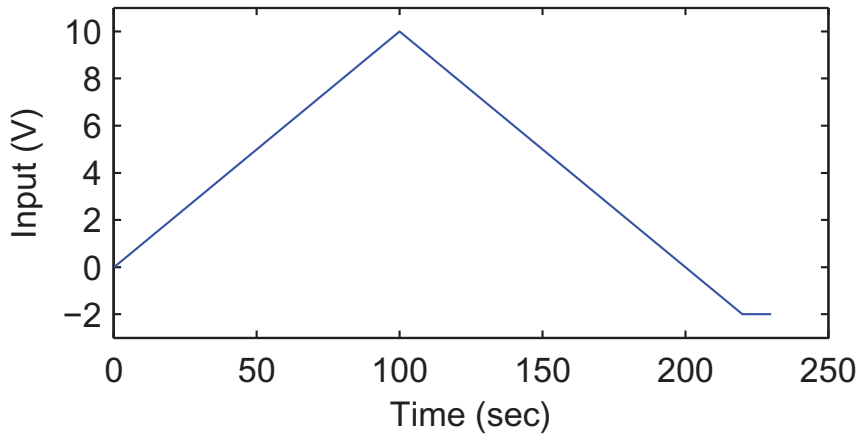

Figure 3.1. Loading history applied to the actuator before each of the modeling experiments.

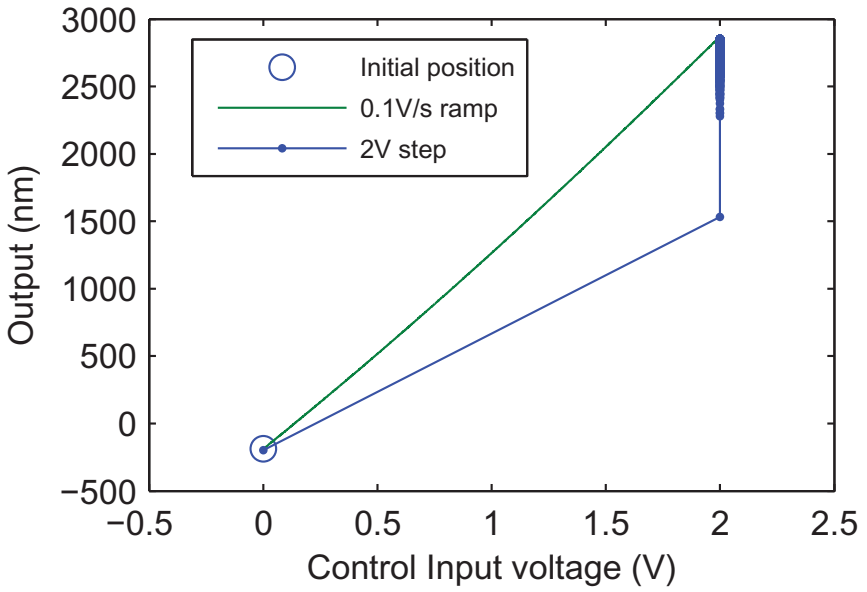

Figure 3.2. Open-loop system response to a 0.1V/s ramp input and a 2V step input, both starting from the same initial position and loading history.

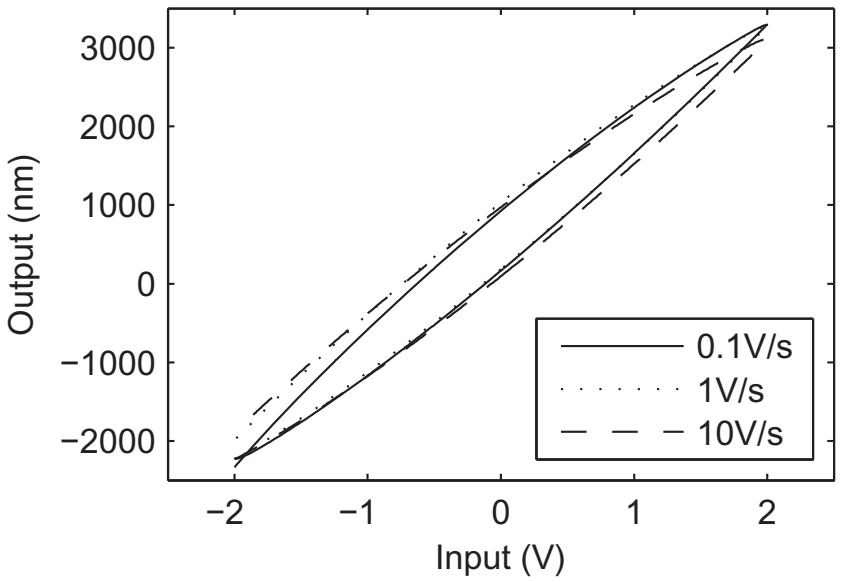

Figure 3.3. Open-loop system response to a 4Vpp triangular input at different rates, all starting from the same initial position and loading history.

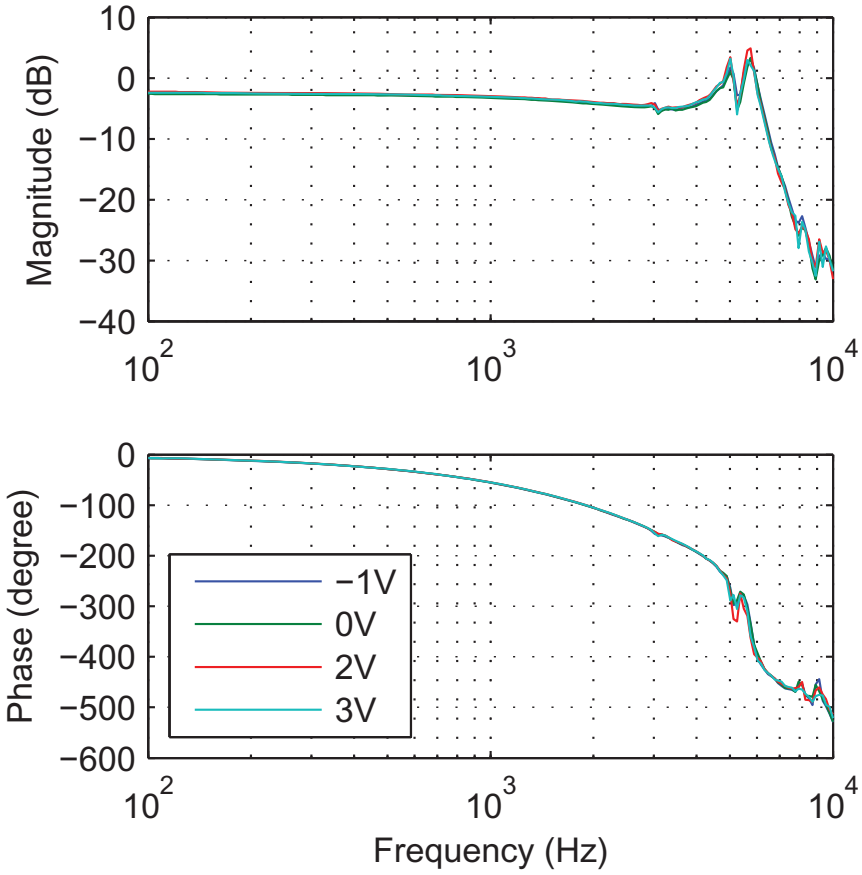

Figure 3.4. Frequency responses of the stage with small amplitude sweeping sinusoidal excitation inputs at different offsets.

Creep Dynamics

To identify the dynamics that governs the hysteretic output, we apply a 2V step input to the actuator. Figure 3.5 shows the response of the actuator over a period of 10 seconds. The resonance of the stage has been removed by a second-order notch filter and the flat response in the first 10^{-4} second is likely due to sampling and sensor delay.

After a very fast response at the beginning, the actuator output continues to drift over time. The drift rate becomes lower and lower as time progresses. This drift, sometimes called creep or relaxation, is often modeled by using a series of linear first-order systems [35], which is simple and effective, but the question is how many terms to include.

Although we can use as many terms as necessary to fit the response, we consider it unnecessary for feedback control, because (i) The drift rate may not be the same over the entire range of operation; (ii) A large number of parameters need to be identified; (iii) Uncertainties in slow, stable dynamics can be compensated very effectively by feedback control with fast on-line parameter adaptation. Modeling the system to the last bit of detail increases computational burden but provides little benefit when closed-loop control is able to compensate most of the uncertainties.

Since most of the fast stage response happens within the first 0.01 second and the control bandwidth is up to 200 Hz, we are mainly concerned with the dynamics that dominate over this period. Figure 3.6 shows the 2-volt step response in linear time domain during the first 0.005 seconds. After filtering out the resonance dynamics and accounting for time-delays due to the amplifier and the sensor electronics [11], we obtain a least squares fit of the response using only two first-order transfer functions $K_{ss}(\frac{0.82}{0.000152s+1} + \frac{0.18}{0.00236s+1})$.

Since these parameters are dependent on the input level, they are not directly used to calculate controller parameters. They serve as a motivation for our final model structure for control and provide initial estimates of the range of parameter variations

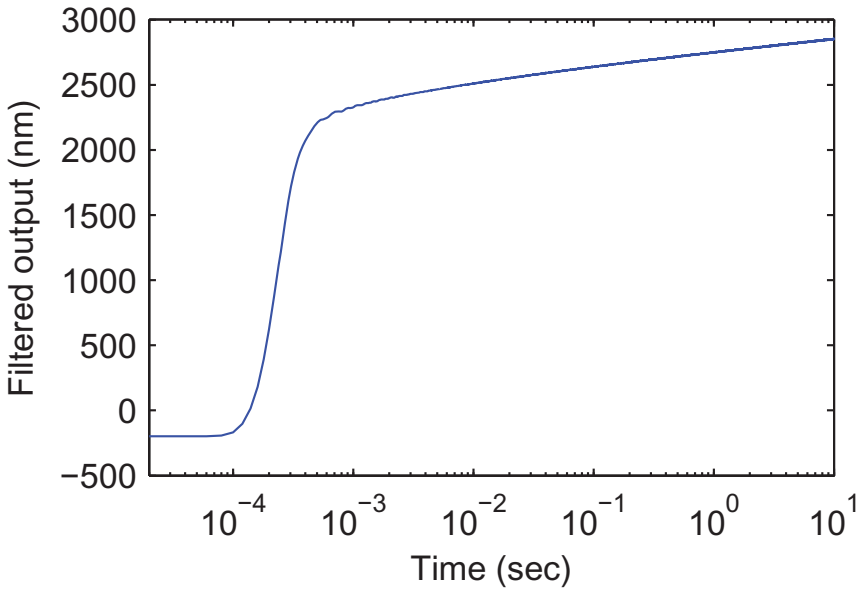

Figure 3.5. 2V step response of the stage over 10 seconds.

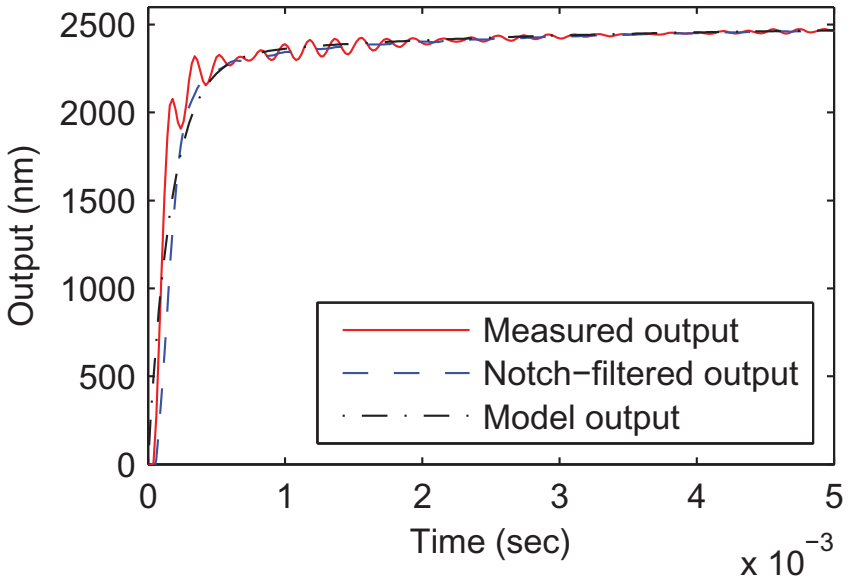

Figure 3.6. 2V step response of the stage in the first 0.005 seconds.

to be adapted. The time constant of the first dynamics, at $0.000152s$, is 2 orders of magnitude smaller than that of the second one at $0.00236s$ and far beyond our desired

bandwidth of 200 Hz. Therefore these dynamics are neglected and will be modeled as a feed-through gain. The second first-order dynamics thus become the dominant dynamics of the system within the frequency range that we consider. Based on these observations, we propose the following simple overall system model for control design

$$\begin{aligned} \tau \dot{x}_h &= -x_h + b_1 g_t(u), \\ y &= x_h + b_0 g_t(u), \end{aligned} \tag{3.1}$$

where $g_t(u)$ is a function that maps the input u to the total output of the dipole domains that will switch at steady state. The feed-through gain b_0 represents the fraction of dipole domains that switch instantaneously, and $b_1 = 1 - b_0$ is the fraction of dipole domains that do not. The state x_h captures the number of dipole domains that are switching over time, with τ being their average time constant.

3.3 Adaptive Robust Control of Piezoelectric Actuators

3.3.1 Design Model and Assumptions

The hysteresis mapping $g_t(u)$ in (3.1) is not a simple function. It changes whenever the output changes direction, as we have observed in Chapter 2, because it describes the internal state of the dipole domains and depends on the past history of actuator displacement. Therefore, we only capture the overall gain of the system and lump the rest as an unknown disturbance to be compensated by fast adaptation and robust feedback. We would like the controller to achieve decent performance on its own without any explicit hysteresis compensation. The performance will then be improved further when the unknown disturbance becomes almost non-hysteretic when we eventually use hysteresis friction feedforward together with the feedback controller.

Replacing $g_t(u)$ by the function

$$g_t(u) = k_u u + d(t), \tag{3.2}$$

the system equations are further simplified to

$$\begin{aligned} \tau \dot{x}_h &= -x_h + b_1[k_u u + d(t)], \\ y &= x_h + b_0[k_u u + d(t)]. \end{aligned} \tag{3.3}$$

The term $d(t)$ represents the time-varying mismatch between $k_u u$ and $g_t(u)$, which is bounded by the maximum hysteresis at each input level. This is easily measurable from the outer-loop in a quasi-static experiment, such as the one in Figure 3.3. The parameter k_u captures the slope of the hysteresis loop that covers the entire range of desired operation, so it depends on the desired length of travel and prior displacement, but an estimate of its range is also readily available from the quasi-static full-loop loading experiment we discussed in Chapter 2.

To put the model into the standard form for subsequent adaptive robust control design, we rewrite (3.3) by defining the state vector $\vec{x} = [x_1, x_2]^T = [y, u]^T$ and using $v = \dot{u}$ as a virtual input (also noting the identity $b_0 + b_1 = 1$)

$$\begin{aligned} \frac{1}{b_0 k_u}\dot{x}_1 &= -\frac{1}{\tau b_0 k_u}x_1 + \frac{1}{\tau b_0}x_2 + \frac{1}{k_u}[\frac{1}{\tau b_0}d + \dot{d}] + v, \\ \dot{x}_2 &= v, \\ y &= x_1. \end{aligned} \tag{3.4}$$

The unknown parameter set $\theta = [\theta_1, \theta_2, \theta_3, \theta_4]$, to be adapted online, are defined as $\theta_1 = \frac{1}{b_0 k_u}$, $\theta_2 = \frac{1}{\tau b_0 k_u}$, $\theta_3 = \frac{1}{\tau b_0}$, and $\theta_4 = d_n$, the nominal value of the term $\frac{1}{k_u}[\frac{1}{\tau b_0}d + \dot{d}]$. Equation (3.4) is now linearly parameterized in terms of θ as

$$\theta_1 \dot{x}_1 = -\theta_2 x_1 + \theta_3 x_2 + \theta_4 + \Delta + v, \tag{3.5}$$

$$\dot{x}_2 = v, \tag{3.6}$$

where $\Delta = \frac{1}{k_u}[\frac{1}{\tau b_0}d + \dot{d}] - d_n$ is the uncertain variation between the lumped discrepancy term and its nominal value. Since the hysteretic discrepancy is bounded in proportion to dipole domains that can switch in the specified input range, the domains that switch under the same input are similar, and domains do not switch infinitely fast, we can make the following practical assumption on the parameters [100], with the notation

that the relational operator "<" used hereinafter between two vectors is performed in terms of the corresponding elements of the vectors:

Assumption 3.1 *The extent of parametric uncertainties and uncertain nonlinearities is known, i.e.,*

$$\begin{aligned} \theta &\in \Omega_\theta \triangleq \{\theta :\ \theta_{min} < \theta < \theta_{max}\}, \\ \Delta &\in \Omega_\Delta \triangleq \{\Delta :\ \|\Delta\| \leq \delta_\Delta\}, \end{aligned} \tag{3.7}$$

where $\theta_{min} = [\theta_{1min}, \cdots, \theta_{4min}]^T$, $\theta_{max} = [\theta_{1max}, \cdots, \theta_{4max}]^T$, *and* δ_Δ *are all known.*

Under Assumption 3.1, the discontinuous projection based ARC design [95, 100] is applied to (3.3) to solve the robust tracking control problem. Let $\hat{\theta}$ denote the estimate of θ and $\tilde{\theta}$ the estimation error ($\tilde{\theta} = \hat{\theta} - \theta$). The parameter estimate $\hat{\theta}$ is updated through the parameter adaptation law

$$\dot{\hat{\theta}} = \text{Proj}_{\hat{\theta}}(\Gamma \tau_e), \tag{3.8}$$

where Γ is any symmetric positive definite adaptation rate matrix (for simplicity, Γ is assumed to be a diagonal matrix in the sequel), τ_e is an adaptation function to be specified later, and the projection mapping $\text{Proj}_{\hat{\theta}}(\bullet) = \left[\text{Proj}_{\hat{\theta}_1}(\bullet_1), \cdots, \text{Proj}_{\hat{\theta}_4}(\bullet_4)\right]^T$ is component-wise defined by

$$\text{Proj}_{\hat{\theta}_i}(\bullet_i) = \begin{cases} 0 & \text{if} \begin{cases} \hat{\theta}_i = \theta_{i_{\max}} & \text{and } \bullet_i > 0, \text{ or} \\ \hat{\theta}_i = \theta_{i_{\min}} & \text{and } \bullet_i < 0; \end{cases} \\ \bullet_i & \text{otherwise,} \end{cases} \tag{3.9}$$

which has the following properties [101]:

$$\begin{aligned} &\text{P1.} \quad \hat{\theta} \in \bar{\Omega}_\theta = \{\hat{\theta} :\ \theta_{min} < \hat{\theta} < \theta_{max}\}, \\ &\text{P2.} \quad \tilde{\theta}^T(\Gamma^{-1}\text{Proj}_{\hat{\theta}}(\Gamma\bullet) - \bullet) \leq 0,\ \forall \bullet\,. \end{aligned} \tag{3.10}$$

3.3.2 ARC Controller Design

Defining the difference between the plant output y and desired output y_d as the tracking error $e = y - y_d = x_1 - y_d$, the error dynamics of the system become

$$\begin{aligned} \theta_1 \dot{e} &= \theta_1 \dot{x}_1 - \theta_1 \dot{y}_d \\ &= -\theta_1 \dot{y}_d - \theta_2 x_1 + \theta_3 x_2 + \theta_4 + \Delta + v \\ &= \varphi(\vec{x})^T \theta + \Delta + v, \end{aligned} \tag{3.11}$$

where $\varphi(\vec{x})^T = [-\dot{y}_d, -x_1, x_2, 1]$. Using the standard direct ARC design [100], the following control law is synthesized, which consists of two parts given by

$$\begin{aligned} v = v_a + v_s, \quad & v_a = -\varphi(\vec{x})^T \hat{\theta}, \\ & v_s = v_{s_1} + v_{s_2} \\ & v_{s_1} = -ke, \end{aligned} \tag{3.12}$$

where v_a is the dynamic model compensation term that cancels the known dynamics for perfect tracking, and v_s is the robust control law consisting of two parts: v_{s_1} is a simple proportional feedback that stabilizes the nominal system; and v_{s_2} is a robust feedback that attenuates the effect of all model uncertainties, which is required to satisfy the following two constraints

$$\begin{aligned} &\text{C1.} \quad e[-\varphi^T \tilde{\theta} + \Delta + v_{s_2}] \leq \varepsilon, \\ &\text{C2.} \quad e v_{s_2} \leq 0, \end{aligned} \tag{3.13}$$

where ε is a positive design parameter representing the attenuation level of the model uncertainties. The constraint C1 ensures that v_{s_2} will dominate the model uncertainties coming from both parametric uncertainties and uncertain nonlinearities to achieve the guaranteed attenuation level ε, and constraint C2 ensures that v_{s_2} is dissipative and does not interfere with the parameter adaptation. Several specific forms of v_{s_2} that satisfy (3.13) are available [96, 97, 100], with one of the simplest being

$$v_{s_2} = -\frac{1}{4\varepsilon} h^2 e, \tag{3.14}$$

where $h \geq \|\theta_{max} - \theta_{min}\| \, \|\varphi\| + \Delta$. It is chosen for our experimental implementation due to its computational simplicity. With this ARC design, we have the following theoretical performance:

Theorem 3.2 *If the adaptation function in (3.8) is chosen as*

$$\tau_e = \varphi(\vec{x})e, \tag{3.15}$$

the ARC law (3.12) with the parameter adaptation law (3.8) guarantees that,

***A**. The magnitude of tracking error is bounded above by*

$$|e|^2 \leq \exp(-\frac{2k}{\theta_1}t)|e(0)|^2 + \frac{\varepsilon}{k}[1 - \exp(-\frac{2k}{\theta_1}t)], \tag{3.16}$$

where the exponential decay rate $\frac{2k}{\theta_1}$ and the magnitude of final tracking error ($|e(\infty)| \leq \sqrt{\frac{\varepsilon}{k}}$) can be directly tuned by the controller parameters ε and k.

***B**. After a finite time, if there exist only parametric uncertainties (i.e., $\Delta = 0, \forall t \geq t_0$), then in addition to the transient error bounds in part A, asymptotic tracking is achieved (i.e., $e \to 0$ as $t \to 0$).*

Proof Defining a positive definite function $V_s = \frac{1}{2}\theta_1 e^2$ and differentiating, also noting condition C1 of (3.13), we have

$$\begin{aligned} \dot{V}_s &= \theta_1 e\dot{e} \\ &= e[-ke + v_s + \Delta - \varphi^T\tilde{\theta}] \\ &\leq -ke^2 + \varepsilon \\ &= -\frac{2k}{\theta_1}V_s + \varepsilon, \end{aligned} \tag{3.17}$$

therefore $V_s \leq \exp(-\frac{2k}{\theta_1}t)V_s(0) + \frac{\varepsilon\theta_1}{2k}[1 - \exp(-\frac{2k}{\theta_1}t)]$ and $|e|^2 = \frac{2V_s}{\theta_1}$, which leads to part A.

When $\Delta = 0$, define another p.d. function $V_a = \frac{1}{2}\theta_1 e^2 + \frac{1}{2}\tilde{\theta}^T\Gamma^{-1}\tilde{\theta}$, whose derivative is

$$\begin{aligned} \dot{V}_a &= \theta_1 e\dot{e} + \tilde{\theta}^T\Gamma^{-1}\dot{\hat{\theta}} \\ &= e[-ke + v_s - \varphi^T\tilde{\theta}] + \tilde{\theta}^T\Gamma^{-1}\dot{\hat{\theta}}. \end{aligned} \tag{3.18}$$

Noting condition C2 of (3.13) and the adaptation function (3.15), we have

$$\begin{aligned}
\dot{V}_a &= -ke^2 + v_s e + \tilde{\theta}^T(\Gamma^{-1}\dot{\hat{\theta}} - \varphi e) \\
&\leq -ke^2 + \tilde{\theta}^T(\Gamma^{-1}\dot{\hat{\theta}} - \varphi e) \\
&= -ke^2 + \tilde{\theta}^T(\Gamma^{-1}\mathrm{Proj}_{\hat{\theta}}(\Gamma\varphi e) - \varphi e) \\
&\leq -ke^2 \\
&\leq 0, \qquad (3.19)
\end{aligned}$$

which leads to the asymptotic tracking in part B by applying Babarlat's lemma [100, 102]. ■

Since we introduced an integrator for the input voltage to formulate the problem into the standard form required for ARC design, the augmented system (3.4) becomes a relative degree one system with two states. The resulting one-dimensional internal dynamics for x_2 needs to be bounded-input-bounded-output (BIBO) stable for the actual control input to be bounded and implementable. Substituting the ARC law into the internal dynamics (3.6), we have

$$\dot{x}_2 = -\hat{\theta}_3 x_2 + [\hat{\theta}_1 \dot{y}_d + \hat{\theta}_2 x_1 - \hat{\theta}_4 - ke - \frac{h^2}{4\varepsilon}e]. \qquad (3.20)$$

Defining a p.d. function $V_2 = \frac{1}{2}x_2^2$ and differentiating,

$$\dot{V}_2 = x_2\dot{x}_2 = -\hat{\theta}_3 x_2^2 + [\hat{\theta}_1 \dot{y}_d + \hat{\theta}_2 x_1 - \hat{\theta}_4 - ke - \frac{h^2}{4\varepsilon}e]x_2. \qquad (3.21)$$

Since all the terms in the square bracket are bounded, we denote the upper bound of the entire term by $\bar{b}$ and also notice that $0 < \hat{\theta}_3 < \theta_{3_{min}}$, therefore

$$\begin{aligned}
\dot{V}_2 &\leq -\theta_{3_{min}} x_2^2 + \bar{b}x_2 \\
&= -(1-\lambda)\theta_{3_{min}} x_2^2 - \lambda\theta_{3_{min}} x_2^2 + \bar{b}x_2 \\
&= -(1-\lambda)\theta_{3_{min}} x_2^2 - \lambda\theta_{3_{min}}\left(x_2 - \frac{\bar{b}}{2\lambda\theta_{3_{min}}}\right)^2 \\
&\quad + \frac{\bar{b}^2}{4\lambda\theta_{3_{min}}} \\
&\leq -(1-\lambda)\theta_{3_{min}} x_2^2 + \frac{\bar{b}^2}{4\lambda\theta_{3_{min}}}, \qquad (3.22)
\end{aligned}$$

where the arbitrary constant $\lambda \in (0, 1)$.

Equation (3.22) implies $V_2 \leq x_2^2(0)e^{-(1-\lambda)\theta_{3_{min}}t} + \frac{\bar{b}^2}{4\lambda\theta_{3_{min}}}[1-(1-\lambda)\theta_{3_{min}}t] \leq x_2^2(0) + \frac{\bar{b}^2}{4\lambda\theta_{3_{min}}}$, therefore $|x_2| = \sqrt{2V_2} \leq \sqrt{2x_2^2(0) + \frac{\bar{b}^2}{2\lambda\theta_{3_{min}}}}$ and so $x_2 \in L_\infty$. ■

3.4 Experimental Results

3.4.1 Controller Parameters

The dSPACE controller board executes the ARC algorithm at a sampling frequency of 50 kHz, and the controller dynamics are integrated by forward difference. The controller parameters include the bounds of parameter variations, adaptation gains, and feedback gains, which are selected as follows.

The slope k_u will be bounded by $\frac{dy}{du}$ along a loop curve, which is between 0.7 and 1.2. The fraction b_0 from the step response in Section 3.2.2 was 0.82. We assume that it can vary from 0.6 to 0.9. The time constant τ was 2.36×10^{-3} and it is assumed to be within the same magnitude between 1×10^{-3} and 5×10^{-3}. For a loop starting from zero input and spanning less than 2.5 microns, which is what we will attempt to track, the offset of the model can be found from the outer hysteresis loop to be less than 0.25.

Based on these assumed physical bounds, the bounds for the parameters θ_1 through θ_4 are roughly $\theta_{min} = [0.9,\ 180,\ 220,\ -600]^T$ and $\theta_{max} = [2.4,\ 2400,\ 1670,\ 600]^T$. The magnitude of Δ is assumed to be less than $d_{max} = 1200$. The initial values for the model parameters are set to $\hat{\theta}(0) = [1.6,\ 600,\ 600,\ 0]^T$, which are within the expected bounds but arbitrarily chosen. Using different values results in minor differences in transient error but has no effect on steady state performance.

There is no quantitative method for the selection of the adaptation and feedback gains. However, there are effective heuristics that borrow insights from linear control design. For a linear system with a linear controller, its performance is determined by the poles of the closed-loop error dynamics, which are typically chosen to be well

damped with a bandwidth higher than that of the desired trajectory. For the linear, nominal part of our error dynamics,

$$\ddot{e} + \frac{k}{\theta_1}\dot{e} + \frac{\gamma_4}{\theta_1}e = 0 \tag{3.23}$$

we need to pick the gains k and γ_4 such that it's well damped and its bandwidth is above our desired bandwidth of at least 100Hz. Though theoretically we can reduce ε to arbitrarily bound the transient error, in practice we will excite the resonant dynamics of the stage if we make it too small and therefore the robust feedback too aggressive. The rest of the adaptation gains are picked by dividing γ_4 with the regressor bounds, so that the adaptation dynamics are no faster than the linear integral feedback. Starting from the initial set of values, these control gains are manually tuned further for better performance. The final values are $k = 7000$ and $\varepsilon = 8\times10^{10}$. The adaptation rates are chosen as $\Gamma = \text{diag}\{8,\ 8\times10^5,\ 8\times10^5,\ 1\times10^6\}$.

3.4.2 Trajectory Filtering

The initial error is an important component of the upper bound for transient error (Equation 3.16). To reduce transient tracking error, the desired trajectory y_d is generated by filtering the reference trajectory y_r with a second order stable system

$$\ddot{y}_d + 2\zeta\omega_n\dot{y}_d + \omega_n^2 y_d = \ddot{y}_r + 2\zeta\omega_n\dot{y}_r + \omega_n^2 y_r, \tag{3.24}$$

with $\zeta = 1$ and $\omega_n = 100\text{Hz} = 200\pi\,\text{rad/sec}$. The initial conditions for the desired trajectory are set to $y_d(0) = x_1(0)$, $\dot{y}_d(0) = \dot{x}_1(0)$.

This is crucial for the experiments on the piezoelectric stage, because it is generally very hard to move the position back to zero and maintain it without careful input planning before shutting off the stage. When the stage is turned back on, it usually starts from an undesirable non-zero initial position that is different from that of the reference trajectory. The desired trajectory generated by the filter provides a quick and smooth transition from the initial position of the stage to the true reference

trajectory during the first 0.01s, after which the desired trajectory converges to the reference trajectory.

3.4.3 Tracking Performance

To quantify the performance of our controller, the following performance indices will be used:

(I1) $L_2[e] = \sqrt{\frac{1}{T_f}\int_0^{T_f} |e(t)|^2 dt}$, the scalar valued L_2 norm of the tracking error, a.k.a. the RMS error, is used as a measure of *average tracking performance*, where T_f represents the total running time;

(I2) $e_M = \max_t\{|e(t)|\}$, the maximum absolute value of the tracking error, is used as a measure of *transient performance*;

(I3) $e_F = \max_{T_f-2T\le t\le T_f}\{|e(t)|\}$, the maximum absolute value of the tracking error during the last 2 periods of the experiment, is used as a measure of *final tracking accuracy* for periodic trajectories.

Sinusoidal Trajectories

Table 3.1.
Tracking error for a 2.4 μm, 100-Hz sinusoidal trajectory.

Indices	e_M (nm)	$L_2[e]$ (nm)	e_F (nm)
Values	50.4	7.08	10.3

Figure 3.7 shows the tracking error in the first 10 periods along with the estimated parameters for a 100Hz sinusoidal trajectory $y_r(t) = 1200\,[1-\cos(2\pi f t)]$(unit:nm), which has a total travel of 2400nm. The performance indices are given in Table 3.1. The maximum error $e_M = 50.4$nm, which is 2.1% of the total travel and occurs during

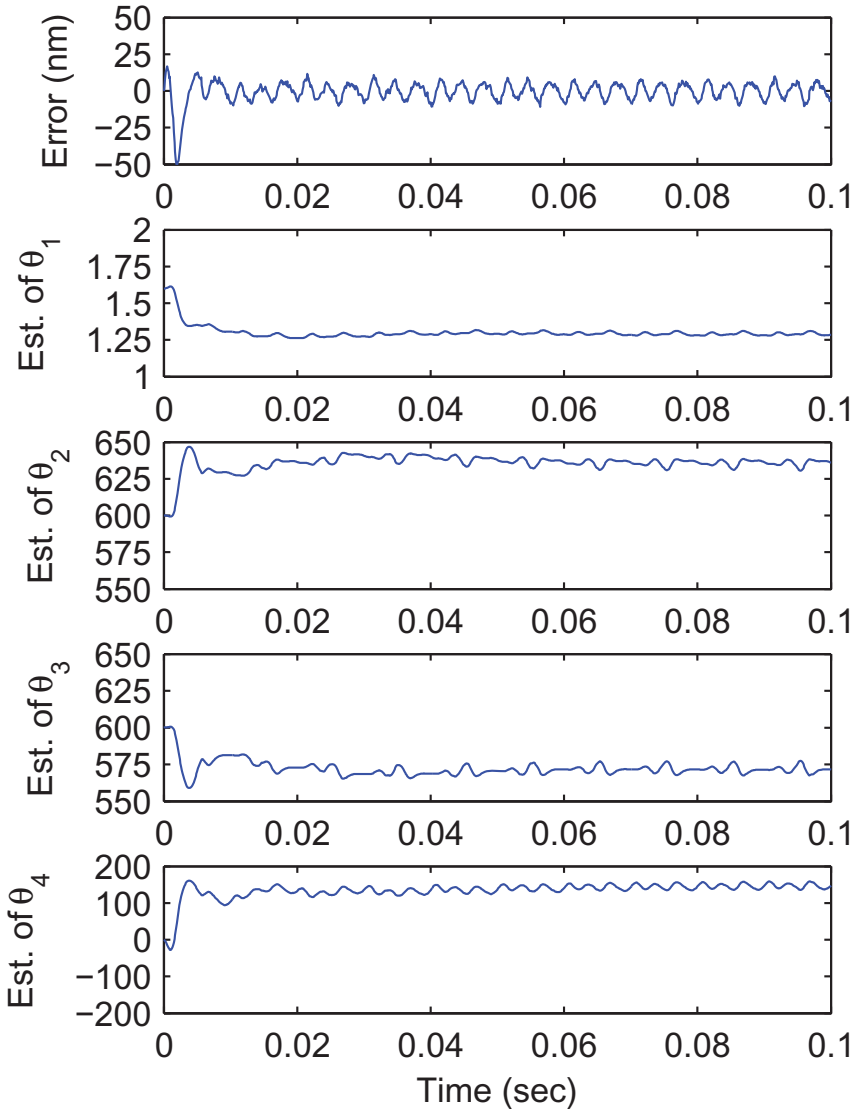

Figure 3.7. Tracking error and parameter estimates for a 100Hz sinusoid.

the first period when the parameters are far from their converged values. The average error $L_2[e] = 7.08$nm is only 0.3% of the total travel. The final maximum tracking error $e_F = 10.3$nm is less than 0.5% of the total travel and on the same magnitude of the sensor noise level.

From the estimated parameters θ_2 and θ_3, the "physical" parameter k_u is back calculated and overlayed on top of the stage response in Figure 3.8. The average

slope of the loop is successfully captured by the estimated parameter, demonstrating the effectiveness of the adaptation. There is, however, no guarantee that the parameters will converge to their true values, because our trajectories do not usually provide enough persistent excitation and the adaptation is very slow when error is too small. We are able to use very fast adaptation rates without destabilizing the system, because the robust feedback law in ARC guarantees stability as long as the parameters are bounded in the prescribed range, regardless of how they change. The good adaptation shown here is also facilitated by the filtered trajectory. Being a combination of the sinusoidal reference signal and the transient response of a second order transfer function, it gives a persistent excitation of enough order during the initial period than just the sine wave itself.

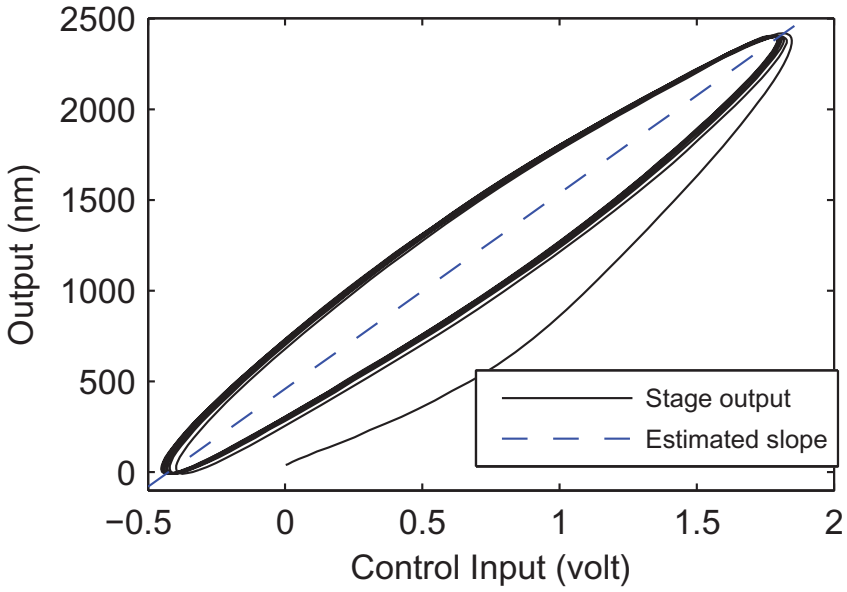

Figure 3.8. Input-output loop for the 100Hz sinusoid.

Point-to-point Step Trajectories

Figure 3.9 shows the tracking error in the first 10 periods along with the estimated parameters for a 2400nm peak-to-peak square wave trajectory with 50% duty cycle

and a period of 0.1 second. The error given in Figure 3.9 is for the filtered desired trajectory. It shows how well the actuator response follows the response of a second order transfer function. Figure 3.10 shows the first 20 ms of the response. The stage follows the desired 2nd order response almost perfectly with a settling time less than 10 ms. The stage response converges to each new set-point after about 20ms with no steady-state error.

3.5 Combining Hysteresis Feedforward and Adaptive Robust Feedback

Now that we have confirmed the individual effectiveness of the hysteresis feedforward and the adaptive robust controller, they are finally combined for the best performance (Figure 3.11). The hysteresis "friction" is predicted from the desired trajectory using the extended Dahl model with memory. Although adding a disturbance feedforward does not affect the stability of the feedback loop, the practical performance depends on careful initialization of both the actuator position and the trajectory.

Without a full-loop actuator initialization, the feedforward signal may not reduce the hysteresis. It may instead add to the disturbance Δ of the original system in equation 3.5, until the historical minor loops are all wiped out when the actuator has traversed the reach of the trajectory. With initialization, the feedforward model matches the true hysteresis and cancels most of the unstructured uncertainty, when the actuator starts from a known state after its loading history has been erased by a full loop. The remaining uncertainties in the gain and offset of the system are then handled by adaptation and robust feedback.

The actuator may form small inner loops due to initial transient oscillations that are not canceled well by the feedforward model, causing larger transient errors than without feedforward. This did not cause an issue for us, because trajectory initialization in the feedback loop ensures the initial transient error is small. The parameters of the initialization filter should be picked such that y_d and y_r go in the same direc-

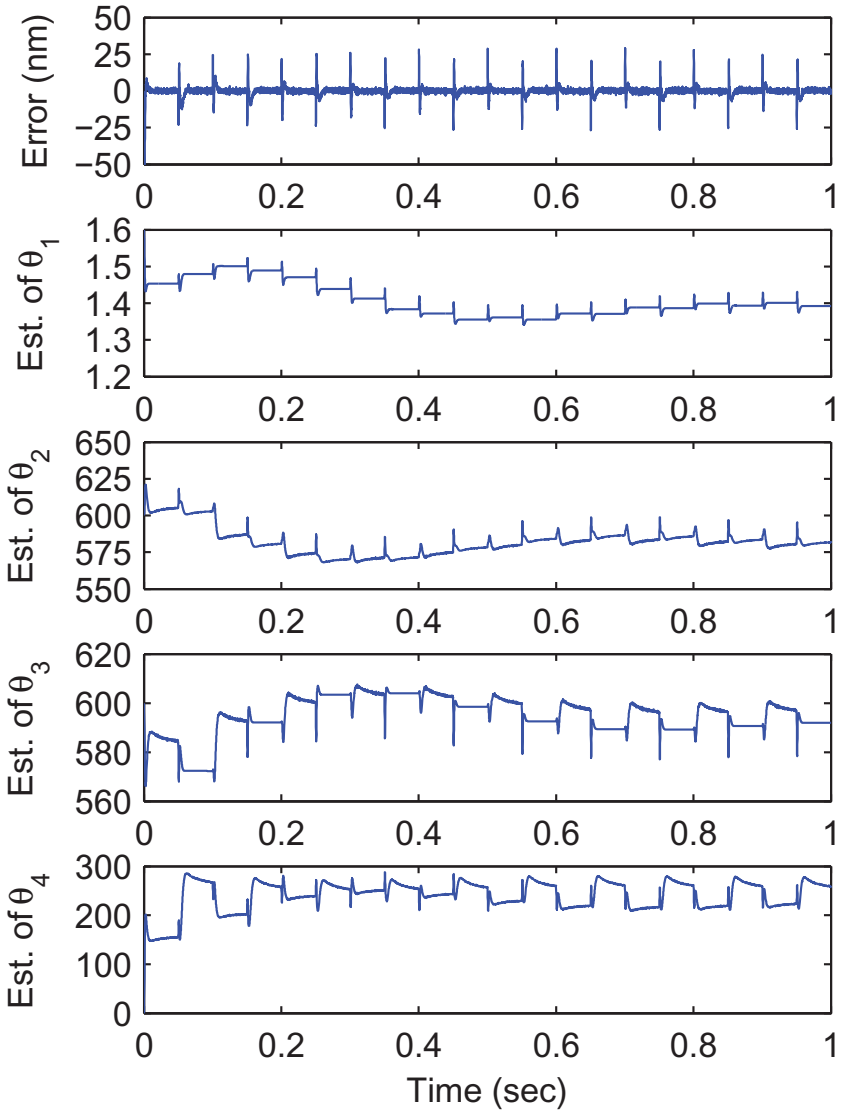

Figure 3.9. Tracking error and parameter estimates for step-like trajectories.

tion initially and quickly converge before the direction of y_r changes, otherwise the actuator will form a small reversal loop at the beginning that is not canceled well during the transient. These considerations don't affect theoretical stability and final tracking error, but are key to good transient tracking in practice.

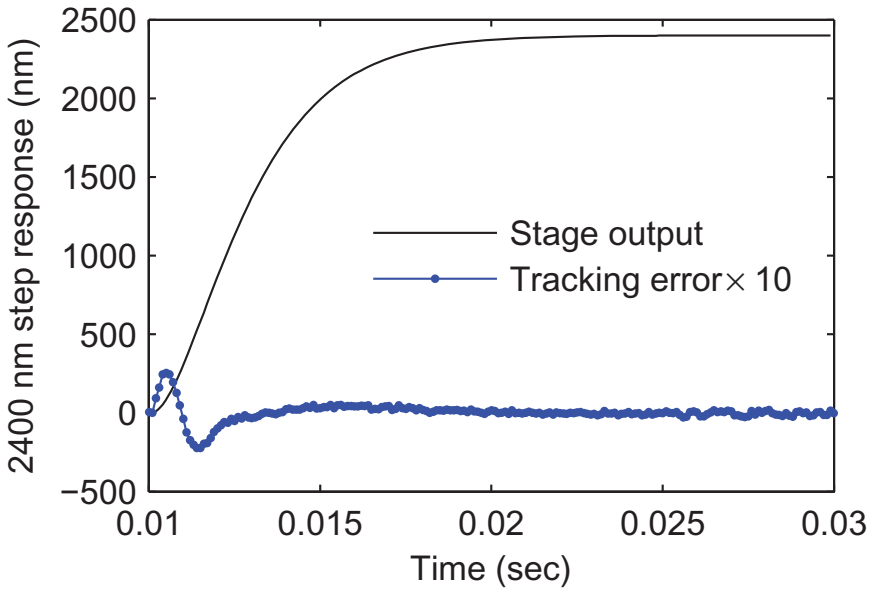

Figure 3.10. Magnified step response of the stage.

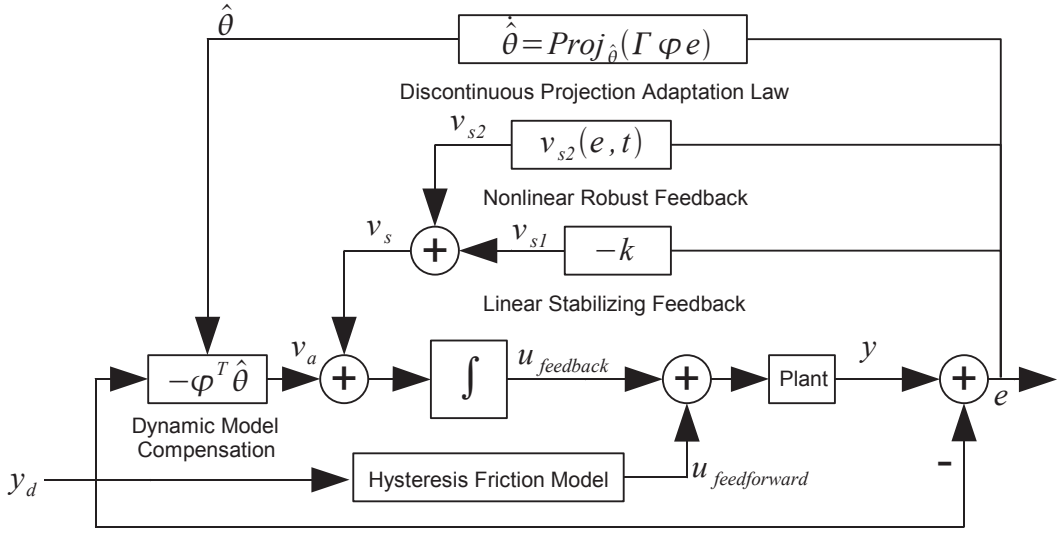

Figure 3.11. Controller structure combining both adaptive robust feedback and hysteresis friction feedforward.

3.5.1 Sinusoidal Trajectory

Figure 3.12 shows the performance for a 100 Hz sinusoidal trajectory with a peak-peak amplitude of 10 microns. The tracking is almost perfect after the first period. The largest tracking error during the 20th period is 0.016 micron, or 0.16% of the peak-peak amplitude.

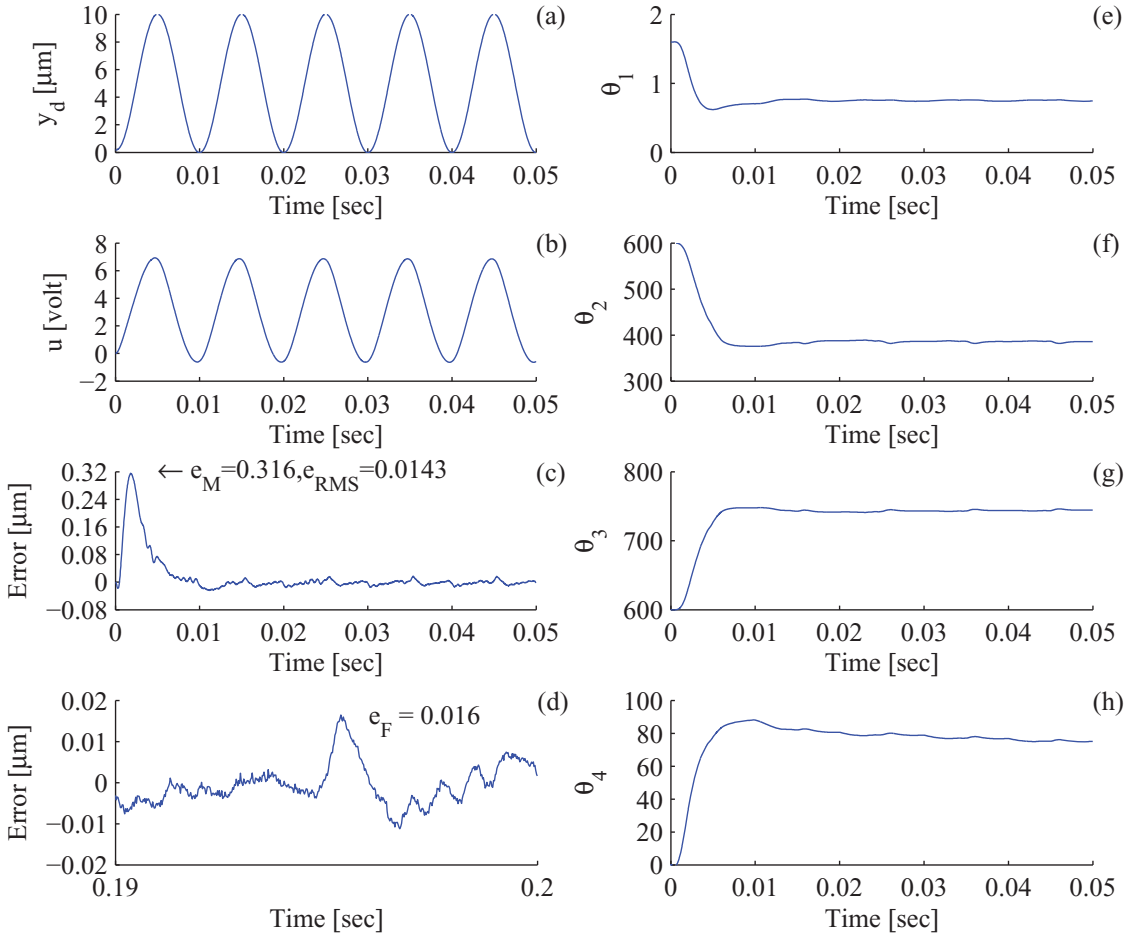

Figure 3.12. Tracking error and parameter estimates for a 10μm, 100-Hz sinusoid using ARC with Dahl friction feedforward. The tracking is very good after the first period. (a) Desired trajectory; (b) Control input; (c) Tracking error during the first 5 periods of the sinusoidal trajectory; (d) Final tracking error during the 20th period, which is only 0.16% of the trajectory amplitude; (e-h) Parameter estimates of θ_1, θ_2, θ_3, and θ_4.

3.5.2 Multi-sine Trajectories

Here we repeat the exact same trajectories used by Bashash and Jalili in their 2007 TCST paper [63]. Their results have been obtained three years before on an identical actuator and a similar dSPACE prototyping system, which provide a rare opportunity for direct comparison of contemporary experimental results. Table 3.2 shows 6 different trajectory profiles from [63] and Table 3.3 compares the tracking performance between their design and ours. The orders of the profiles are retained from [63] for easier verification by the reader.

Table 3.2.
Trajectory profiles from reference [63].

	Desired trajectory profile (μm)
(a)	$3 - 3\cos(20\pi t)$
(b)	$4 - 4[\cos(2\pi t) + \cos(6\pi t) + \cos(10\pi t) + \cos(20\pi t)]$
(c)	$3 - 3\cos(100\pi t)$
(d)	$4 - 4[\cos(20\pi t) + \cos(30\pi t) + \cos(80\pi t) + \cos(100\pi t)]$
(e)	$3 - 3\cos(200\pi t)$
(f)	$4 - 4[\cos(60\pi t) + \cos(100\pi t) + \cos(140\pi t) + \cos(200\pi t)]$

Figure 3.13 shows our results for cases (a), (c) and (e), which are single sinusoids at 10, 50 and 100 Hz with 6 microns peak to peak. In the first column of subplots are the desired trajectories. The middle column shows the tracking error for the first 5 periods, and the last column shows the final tracking error for the 20th period after more adaptation.

We have previously demonstrated good performance for a 100-Hz sinusoid of 10 microns in Section 3.5.1. The single-sine trajectories here are less demanding in both amplitude and frequency, and the tracking errors from our controller are consistently close to the noise level. Our maximum errors are slightly larger, but it only hap-

Table 3.3.
Tracking error comparison between our controller and the controller in [63]

	Hysteresis Inverse + Sliding Mode [63]		Dahl Friction Feedforward + ARC	
	Max error (%)	MSE (μm)	Max error (%)	MSE (μm)
(a)	1.04	0.03	1.1	3.7×10^{-5}
(b)	0.84	0.02	0.76	4.0×10^{-5}
(c)	1.40	0.03	2.4	1.1×10^{-4}
(d)	1.16	0.02	1.9	5.5×10^{-5}
(e)	2.32	0.07	4.2	1.8×10^{-5}
(f)	1.83	0.03	3.0	7.0×10^{-5}

pens during the initial transient. Adaptation settles within a couple periods and the subsequent error drops to extremely low levels, as is shown in Figure 3.13.a2.

Figure 3.14 shows cases (b), (d) and (f), which are multi-sine trajectories that form minor loops in actuator response and more challenging than the single sinusoids. The trajectory profiles are in the first column, and the second column shows the tracking error for the first two periods of the slowest component of the sines.

Our mean-squared tracking errors for all six profiles are smaller *by more than 2 orders of magnitude*. Note that Figures 3.13 and 3.14 are annotated with the RMS errors of our results instead of MSE. Our MSE in Table 3.3 for the multi-sine trajectories are [0.000040, 0.000055, 0.000070] compared to their MSE of [0.02, 0.02, 0.03].

The controller in [63] has a Preisach-type hysteresis inverse between the feedback controller and the plant, and the feedback controller is a sliding-mode controller designed around the 2nd-order resonance dynamics of the actuator stage. Since the stage resonance is at 5.6 kHz, this dynamics is negligibly fast when the actuator is only tracking a 100-Hz trajectory. Their sliding-mode controller is essentially attenuating the uncertainties in their hysteresis inverse alone, whereas we design around

the slower, dominant dynamics of the actuator and adapt all the parameters online for better steady-state performance. Our hysteresis model is used as a disturbance feedforward outside of the feedback loop, which doesn't introduce modeling uncertainties in the loop gain when the hysteresis inverse becomes less accurate at higher frequencies.

3.6 Conclusions

For a piezoelectric actuator with resonant frequencies far beyond the application bandwidth, the dominant dynamics that should be used for control design is the domain switching dynamics. Experimental results show that, even at low input rates, the hysteretic nonlinearity is *rate-dependent*, and the dipole domain switching, the cause of this rate-dependence, cannot be assumed to occur instantaneously and independent of input-rate. Instead, the switching dynamics should be explicitly accounted for if high precision closed-loop control is desired.

A simple control-oriented nonlinear first-order model is enough to achieve a good balance between the engineering efforts needed for detailed rate-dependent hysteresis modeling and the achievable overall control performance through advanced model-based controls. The model structure captures the major characteristics of various piezoelectric effects, including the rate-dependent hysteresis nonlinearity, the drifting, and the broad spectrum of domain switching time constants, but the parameters do not need to be identified offline to extreme accuracy. The model is linearly parameterized by only four parameters so that on-line fast parameter adaptation can be used to effectively compensate for the effect of unknown hysteresis model parameters and uncertainties.

An adaptive robust controller (ARC) using discontinuous projection based online parameter estimation is able to meet the design objective and demonstrate the effectiveness of the holistic approach. Experimental results from tracking control of sinusoidal trajectories up to 100 Hz show tracking error on the magnitude of the sen-

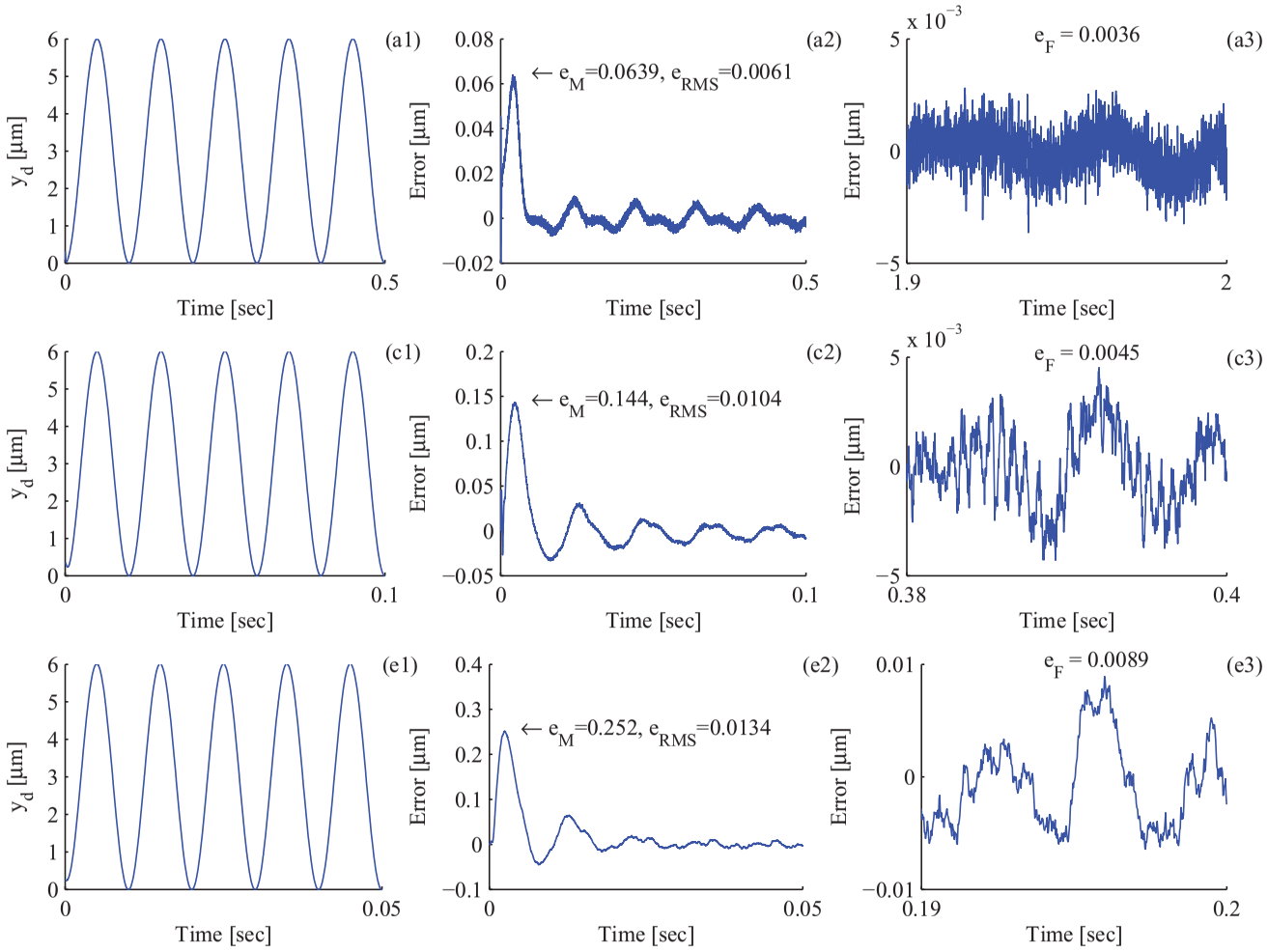

Figure 3.13. Tracking error for single-sine trajectories. Left to right (1, 2, 3): Desired trajectory and transient error during the first 5 periods and final error during the 20th period. Top to bottom (a, c, e): Results for profiles (a), (c), and (e) in Table 3.2.

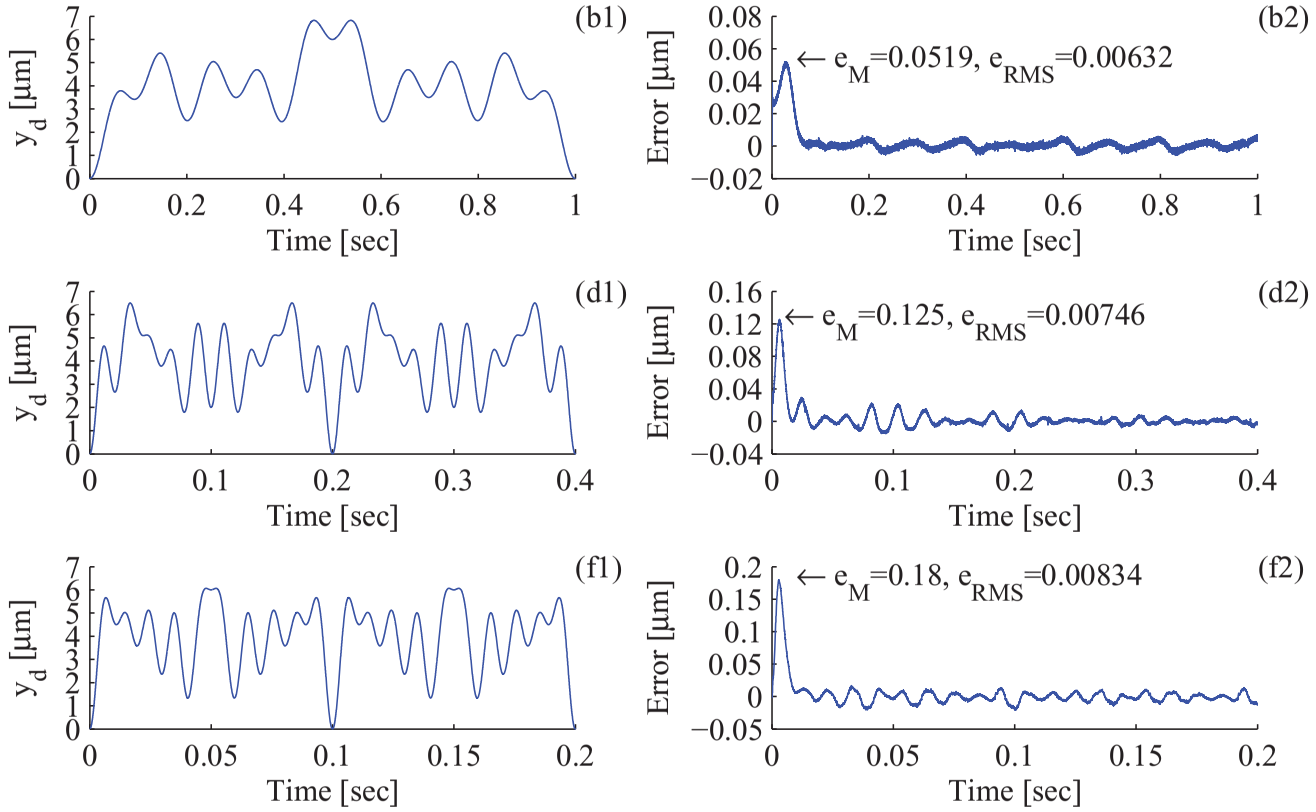

Figure 3.14. Tracking error for multi-sine trajectories. Left and right (e.g., b1 and b2): Desired trajectory and transient error. Top to bottom: Results for profiles (b), (d), and (f) in Table 3.2.

sor noise level, which demonstrate that good tracking accuracy is possible without exact knowledge of hysteresis or offline identification of a complex model, when advanced adaptive robust controls are used to generate better dynamic compensation via on-line adaptation and to reduce transient error via robust feedback.

Reducing unstructured uncertainty is one of the keys to good tracking performance in adaptive robust control. When the hysteresis friction model is combined with the adaptive robust controller, much of the unstructured uncertainty coming from hysteresis is canceled, which helps reduce tracking errors to a level that is orders of magnitude smaller than previously reported results on the same actuator.

4. SINGLE-LOOP PERIODIC TRAJECTORY TRACKING CONTROL

4.1 Introduction

In chapter 3, we modeled the overall slope of the hysteretic input-output relationship and left the discrepancy to be compensated by fast adaptation and robust feedback. We have proved asymptotic tracking when only parametric uncertainties are present, but in reality the unmodeled part of the hysteresis always remains. Reducing non-parametric uncertainty is key to better steady-state tracking. Even though the friction model cancels most of the hysteresis, a small amount of uncertainty still exists in the model. Since the friction model is identified offline and not adapted, it is a static feedforward that cannot be improved by feedback.

The difficulty for perfect tracking is much reduced when the desired trajectory is periodic or repetitive. Experimentally, when a piezoelectric actuator is driven by a periodic input, it converges to a steady-state hysteresis loop after a certain number of cycles, a phenomenon commonly known as "accommodation" [20]. It indicates that under the same periodic input, the dipole domains that will switch in each cycle are almost the same. Therefore for periodic trajectories, the required input is highly periodic.

The periodic input can be adapted by methods such as iterative learning control (ILC), which updates the input signal using the error signal from the previous period and avoids inverting complex nonlinear models. This has been shown to achieve exact tracking for a piezoelectric positioner [34], but the stability and error convergence of their method is theoretically guaranteed only for trajectories that satisfy the classic Preisach model, which are slow or pseudo-static trajectories. Though easy to implement, such a method require large computer memory and are sensitive to noise because the physical dependence of the unknown nonlinearity over the same period

is overlooked. The known dynamics of the system are also hard to be incorporated. The tracking error in [34] converges to zero after almost 50 periods. This may be too long for real-world applications.

A remedy to this problem is proposed by Xu and Yao in [103]. By recognizing the physical dependence of the values of periodic uncertainties over the same period and using certain known basis functions to capture such dependence, only the amplitudes of the basis functions are needed for parameterization, which can be easily adapted online. It also overcomes the sensitivity to noise because the basis functions naturally smooth out the effect of random noise. Incorporated with the adaptive robust control (ARC) scheme, it guarantees good transient performance, fast convergence, and almost perfect tracking when a sufficient number of basis functions are used to parameterize the unknown periodic nonlinearity.

In this chapter, we assume the same plant dynamics as in Chapter 3, but the explicit hysteresis model from Chapter 2 will not be used. Instead, we approximate the hysteretic discrepancy term by a series of harmonic basis functions. The adaptive robust control scheme is applied to the model, which adapts the unknown parameters using a discontinuous projection based method, and the uncompensated nonlinearities are attenuated by robust control laws.

Without using an explicit model for hysteresis, the steady-state tracking error is reduced to almost the sensor noise level for sinusoidal trajectories up to 100 Hz and pseudo-triangular (with smoothed turnaround points) trajectories up to 50 Hz. Tracking error converges to almost the sensor noise level after only a few periods, demonstrating the effectiveness of the method.

4.2 Revisiting the System Model

In Chapter 3, we have reduced our overall model to a simple first order system

$$\begin{aligned} \tau \dot{x_h} &= -x_h + b_1 g_t(u), \\ y &= x_h + b_0 g_t(u), \end{aligned} \tag{4.1}$$

where $g_t(u)$ is a hysteretic mapping from the input u to the steady-state output of the system, b_0 the feed-through gain, and b_1 the input gain of the first order dynamics. Replacing $g_t(u)$ by a linear gain plus a time varying disturbance,

$$g_t(u) = k_u u + d_g(t), \tag{4.2}$$

the system equations are simplified to

$$\begin{aligned} \tau \dot{x_h} &= -x_h + b_1[k_u u + d_g(t)], \\ y &= x_h + b_0[k_u u + d_g(t)]. \end{aligned} \tag{4.3}$$

The term $d_g(t)$ represents the time-varying mismatch between $k_u u$ and $g_t(u)$. The parameter k_u captures the average slope of the hysteresis loop that covers the entire range of desired operation.

Defining the system state vector $[x_1, x_2]^T = [y, u]^T$ and using $v = \dot{u}$ as a virtual input (also noting the identity $b_0 + b_1 = 1$), we rewrite (4.3) as

$$\begin{aligned} \frac{1}{b_0 k_u}\dot{x}_1 &= -\frac{1}{\tau b_0 k_u}x_1 + \frac{1}{\tau b_0}x_2 + \frac{1}{k_u}[\frac{1}{\tau b_0}d_g + \dot{d}_g] + v, \\ \dot{x}_2 &= v, \\ y &= x_1. \end{aligned} \tag{4.4}$$

4.3 Harmonic Function Approximation

The term $\frac{1}{k_u}[\frac{1}{\tau b_0}d_g + \dot{d}_g]$ in (4.4), representing the uncertain nonlinearity from hysteresis, was parameterized as an unknown nominal value plus an unstructured disturbance in Chapter 3, because that's all we know about the uncertainty when

the trajectory is arbitrary[1]. When the desired trajectory is periodic, however, the uncertainty term also becomes highly periodic with the same period. We can further approximate the uncertainty using a finite Fourier series

$$\begin{aligned}\frac{1}{k_u}[\frac{1}{\tau b_0}d_g + \dot{d}_g] &= \frac{A_0}{2} + \sum_{n=1}^{m}(A_n \cos n\omega t + B_n \sin n\omega t) + \Delta \\ &= \Phi_d^T \theta_d + \Delta, \end{aligned} \tag{4.5}$$

where $\theta_d = [A_0/2,\ A_1,\ B_1,\ \cdots,\ A_m,\ B_m]^T$ represent the unknown Fourier coefficients, $\Phi_d^T = [1,\ \cos\omega t,\ \sin\omega t,\ \cdots,\ \cos m\omega t,\ \sin m\omega t]$ are the basis functions, and Δ is the unknown variation between the series and the true nonlinearity. Since the mechanical system has a finite bandwidth, the first few terms will be enough for a good approximation in practice.

To use parameter adaptation, we define the unknown parameter set $\theta^T = [\theta_1,\ \theta_2,\ \theta_3,\ \theta_d^T]$ with $\theta_1 = \frac{1}{b_0 k_u}$, $\theta_2 = \frac{1}{\tau b_0 k_u}$, and $\theta_3 = \frac{1}{\tau b_0}$. The state space equation (4.4) is now linearly parameterized in terms of θ as

$$\theta_1 \dot{x}_1 = -\theta_2 x_1 + \theta_3 x_2 + \Phi_d^T \theta_d + \Delta + v, \tag{4.6}$$

$$\dot{x}_2 = v. \tag{4.7}$$

4.4 Controller Design

The model is structurally identical to the plant model in Chapter 3, except for the additional parameters and harmonic regressors for the periodic uncertainty. Therefore the assumptions, procedures and stability proofs are almost identical to those in Section 3.3. They have been published separately [104] and are included here for completeness.

[1]Though the trajectories in Chapter 3 were all periodic, we never exploited the periodicity in our controller design.

4.4.1 Design Assumptions

The diaturbance from hysteresis is bounded in proportion to dipole domains that can switch in the specified input range. The domains that switch under the same input are similar, and domains do not switch infinitely fast. With these physical properties in mind, we can make the following practical assumption on the parameters [100], with the notation that the relational operator "$<$" used hereinafter between two vectors is performed in terms of the corresponding elements of the vectors:

Assumption 4.1 *The extent of parametric uncertainties and uncertain nonlinearities is known, i.e.,*

$$\begin{aligned} \theta &\in \Omega_\theta \triangleq \{\theta :\ \theta_{\min} < \theta < \theta_{\max}\}, \\ \Delta &\in \Omega\Delta \triangleq \{\Delta\ \ \|\Delta(x,t)\| \le \delta(x,t)\}, \end{aligned} \tag{4.8}$$

where $\theta_{\min}$, $\theta_{\max}$, and $\delta(x,t)$ are known.

Under the assumption, the discontinuous projection based ARC design is applied to (4.3) to solve the robust tracking control problem. Specifically, the parameter estimation $\hat{\theta}$ is updated through a parameter adaptation law of the form

$$\dot{\hat{\theta}} = \mathrm{Proj}_{\hat{\theta}}(\Gamma\tau) \tag{4.9}$$

where Γ is any symmetric positive definite adaptation rate matrix (for simplicity, Γ is assumed to be a diagonal matrix), τ is an adaptation function to be specified later, and the projection mapping $\mathrm{Proj}_{\hat{\theta}}(\bullet)$ is defined by

$$\mathrm{Proj}_{\hat{\theta}}(\bullet) = \begin{cases} 0 & \text{if} \begin{cases} \hat{\theta}_i = \hat{\theta}_{\max} & \text{and } \bullet > 0, \text{ or} \\ \hat{\theta}_i = \hat{\theta}_{\min} & \text{and } \bullet < 0; \end{cases} \\ \bullet & \text{otherwise,} \end{cases} \tag{4.10}$$

which has the following properties [101]:

$$\begin{aligned} &\text{P1.} \quad \hat{\theta} \in \bar{\Omega}_\theta = \{\hat{\theta} :\ \theta_{\min} < \hat{\theta} < \theta_{\max}\}, \\ &\text{P2.} \quad \tilde{\theta}^T(\Gamma^{-1}\mathrm{Proj}_{\hat{\theta}}(\Gamma\bullet) - \bullet) \le 0,\ \forall \bullet\,. \end{aligned} \tag{4.11}$$

4.4.2 ARC Design

Defining $e = x_1 - y_d$ as the tracking error, the error dynamics of the system becomes

$$\begin{aligned} \theta_1 \dot{e} &= \theta_1 \dot{x}_1 - \theta_1 \dot{y}_d \\ &= -\theta_1 \dot{y}_d - \theta_2 x_1 + \theta_3 x_2 + \Phi_d^T \theta_d + \Delta + v \\ &= \varphi^T \theta + \Delta + v, \end{aligned} \tag{4.12}$$

where $\varphi^T = [-\dot{y}_d,\, -x_1,\, x_2,\, \Phi_d^T]$. The following ARC control law is used, which consists of two parts given by

$$\begin{aligned} v = v_a + v_s, \quad v_a = -\varphi^T \hat{\theta}, \\ v_s = v_{s_1} + v_{s_2},\ v_{s_1} = -ke, \end{aligned} \tag{4.13}$$

where v_a is the adjustable model compensation needed for achieving perfect tracking, and v_s is the robust control law consisting of two parts: v_{s_1} is a simple proportional feedback used to stabilize the nominal system, and v_{s_2} is a robust feedback used to attenuate the effect of model uncertainties, which is required to satisfy the following two constraints

$$\begin{aligned} &\text{C1.} \quad e[-\varphi^T \tilde{\theta} + \Delta(x,t) + v_{s_2}] \le \varepsilon, \\ &\text{C2.} \quad v_{s_2} e \le 0, \end{aligned} \tag{4.14}$$

where ε is a positive design parameter representing the attenuation level of the model uncertainties. In (4.14), constraint C1 is used to represent the fact that v_{s_2} is synthesized to dominate the the model uncertainties coming from both parametric uncertainties and unmodeled nonlinearities to achieve the guaranteed attenuation level ε, and the passivity constraint C2 is imposed to ensure that introducing v_{s_2} does not interfere with the nominal parameter adaptation process. A simple form of v_{s_2} that satisfy (4.14) is

$$v_{s_2} = -\frac{1}{4\varepsilon} h^2 e, \tag{4.15}$$

where $h \ge \|\theta_{\max} - \theta_{\min}\| \, \|\varphi\| + \delta(x,t)$. It is used in our experimental implementation for computational simplicity. The ARC design above has the following theoretical performance:

Theorem 4.2 *If the adaptation function in (4.9) is chosen as*

$$\tau = \varphi(x)e, \tag{4.16}$$

then the ARC law (4.13) with the parameter adaptation law (4.9) guarantees that

A. *In general, all signals are bounded and the tracking error is bounded by*

$$|e|^2 \leq \exp(-\frac{2k}{\theta_{1max}}t)\frac{2|e(0)|^2}{\theta_1} + \frac{\varepsilon\theta_{1max}}{2k}[1-\exp(-\frac{2k}{\theta_{1max}}t)]. \tag{4.17}$$

The exponential converging rate $\frac{2k}{\theta_{1max}}$ *and the size of the final tracking error (*$|e(\infty)| \leq \sqrt{\frac{\varepsilon\theta_{1max}}{2k}}$*) can be freely adjusted by the controller parameters* ε *and* k *in a known form.*

B. *If after a finite time, there exist parametric uncertainties only (i.e.,* $\Delta(x,t) = 0, \forall t \geq t_0$*), then in addition to the results in A, zero tracking error is achieved, i.e.,* $e \to 0$ *as* $t \to \infty$.

Proof Defining a positive definite function $V_s = \frac{1}{2}\theta_1 e^2$ and differentiating, also noting constraint C1 of (4.14), we have

$$\begin{aligned}
\dot{V}_s &= \theta_1 e\dot{e} \\
&= e[-ke + v_s + \Delta - \varphi^T\tilde{\theta}] \\
&\leq -ke^2 + \varepsilon \\
&\leq -\frac{2k}{\theta_{1max}}V_s + \varepsilon,
\end{aligned} \tag{4.18}$$

therefore $V_s \leq \exp(-\frac{2k}{\theta_{1max}}t)V_s(0) + \frac{\varepsilon\theta_{1max}}{2k}[1-\exp(-\frac{2k}{\theta_{1max}}t)]$. Substituting $|e|^2 = \frac{2V_s}{\theta_1}$ back leads to part A.

When $\Delta = 0$, define another positive definite function $V_a = \frac{1}{2}\theta_1 e^2 + \frac{1}{2}\tilde{\theta}^T\Gamma^{-1}\tilde{\theta}$, whose derivative is

$$\begin{aligned}
\dot{V}_a &= \theta_1 e\dot{e} + \tilde{\theta}^T\Gamma^{-1}\dot{\hat{\theta}} \\
&= e[-ke + v_s - \varphi^T\tilde{\theta}] + \tilde{\theta}^T\Gamma^{-1}\dot{\hat{\theta}}.
\end{aligned} \tag{4.19}$$

Noting constraint C2 in (4.14) and the adaptation function (4.16), we have

$$\begin{aligned}
\dot{V}_a &= -ke^2 + v_s e + \tilde{\theta}^T(\Gamma^{-1}\dot{\hat{\theta}} - \varphi e) \\
&\leq -ke^2 + \tilde{\theta}^T(\Gamma^{-1}\dot{\hat{\theta}} - \varphi e) \\
&= -ke^2 + \tilde{\theta}^T(\Gamma^{-1}\mathrm{Proj}_{\hat{\theta}}(\Gamma\varphi e) - \varphi e) \\
&\leq -ke^2 \\
&\leq 0, \qquad (4.20)
\end{aligned}$$

which leads to the asymptotic tracking in part B by easily verifying $\dot{e} \in L_\infty$ and applying Barbalat's Lemma. ■

In addition, the system (4.4) has relative degree one, the internal dynamics for x_2 needs to be BIBO stable for the actual control input to be bounded and implementable. Substituting the ARC law into the internal dynamics (4.7), we have

$$\dot{x}_2 = -\hat{\theta}_3 x_2 + [\hat{\theta}_1 \dot{y}_d + \hat{\theta}_2 x_1 - \Phi_d^T \hat{\theta}_d - ke - \frac{h^2}{4\varepsilon} e]. \qquad (4.21)$$

Defining a positive definite function $V_2 = \frac{1}{2}x_2^2$ and differentiating,

$$\dot{V}_2 = x_2 \dot{x}_2 = -\hat{\theta}_3 x_2^2 + \left[\hat{\theta}_1 \dot{y}_d + \hat{\theta}_2 x_1 - \Phi_d^T \hat{\theta}_d - ke - \frac{h^2}{4\varepsilon} e\right] x_2. \qquad (4.22)$$

Since all the terms in the square bracket are bounded, we denote the upper bound of the entire term by $\bar{b}$ and also notice that $0 < \hat{\theta}_3 < \theta_{3min}$, therefore

$$\begin{aligned}
\dot{V}_2 &\leq -\theta_{3min} x_2^2 + \bar{b} x_2 \\
&= -(1-\lambda)\theta_{3min} x_2^2 - \lambda\theta_{3min} x_2^2 + \bar{b} x_2 \\
&= -(1-\lambda)\theta_{3min} x_2^2 - \lambda\theta_{3min}\left(x_2 - \frac{\bar{b}}{2\lambda\theta_{3min}}\right)^2 \\
&\quad + \frac{\bar{b}^2}{4\lambda\theta_{3min}} \\
&\leq -(1-\lambda)\theta_{3min} x_2^2 + \frac{\bar{b}^2}{4\lambda\theta_{3min}}, \qquad (4.23)
\end{aligned}$$

where the arbitrary constant $\lambda \in (0,1)$. Equation (4.23) implies $V_2 \leq V_b(t) = x_2^2(0)e^{-(1-\lambda)\theta_{3min}t} + \frac{\bar{b}^2}{4\lambda\theta_{3min}}\left[1 - (1-\lambda)\theta_{3min}t\right] \leq x_2^2(0) + \frac{\bar{b}^2}{4\lambda\theta_{3min}}$, therefore $|x_2| = \sqrt{2V_2} \leq \sqrt{2V_b(t)} \leq \sqrt{2x_2^2(0) + \frac{\bar{b}^2}{2\lambda\theta_{3min}}}$ and so x_2 is bounded. ■

4.5 Experimental Results

4.5.1 Controller Parameters

The dSPACE controller board executes the ARC algorithm at a sampling frequency of 10 kHz. We will measure the response to sinusoidal trajectories and triangular trajectories with rounded corners. A power spectrum analysis of the hysteresis loops suggests that only the offset term $A_0/2$ and the odd number harmonics are significant due to the symmetry of our desired trajectories, so $n = [1, 3, 5, \cdots]$. In the experiments, using up to $n = 5$ is enough to get the error close to the noise level, and thus $\Phi_d^T \theta_d$ contains 7 terms.

Using the same procedure as in Section 3.4.1, the initial values for the parameters are set to $\hat{\theta}(0) = [1.6, 600, 600, 0, 0, 0, 0, 0, 0, 0]^T$. The bounds of variations are estimated as $\theta_{min} = [0.9, 180, 220, -500, -500, -500, -500, -500, -50, -50]^T$ and $\theta_{max} = [2.4, 2400, 1670, 500, 500, 500, 500, 500, 50, 50]^T$. The magnitude of Δ is assumed to be less than $d_{max} = 500$. The parameters used for the ARC controller are $k_1 = 8000$ and $\varepsilon = 10^{10}$. The adaptation rates are chosen as $\Gamma = \text{diag}\{8, 8 \times 10^5, 8 \times 10^5, 2 \times 10^6, 2 \times 10^6, 2 \times 10^6, 2 \times 10^6, 2 \times 10^6, 2 \times 10^6, 2 \times 10^6\}$.

4.5.2 Tracking Performance

To quantify the performance of our controller, we will use the same performance indices as we did in Chapter 3:

(I1) $L_2[e] = \sqrt{\frac{1}{T_f} \int_0^{T_f} |e(t)|^2 dt}$, the scalar valued L_2 norm of the tracking error, is used as a measure of *average tracking performance*, where T_f represents the total running time;

(I2) $e_M = \max_t \{|e(t)|\}$, the maximum absolute value of the tracking error, is used as a measure of *transient performance*.

(I3) $e_F = \max_{T_f-2T \le t \le T_f} \{|e(t)|\}$, the maximum absolute value of the tracking error during the last 2 periods, is used as a measure of *final tracking accuracy* for general periodic trajectories.

Sinusoidal Trajectories

Figure 4.1 shows the tracking error in the first 10 periods for a 100Hz sinusoidal trajectory $r(t) = [1 - cos(2\pi ft)] * 1200[nm]$, which corresponds to a total travel of 2400nm. The maximum error $e_M = 33.6$nm, which is 1.4% of the total travel. The average error $L_2[e] = 4.36$nm, which translates to less than 0.2% of the total travel. The final tracking error $e_F = 3.07$nm is only 0.13% of the total travel and almost the same as the sensor noise level.

The estimates of the 4 major parameters (θ_1 through θ_3 and the static component of the harmonic approximation) are shown in Figure 4.2. The parameters have almost stopped adapting after the first two periods because the error has already converged to such a small value. The direct ARC algorithm used here only aims to reduce tracking error. It does not require nor guarantee parameter convergence, which can only happen if persistent excitation is satisfied. The major parameter estimates are very reasonable, even though the simple trajectory may not provide enough excitation, because the trajectory generated from the all-pass filter contains not only the reference trajectory but also a decaying signal from initial position, which improves the "richness" of the signal at the beginning.

Figure 4.3 shows the trend of tracking errors as the number of harmonic functions increases. The transient error is not affected much, as it is determined mostly by the robust feedback gain, but the average error and final tracking error decrease as we increase the highest order of harmonics used to approximate the uncertain nonlinearity.

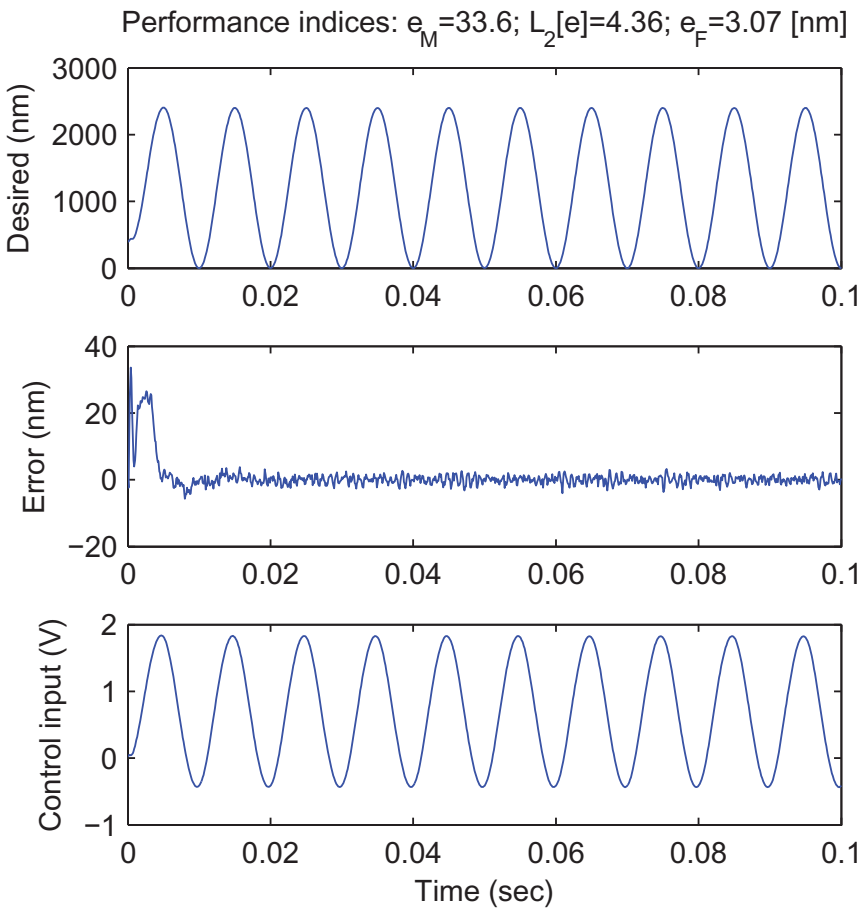

Figure 4.1. Tracking error for a 100Hz sinusoid.

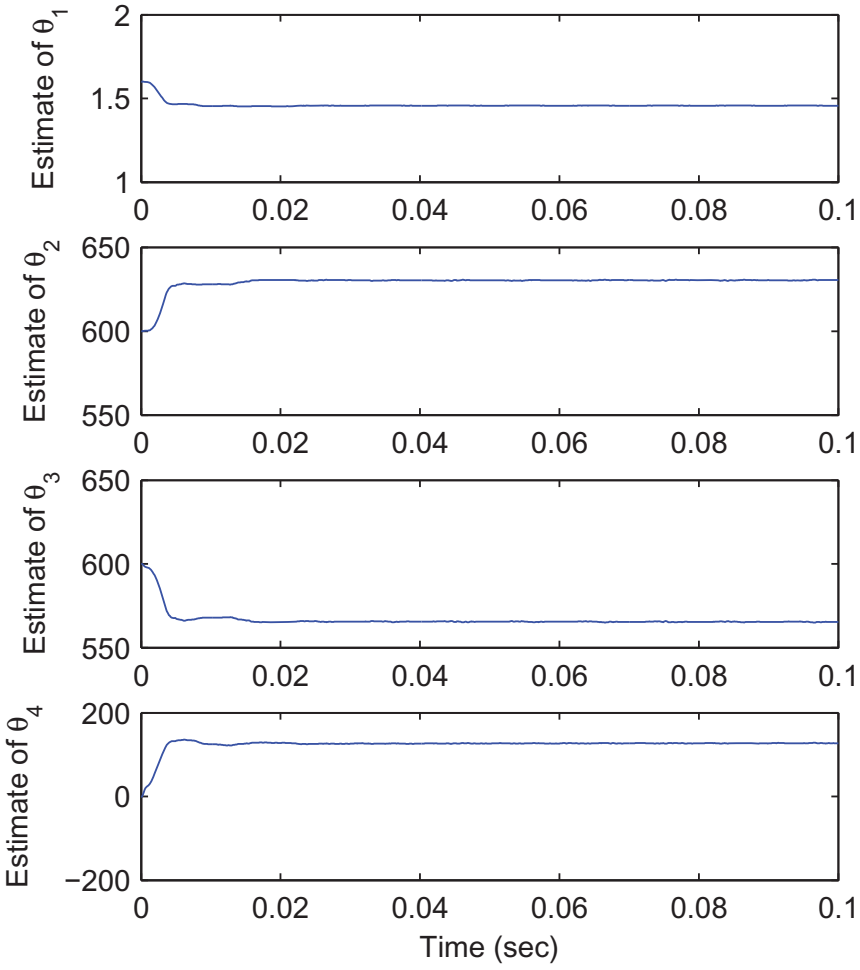

Figure 4.2. Major parameter estimates for a 100Hz sinusoid.

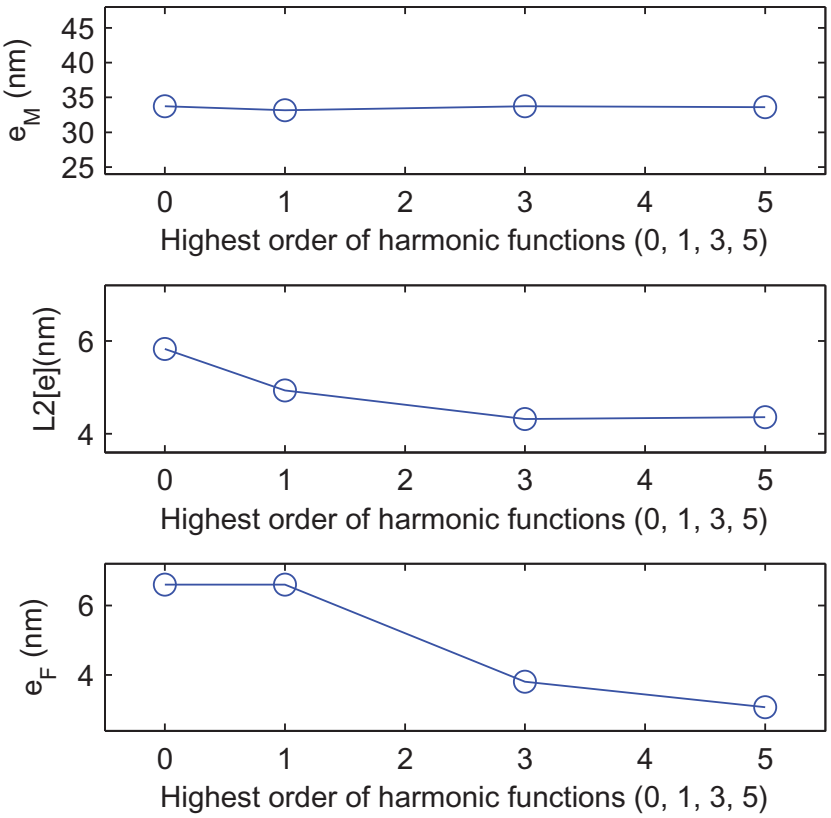

Figure 4.3. Tracking error v.s. highest order of harmonic functions.

Pseudo-triangular Trajectories

Figure 4.4 shows the tracking error in the first 10 periods for a 50 Hz pseudo-triangular trajectory. The constant velocity sections of the trajectory have a length of 2400 nm and occupy 80% of the period. The turn-around points are connected by smooth constant acceleration sections.

The first 4 estimated parameters are shown in Figure 4.5. The tracking performance is not as good as that of sinusoidal trajectory, which is expected because the uncertain nonlinearity when tracking triangular wave would take a lot more harmonics to approximate, but even with the same number of harmonics as before, the final tracking error is already down to 7.22nm, or 0.3% of the constant velocity scan length. If more stringent performance is required, more harmonics should be included. The same decreasing trend in error is observed as we increase the highest order of harmonics used, which is shown in Figure 4.6.

4.6 Using Harmonic Functions of Displacement

The uncertainty from hysteresis loops formed by periodic trajectories is fundamentally a function of displacement. We may also approximate the periodic uncertainty using harmonics of displacement instead of time.

4.6.1 Controller Modification

Instead of approximating the uncertainty as

$$\begin{aligned} \frac{1}{k_u}[\frac{1}{\tau b_0}d_g + \dot{d}_g] &= \frac{A_0}{2} + \sum_{n=1}^{m}(A_n \cos n\omega t + B_n \sin n\omega t) + \Delta \\ &= \Phi_d^T \theta_d + \Delta, \end{aligned} \tag{4.24}$$

as we did in section 4.3, we now have

$$\begin{aligned} \frac{1}{k_u}[\frac{1}{\tau b_0}d_g + \dot{d}_g] &= \frac{A_0}{2} + \sum_{n=1}^{m}(A_n \cos n\omega_s s(t) + B_n \sin n\omega_s s(t)) + \Delta \\ &= \Phi_d^T \theta_d + \Delta, \end{aligned} \tag{4.25}$$

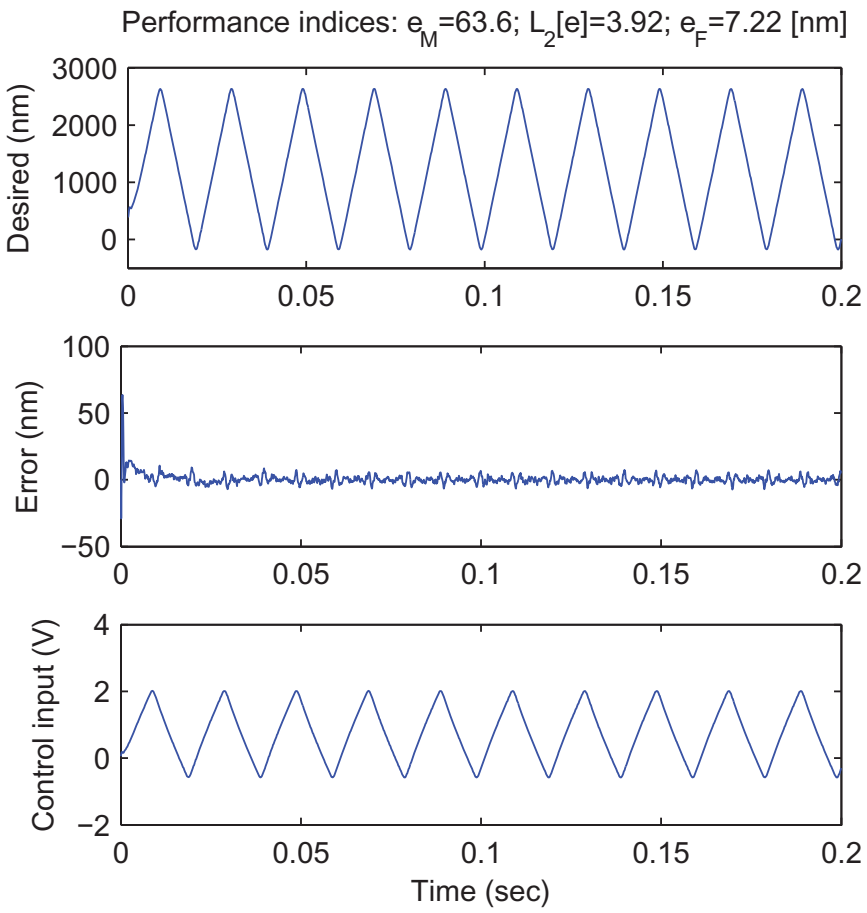

Figure 4.4. Tracking error for a 50Hz pseudo-triangular trajectory.

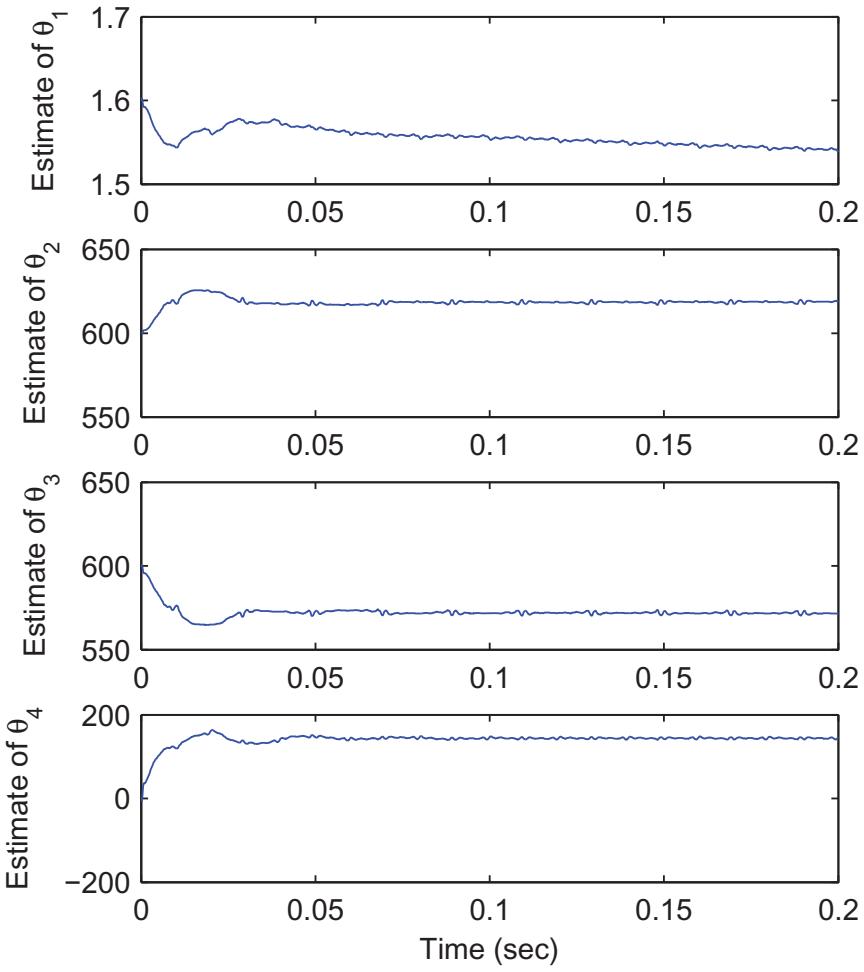

Figure 4.5. Major parameter estimates.

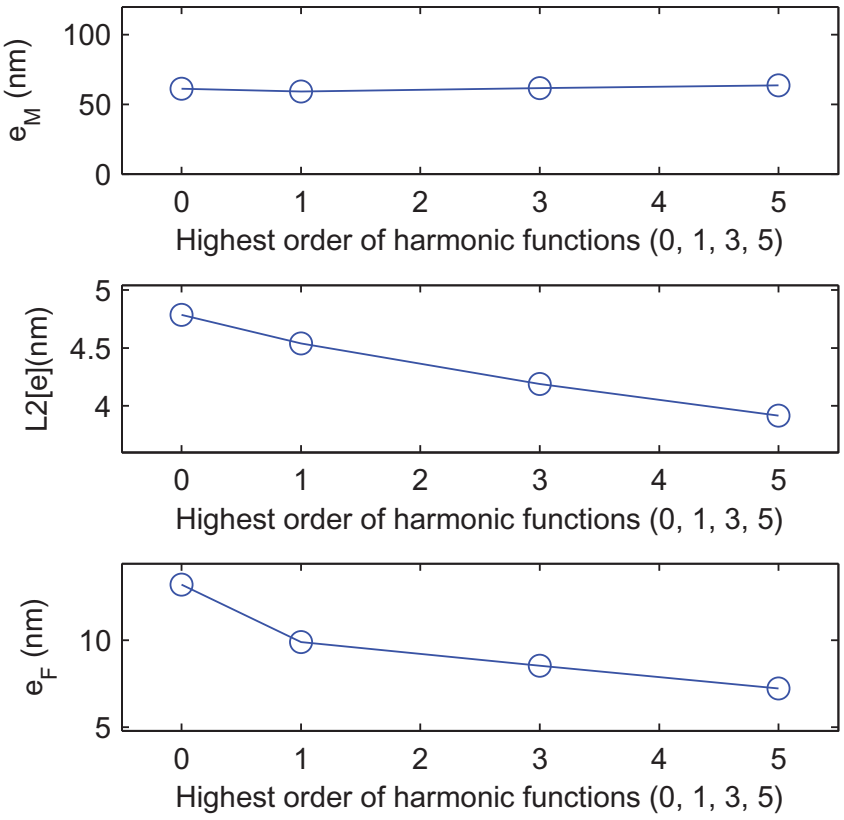

Figure 4.6. Tracking error v.s. highest order of harmonic functions.

where $s(t) = \int_0^t |\dot{y}_d(\tau)|\, d\tau$ is the absolute displacement calculated from the desired trajectory y_d, and ω_s is the frequency in the displacement domain. The rest of the controller remains the same.

4.6.2 Experimental Results

Fewer harmonic functions of displacement are needed to approximate the hysteresis. Figure 4.7 shows the performance of the controller with only the first harmonics for a 100-Hz, 9μm sinusoidal trajectory. Without an explicit hysteresis model, we have reduced the final tracking error to 0.023μm, or 0.26% of the trajectory span, almost to the level achieved by the final controller in Chapter 3.

Including the 2nd harmonics in the series did not significantly reduce error in the experiments, but made it much harder to choose the adaptation parameters, keep the controller stable and balance the transient and steady-state error. A sinusoid in displacement, when expressed in time, contains more than one frequency. The energy of the high frequency component may have enough power near the resonant frequency of the stage. When adapted quickly, the higher harmonics sometimes excite the resonance in the actuator. No further investigation was done in this research.

4.7 Limitations

Although approximation can be improved by including more and more harmonic basis functions, the frequency of higher harmonics inevitably approach the resonant frequency of the actuator. Unless the resonance dynamics is included in the closed-loop design to achieve higher closed-loop bandwidth, the tracking performance cannot be improved further, because exciting the unmodeled dynamics can destabilize the controller. The sampling frequency of the control system will also limit the number of harmonics that can be used.

When harmonic functions of time are used as part of the dynamic feedforward signal, they do not excite the unmodeled resonance at steady-state if the selected

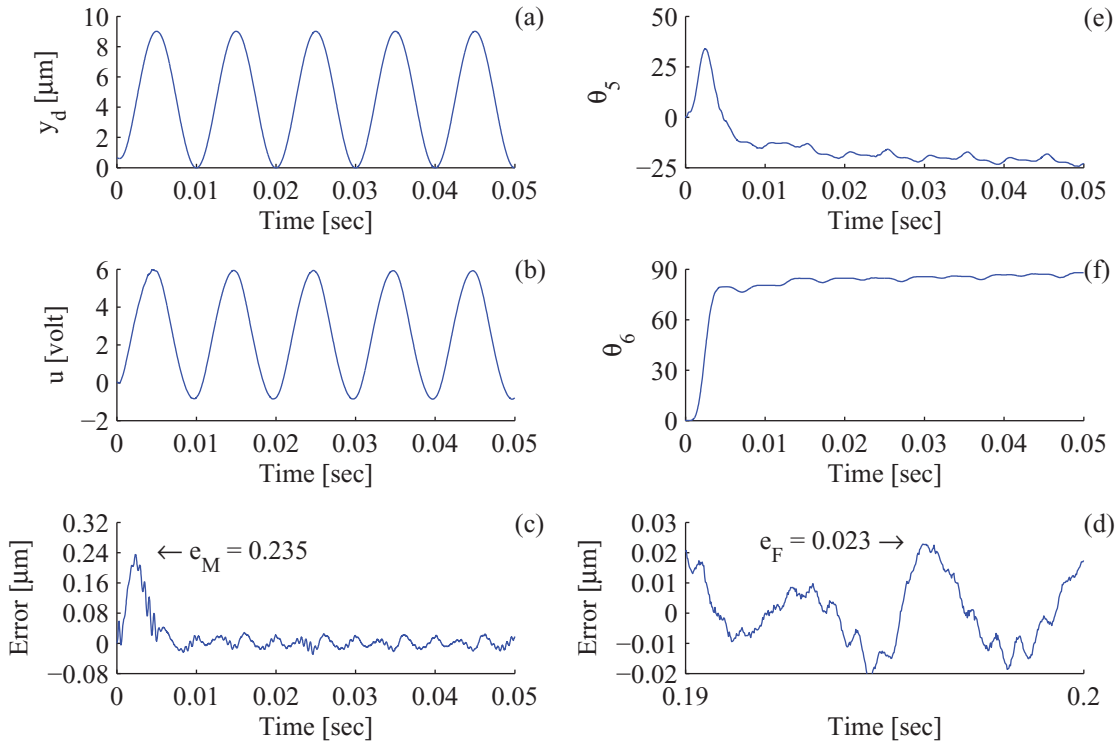

Figure 4.7. Tracking performance using periodic functions of displacement.

harmonics are well below the resonant frequency. We should also keep their adaptation gain small to avoid exciting resonance in the actuator during transient.

With harmonic functions of displacement, it becomes much less straightforward. A harmonic function with a single frequency in displacement s may contain multiple frequency components when expressed in time t, except for perfect triangular trajectories, where the absolute displacement is linear in time, $s = t \times |slope|$. It is not advisable to blindly increase the number of approximation functions without knowing that high frequency effects are well damped, either by design of the hardware system itself or by including the higher order dynamics in the plant model.

4.8 Conclusion

Tracking performance for single-loop periodic trajectories can be drastically improved by approximating the hysteresis uncertainty with a series of harmonic functions. Two types of functions have been used—sinusoidal functions of time and sinusoidal functions of displacement.

Using harmonic functions of time, tracking performance is improved as more and more harmonics are included. Harmonic functions of displacement provides better approximation to the hysteresis and only the harmonics at the fundamental frequency are needed to achieve good performance. In both cases, performance is limited by the resonance dynamics of the actuator stage.

5. CONCLUSIONS

5.1 Contributions

Three major contributions have been made in this dissertation:

- A numerically efficient hysteresis model that captures the essential properties of hysteresis in a piezo-electric actuator. The history-dependent hysteresis model is symmetric in both directions, simplifying implementation and reducing parameters, and the asymmetric response is assumed to be caused by other nonlinear effects such as a nonlinear distribution of internal electric field. The hysteretic friction model requires only two parameters, and the position-dependent nonlinearity is approximated by a polynomial. All parameters can be identified from a pseudo-static major loop alone. Hysteresis effect is reduced 15-fold to less than 1% of the output range.

- An adaptive robust controller design that recognizes the domain-switching dynamics as the dominant dynamics and accounts for both parametric and nonparametric uncertainties in the model. When combined with disturbance feedforward using the hysteresis model, it achieves tracking errors that are orders of magnitude smaller than those published in contemporary literature on the same actuator.

- An alternative compensation scheme that reduces tracking error to the noise level for periodic trajectories without using an explicit hysteresis model. Nonparametric uncertainty is reduced by exploiting the periodic nature of the uncertainty and parameterizing it with harmonic functions in time and displacement.

Regardless of the method, the philosophy stays the same — parameterize the model as much as possible to reduce the unstructured uncertainty that contributes to tracking error, and leave the rest to adaptation and robust feedback.

5.2 Future Directions

The work in this dissertation can be extended in the following directions:

- So far we have only used the simplest form of the Dahl hysteresis model. A non-integer order or a higher order of the model may provide an even better fit.
- The disturbance feedforward does not include any dynamics. Including the inverse dynamics of a nominal model may further improve its accuracy.
- The amplitude parameter for the hysteresis friction feedforward is fixed. Can we improve performance by adapting it online? Can we adapt more or all of the Dahl model parameters online? Is it possible to use a memory-less hysteresis model and only rely on fast adaptation?
- As frequency increases, the vibrational dynamics of the stage is no longer negligible. To further push the closed-loop bandwidth, the controller must consider the resonance dynamics.

LIST OF REFERENCES

LIST OF REFERENCES

[1] PhysikInstrumente. http://www.physikinstrumente.com/.

[2] Yan Yan, Qingze Zou, and Zhiqun Lin. A control approach to high-speed probe-based nanofabrication. *Nanotechnology*, 20:175301, 2009.

[3] Standards Committee of the IEEE Ultrasonics, Ferroelectrics, and Frequency-ControlSociety. IEEE standard on piezoelectricity. ANSI/IEEE std 176-1987, IEEE, 1987.

[4] Marc Kamlah and Charalampos Tsakmakis. Phenomenological modeling of the non-linear electromechanical coupling inferroelectrics. *International Journal of Solids and Structures*, 36:669–695, 1999.

[5] C. V. Newcomb and I. Flinn. Improving the linearity of piezoelectric ceramic actuators. *IEEE Electronics Letters*, 18:442–444, May 1982.

[6] M. Goldfarb and N. Celanovic. Modeling piezoelectric stack actuators for control of micromanipulation. *IEEE Control System Magazine*, 17(3):69–79, June 1997.

[7] A. J. Fleming and S. O. R. Moheimani. A ground-load charge amplifier for reducing hysteresis in piezoelectrictube scanners. *Review of Scientific Instruments*, 76, June 2005.

[8] Jiashi Yang. *An Introduction to the Theory of Piezoelectricity*, volume 9 of *Advances in Mechanics and Mathematics*. Springer, 2005.

[9] R. C. Smith. *Smart Materials Systems: Model Development*. SIAM, Philadelphia, 2005.

[10] D. S. Bernstein. Ivory ghost. *IEEE Control Systems Magazine*, 27(5):16–17, Oct. 2007.

[11] R. Ramanujam. *Modeling and Control of A Piezoelectric Positioning System*. Master's thesis, Purdue University, West Lafayette, USA, May 2001. MSME Thesis.

[12] Yongkai Xu. *Robust proximate-time-optimal command shaping for motion control: Scanningprobe microscope application*. PhD thesis, Purdue University, May 2006. PhD Thesis.

[13] Jinghua Zhong. *Modeling and Control of Piezoceramic Actuators for Nanopositoning*. Master's thesis, North Carolina State University, Raleigh, NC, August 2003.

[14] R. C. Smith, S. Seelecke, M. J. Dapino, and Z. Ounaies. A unified framework for modeling hysteresis in ferroic materials. *Journal of the Mechanics and Physics of Solids*, 54(1):46–85, 2005.

[15] Jack W. Macki, Paolo Nistri, and Pietro Zecca. Mathematical models for hysteresis. *SIAM Review*, 35(1):94–123, March 1993.

[16] Rostislav Lapshin. Analytical model for the approximation of hysteresis loop and its applicationto the scanning tunneling microscope. *Rev. Sci. Instrum.*, 66(9):4718–4730, Sep. 1995.

[17] Saeid Bashash and Nader Jalili. Feedforward hysteresis compensation in trajectory control of piezoelectrically-drivennanostagers. In *Smart Structures and Materials 2006: Smart Structures and Integrated Systems*, volume 6173, 2006.

[18] Jenö Takacs. *The T(x) Model for the Description of Hysteresis*. Wiley, Sep. 2003.

[19] F. Preisach. Über die magnetische nachwirkung. *Zeitschrift für Physik A Hadrons and Nuclei*, 94:277–302, 1935. 10.1007/BF01349418.

[20] Isaak Mayergoyz. *Mathematical Models of Hysteresis and Their Applications*. Elsevier Series in Eletrocmagnetism. Elsevier, 2003.

[21] Zs. Szabó, I. Tugyi, Gy. Kádár, and J. Füzi. Identification procedures for scalar preisach model. *Physica B*, 343:142–147, 2004.

[22] R. C. Smith. *Smart Materials Systems: Model Development*. SIAM, Philadelphia, 2005.

[23] R. B. Gorbet. *Control of Hysteresis systems with Preisach Representations*. PhD thesis, University of Waterloo, Waterloo, Canada, 1997. PhD Thesis.

[24] W. S. Galinaitis. *Two methods for modeling scalar hysteresis and their use in controllingactuators with hysteresis*. PhD thesis, Virginia Polytechnic Institute and State University, Blacksburg, VA, 1999. PhD Thesis.

[25] Szabó Zsolt. *Hysteresis models from elementary operators and integral equations*. PhD thesis, Budapest University of Technology and Economics, Budapest, Hungary, 2002.

[26] P. Ge and M. Jouaneh. Tracking control of a piezoceramic actuator. *IEEE Trans. Contr. Syst. Tech.*, 4(3):209–216, 1996.

[27] Saeid Bashash and Nader Jalili. A new constitutive modeling and control paradigm for piezoelectrically-actuated nanostagers. In *Proceedings of IMECE2006*, 2006.

[28] Saeid Bashash and Nader Jalili. Intelligence rules of hysteresis in the feedforward trajectory control of piezoelectrically-driven nanostagers. *Journal of Micromechanics and Microenigneering*, 17:342–349, 2007.

[29] H. Olsson, K. J. Åström, C. Canudas de Wit, M. Gäfvert, and P. Lischinsky. Friction models and friction compensation. *European Journal of Control*, 4:176–195, 1998.

[30] Carrett M. Clayton, Szhchu Tien, Kam K. Leang, Qingze Zou, and Santosh Devasia. A review of feedforward control approaches in nanopositioning for high-speed spm. *Journal of Dynamical Systems, Measurement and Control*, 131:061101, 2009.

[31] Saeid Bashash and Nader Jalili. Robust multiple frequency trajectory tracking control of piezoelectricallydriven micro/nanopositioning systems. *IEEE Transactions on Control System Technology*, 15(5):867–878, Sep. 2007.

[32] Douglas A. Bristow, Jingyan Dong, Andrew G. Alleyne, Placid M. Ferreira, and Srinivasa M. Salapaka. High bandwidth control of precision motion instrumentation. *Review of Scientific Instruments*, 79:103704, 2008.

[33] K. Kuhnen and H. Janocha. Adaptive inverse control of piezoelectric actuators with hysteresis operators. In *Proceedings of the European Control Conference*, page F291, Karlsruhe, Germany, August 1999. Laboratory for Process Automation, University of Saarland, Im Stadtwald,Geb.13, Saarbrucken Germany; klaus@lpa.uni-sb.de.

[34] Kam K. Leang and Santosh Devasia. Iterative feedforward compensation of hysteresis in piezo positioners. In *Proceedings of the 42nd IEEE Conference on Decision and Control*, pages 2626–2631, Maui, Hawaii, USA, December 2003.

[35] K. K. Leang and S. Devasia. Design of hysteresis-compensating iterative learning control for piezo-positioners:application to atomic force microscopes. *Mechatronics*, 16:141–158, 2006.

[36] Juan Manuel Cruz-Hernandez and Vincent Hayward. Phase control approach to hysteresis reduction. *IEEE Trans. on Control Systems Technology*, 9(1), 2001.

[37] Jayesh Minase, T-F Lu, B Cazzolato, and S Grainger. A review, supported by experimental results, of voltage, charge and capacitor insertion method for driving piezoelectric actuators. *Precision Engineering*, 34(4):692–700, 2010.

[38] Yusuke Ishikiriyama and Takeshi Morita. Improvement of self-sensing piezoelectric actuator control using permittivity change detection. *Journal of Advanced Mechanical Design, Systems, and Manufacturing*, 4(1):143–149, 2010.

[39] MH Salah, ML McIntyre, DM Dawson, JR Wagner, and E Tatlicioglu. Charge feedback-based robust position tracking control for piezoelectric actuators. *IET control theory & applications*, 6(5):615–628, 2012.

[40] Liang Huang, Yu Ting Ma, Zhi Hua Feng, and Fan Rang Kong. Switched capacitor charge pump reduces hysteresis of piezoelectric actuators over a large frequency range. *Review of Scientific Instruments*, 81(9):094701–094701, 2010.

[41] LS Zhang, YB Liu, L Huang, and ZH Feng. Using output voltage of charge drivers to reduce hysteresis of piezoelectric actuators. *Electronics letters*, 48(12):697–698, 2012.

[42] Andrew J Fleming. Precision charge drive with low frequency voltage feedback for linearization of piezoelectric hysteresis. In *American Control Conference (ACC), 2013*, pages 6022–6026. IEEE, 2013.

[43] Zhang Lian Sheng, Liu Yong Bin, Pan Cheng Liang, and Feng Zhi Hua. Leakage current characterization and compensation for piezoelectric actuator with charge drive. *Sensors and Actuators A: Physical*, 199:116–122, 2013.

[44] Pekka Ronkanen, Pasi Kallio, Matti Vilkko, and Heikki N Koivo. Displacement control of piezoelectric actuators using current and voltage. *Mechatronics, IEEE/ASME Transactions on*, 16(1):160–166, 2011.

[45] Andrew J Fleming and Kam K Leang. Integrated strain and force feedback for high-performance control of piezoelectric actuators. *Sensors and Actuators A: Physical*, 161(1):256–265, 2010.

[46] Ram V Iyer and Xiaobo Tan. Control of hysteretic systems through inverse compensation. *Control Systems, IEEE*, 29(1):83–99, 2009.

[47] Ming-Jyi Jang, Chieh-Li Chen, and Jie-Ren Lee. Modeling and control of a piezoelectric actuator driven system with asymmetric hysteresis. *Journal of the Franklin Institute*, 346(1):17–32, 2009.

[48] Hao Jiang, Hongli Ji, Jinhao Qiu, and Yuansheng Chen. A modified prandtl-ishlinskii model for modeling asymmetric hysteresis of piezoelectric actuators. *Ultrasonics, Ferroelectrics and Frequency Control, IEEE Transactions on*, 57(5):1200–1210, 2010.

[49] Jingyang Peng and Xiongbiao Chen. h_2-optimal digital control of piezoelectric actuators. In *Intelligent Control and Automation (WCICA), 2010 8th World Congress on*, pages 3684–3690. IEEE, 2010.

[50] Lei Liu, Kok Kiong Tan, Si-Lu Chen, Sunan Huang, and Tong Heng Lee. Svd-based preisach hysteresis identification and composite control of piezo actuators. *ISA transactions*, 51(3):430–438, 2012.

[51] Lei Liu, Kok Kiong Tan, Silu Chen, Chek Sing Teo, and Tong Heng Lee. Discrete composite control of piezoelectric actuators for high-speed and precision scanning. *Industrial Informatics, IEEE Transactions on*, 9(2):859–868, 2013.

[52] Jayesh Minase, T-F Lu, B Cazzolato, and S Grainger. Adaptive identification of hysteresis and creep in piezoelectric stack actuators. *The International Journal of Advanced Manufacturing Technology*, 46(9-12):913–921, 2010.

[53] Mohammad Al Janaideh, Subhash Rakheja, and Chun-Yi Su. An analytical generalized prandtl–ishlinskii model inversion for hysteresis compensation in micropositioning control. *Mechatronics, IEEE/ASME Transactions on*, 16(4):734–744, 2011.

[54] Zhi Li, Omar Aljanaideh, Chun-Yi Su, Subhash Rakheja, and M Al Janaideh. Compensation of hysteresis nonlinearity for a piezoelectric actuator using a stop operator-based prandtl-ishlinskii model. In *Advanced Mechatronic Systems (ICAMechS), 2011 International Conference on*, pages 169–174. IEEE, 2011.

[55] Mohamed Edardar, Xiaobo Tan, and Hassan K Khalil. Sliding-mode tracking control of piezo-actuated nanopositioners. In *American Control Conference (ACC), 2012*, pages 3825–3830. IEEE, 2012.

[56] Mohamed Edardar, Xiaobo Tan, and Hassan K Khalil. Tracking error analysis for singularly perturbed systems preceded by piecewise linear hysteresis. In *Decision and Control (CDC), 2012 IEEE 51st Annual Conference on*, pages 3139–3144. IEEE, 2012.

[57] Mohamed Edardar, Xiaobo Tan, and Hassan K Khalil. Closed-loop analysis for systems with fast linear dynamics preceded by hysteresis. In *American Control Conference (ACC), 2013*, pages 3573–3578. IEEE, 2013.

[58] Alex Esbrook and Xiaobo Tan. Harmonic analysis for hysteresis operators with application to control design for systems with hysteresis. In *American Control Conference (ACC), 2012*, pages 1652–1657. IEEE, 2012.

[59] Yanfang Liu, Jinjun Shan, Ulrich Gabbert, and Naiming Qi. Hysteresis and creep modeling and compensation for a piezoelectric actuator using a fractional-order maxwell resistive capacitor approach. *Smart Materials and Structures*, 22(11):115020, 2013.

[60] Yanfang Liu, Jinjun Shan, Ulrich Gabbert, and Naiming Qi. Hysteresis compensation and trajectory preshaping for piezoactuators in scanning applications. *Smart Materials and Structures*, 23(1):015015, 2013.

[61] Saeid Bashash, Nader Jalili, Phillip Evans, and Marcelo J. Dapino. Recursive memory-based hysteresis modeling for solid-state smart actuators. *Journal of Intelligent Material Systems and Structures*, 20:2161–2171, 2009.

[62] Sunan Huang, Kok Kiong Tan, and Tong Heng Lee. Adaptive sliding-mode control of piezoelectric actuators. *Industrial Electronics, IEEE Transactions on*, 56(9):3514–3522, 2009.

[63] Saeid Bashash and Nader Jalili. Robust multiple frequency trajectory tracking control of piezoelectrically driven micro/nanopositioning systems. *IEEE Transactions on Control Systems Technology*, 15(5):867–878, 2007.

[64] Saeid Bashash and Nader Jalili. Robust adaptive control of coupled parallel piezo-flexural nanopositioning stages. *Mechatronics, IEEE/ASME Transactions on*, 14(1):11–20, 2009.

[65] Nader Jalili. *Piezoelectric-based vibration control: from macro to micro/nano scale systems*. Springer, 2010.

[66] Y Cao and XB Chen. A novel discrete arma-based model for piezoelectric actuator hysteresis. *Mechatronics, IEEE/ASME Transactions on*, 17(4):737–744, 2012.

[67] Micky Rakotondrabe. Bouc–wen modeling and inverse multiplicative structure to compensate hysteresis nonlinearity in piezoelectric actuators. *Automation Science and Engineering, IEEE Transactions on*, 8(2):428–431, 2011.

[68] Yung-Tien Liu, Kuo-Ming Chang, and Wen-Zen Li. Model reference adaptive control for a piezo-positioning system. *Precision engineering*, 34(1):62–69, 2010.

[69] Yangmin Li and Qingsong Xu. Adaptive sliding mode control with perturbation estimation and pid sliding surface for motion tracking of a piezo-driven micromanipulator. *Control Systems Technology, IEEE Transactions on*, 18(4):798–810, 2010.

[70] Qingsong Xu and Yangmin Li. Dahl model-based hysteresis compensation and precise positioning control of an xy parallel micromanipulator with piezoelectric actuation. *Journal of dynamic systems, measurement, and control*, 132(4):041011, 2010.

[71] GuoYing Gu and LiMin Zhu. High-speed tracking control of piezoelectric actuators using an ellipse-based hysteresis model. *Review of Scientific Instruments*, 81(8):085104–085104, 2010.

[72] GuoYing Gu and LiMin Zhu. Modeling of rate-dependent hysteresis in piezoelectric actuators using a family of ellipses. *Sensors and Actuators A: Physical*, 165(2):303–309, 2011.

[73] Kam Leang, Qingze Zou, and Santosh Devasia. Feedforward control of piezoactuators in atomic force microscope systems. *Control Systems, IEEE*, 29(1):70–82, 2009.

[74] Kam K Leang, Qingze Zou, and Santosh Devasia. A review of feedforward control approaches in nanopositioning for high-speed spm. *Journal of dynamic systems, measurement, and control*, 131:061101–1, 2009.

[75] Lei Liu, Kok Kiong Tan, Andi Sudjana Putra, and Tong Heng Lee. Compensation of hysteresis in piezoelectric actuator with iterative learning control. In *Advanced Intelligent Mechatronics, 2009. AIM 2009. IEEE/ASME International Conference on*, pages 1300–1305. IEEE, 2009.

[76] Ying Wu and Qingze Zou. Robust inversion-based 2-dof control design for output tracking: piezoelectric-actuator example. *Control Systems Technology, IEEE Transactions on*, 17(5):1069–1082, 2009.

[77] Yan Yan, Qingze Zou, and Zhiqun Lin. A control approach to high-speed probe-based nanofabrication. *Nanotechnology*, 20(17):175301, 2009.

[78] Yan Yan, Haiming Wang, and Qingze Zou. A decoupled inversion-based iterative control approach to multi-axis precision positioning: 3d nanopositioning example. *Automatica*, 48(1):167–176, 2012.

[79] Haiming Wang. *Inversion-Based Control Tools for High-Speed Precision Tracking/Transition in Emerging Applications*. PhD thesis, Rutgers, The State University of New Jersey, 2013.

[80] Jingang Yi, Steven Chang, and Yantao Shen. Disturbance-observer-based hysteresis compensation for piezoelectric actuators. *Mechatronics, IEEE/ASME Transactions on*, 14(4):456–464, 2009.

[81] Hwee Choo Liaw and Bijan Shirinzadeh. Robust adaptive constrained motion tracking control of piezo-actuated flexure-based mechanisms for micro/nano manipulation. *Industrial Electronics, IEEE Transactions on*, 58(4):1406–1415, 2011.

[82] G Gu, L Zhu, C Su, Han Ding, et al. Motion control of piezoelectric positioning stages: modeling, controller design, and experimental evaluation. *Mechatronics, IEEE/ASME Transactions on*, 18(5):1459–1471, 2013.

[83] Sumeet S Aphale, Antoine Ferreira, and SO Moheimani. A robust loop-shaping approach to fast and accurate nanopositioning. *Sensors and Actuators A: Physical*, 204:88–96, 2013.

[84] U. Parlitz, A. Hornstein, D. Engster, F. Al-Bender, V. Lampaert, T. Tjahjowidodo, S. D. Fassois, D. Rizos, C. X. Wong, K. Worden, and G. Manson. Identification of pre-sliding friction dynamics. *Chaos*, 14:420–430, 2004.

[85] Helen. M. S. Georgiou and Ridha Ben Mrad. Electromechanical modeling of piezoceramic actuators for dynamic loading applications. *Journal of Dynamical Systems, Measurement and Control*, 128:558–567, 2006.

[86] Augusto Visintin. *Differential Models of Hysteresis*. Springer, 1994.

[87] P. R. Dahl. A solid friction model. Technical Report TOR-158(3107-18), The Aerospace Corporation, El Segundo, CA, 1968.

[88] P.-A. Bliman and M. Sorine. A system theoretic approach of systems with hysteresis. application to friction modelling and compensation. In *Proceedings of the 2nd European Control Conference*, 1993.

[89] P.-A. Bliman and M. Sorine. Modelling and control of a class of systems with hysteresis. application to friction compensation. In *Proceedings of IEEE Mediterranean Symposium in New Directions in Control Theory and Applications*, 1993.

[90] Jan Swevers, Farid Al-Bender, Chris G. Ganseman, and Tutuko Prajogo. An integrated friction model structure with improved presliding behavior for accurate friction compensation. *IEEE Transactions on Automatic Control*, 45:675–686, 2000.

[91] Y. Q. Ni, J. M. Ko, C. W. Wong, and S. Zhan. Modelling and identification of a wire-cable vibration isolator via a cyclic loading test. In *Proceedings of the Institution of Mechanical Engineers, Part I: Journal of Systems and Control Engineering*, volume 213, pages 163–172. Professional Engineering Publishing, 1999.

[92] A. Al-Majid and R. Dufour. Formulation of a hysteretic restoring force model. application to vibration isolation. *Nonlinear Dynamics*, 27:69–85, 2002.

[93] Jinghua Zhong and Bin Yao. Adaptive robust precision control of piezoelectric positioning stages. In *the IEEE/ASME Conference on Advanced Intelligent Mechatronics (AIM'05)*, pages 189–194, 2005.

[94] Jinghua Zhong and Bin Yao. Adaptive robust precision motion control of a piezoelectric positioning stage. *IEEE Transcations on Control System Technology*, 16(5):1039–1046, March 2008.

[95] Bin Yao. Integrated direct/indirect adaptive robust control of SISO nonlinear systemstransformableto semi-strict feedback forms. In *American Control Conference*, pages 3020–3025, 2003. The O. Hugo Schuck Best Paper (Theory) Award from the American AutomaticControlCouncil in 2004.

[96] Bin Yao and M. Tomizuka. Adaptive robust control of SISO nonlinear systems in a semi-strict feedbackform. *Automatica*, 33(5):893–900, 1997. (Part of the paper appeared in Proc. of 1995 American Control Conference,pp2500-2505,Seattle).

[97] Bin Yao and M. Tomizuka. Adaptive robust control of MIMO nonlinear systems in semi-strict feedbackforms. *Automatica*, 37(9):1305–1321, 2001. Parts of the paper were presented in the *IEEE Conf. on Decision andControl*,pp2346-2351, 1995, and the *IFAC World Congress*, Vol. F,pp335-340,1996.

[98] Li Xu and Bin Yao. Adaptive robust precision motion control of linear motors with negligibleelectricaldynamics: theory and experiments. *IEEE/ASME Transactions on Mechatronics*, 6(4):444–452, 2001.

[99] I.D. Mayergoyz. Mathematical models of hysteresis. In *The IEEE Transactions on Magnetics*, volume MAG-22; No. 5, pages 603–608, 1986.

[100] Bin Yao. High performance adaptive robust control of nonlinear systems: a generalframeworkand new schemes. In *Proc. of IEEE Conference on Decision and Control*, pages 2489–2494, San Diego, 1997.

[101] S. Sastry and M. Bodson. *Adaptive Control: Stability, Convergence and Robustness*. Prentice Hall, Inc., Englewood Cliffs, NJ 07632, USA, 1989.

[102] Bin Yao and M. Tomizuka. Smooth robust adaptive sliding mode control of robot manipulators with guaranteedtransientperformance. *Trans. of ASME, Journal of Dynamic Systems, Measurement and Control*, 118(4):764–775, 1996. Part of the paper also appeared in the *Proc. of 1994 American ControlConference*,pp.1176–1180.

[103] Bin Yao and Li Xu. On the design of adaptive robust repetitive controllers. In *ASME International Mechanical Engineering Congress and Exposition (IMECE'01),IMECE01/DSC-3B-4*, pages 1–9, 2001.

[104] Jinghua Zhong and Bin Yao. Adaptive robust repetitive control of piezoelectric actuators. In *the ASME International Mechanical Engineers Congress and Exposition (IMECE),IMECE2005-81967*, pages 1–8, 2005. Finalist of the Best Student Paper Competition of the ASME Dynamic SystemsandControl Division (DSCD).

VITA

VITA

Jinghua Zhong was born in Guangzhou, China in 1978. From 1991 to 1997, he attended Zhixin High School in Guangzhou. In 2001, he received a Bachelor of Engineering in Precision Instruments, Measurement and Control Technology from Tsinghua University in Beijing, and in 2003, a Master of Science in Mechanical Engineering from North Carolina State University in Raleigh. After 7 years in the Ph.D. program at Purdue University in West Lafayette, He joined Cummins Inc. in 2010 as a senior engineer in controls and diagnostics research.